Technische Universität München

TUM School of Medicine and Health

A T cell monitoring approach using nanobodies directed against the pan-T cell markers CD2 and CD7 as potential immunotherapy tracers

Sandro Bissenberger

Vollständiger Abdruck der von der TUM School of Medicine and Health der Technischen Universität München zur Erlangung eines Doktors der Medizin (Dr.med.) genehmigten Dissertation.

Vorsitz: Prof. Dr. Florian Eyer

Prüfende der Dissertation: 1. Prof. Dr. Angela Krackhardt
2. Priv.-Doz. Dr. Calogero D'Alessandria

Die Dissertation wurde am 01.07.2024 bei der Technischen Universität München eingereicht und durch die TUM School of Medicine and Health am 04.12.2024 angenommen.

Table of Content

Abbreviations

%ID	Percent injected dose
%ID/g	Percent injected dose per gram
[^{18}F]FHBG	9-[4-[^{18}F]fluoro-3-(hydroxymethyl)butyl]guanine
^{111}In	Indium-111
^{131}I	Iodine-131
^{177}Lu	Lutetium-177
^{18}F	Fluor-18
^{68}Ga	Gallium-68
7AAD	7-aminoactinomycine-D
^{89}Zr	Zirconium-89
ADCC	Antibody-dependant cellular cytotoxicity
AML	Acute myeloid leukemia
APC	Antigen-presenting cell
APC	Allophycocyanin
ATC	Adoptive T cell transfer
aTTP	Acquired thrombotic thrombocytopenic purpura
BCMA	B cell maturation antigen
BSA	Bovine serum albumin
CAR	Chimeric antigen receptor
Cas9	CRISPR associated protein 9
CD	Cluster of differentiation
CDC	Complement-dependent cytotoxicity
c_{END}	Endconcentration
CEST	Chemical exchange saturation transfer
CRISPR	Clustered regularly interspaced short palindromic repeats

crRNA	CRISPR RNA
CT	Computed tomography
CTL	Cytotoxic T lymphocyte
CTLA-4	Cytotoxic T-lymphocyte-associated antigen 4
DEPC	Diethyl pyrocarbonate
DFO	Desferrioxamine B
DMSO	Dimethylsulfoxide
DNA	Deoxyribonucleic acid
DOTA	Dodecane tetraacetic acid
DSB	Double strand break
DsRed	Discosoma sp. Red
EDTA	Ethylenediaminetetraacetic acid
EGFR	Epidermal growth factor receptor
ELISA	Enzyme-linked immunosorbent assay
FACS	Fluorescence-activated cell sorting
FBS	Fetal bovine serum
FCS	Fetal calf serum
FcγR	Fc receptor for IgG
FDA	Food and Drug Administration
FITC	Fluorescein isothiocyanate
FWD	Forward
gDNA	Genomic DNA
GFP	Green fluorescent protein
GM-CSF	Granulocyte macrophage colony-stimulating factor
gp100	Glycoprotein 100
gRNA	Guide RNA

HEPES	4-(2-hydroxyethyl)-1-piperazineethanesulfonic acid
HER2	Human epidermal growth factor receptor 2
His-tag	Polyhistidine-tag
HLA	Human leukocyte antigen
HS	Human serum
HSV1-TK	Herpes simplex virus type 1 thymidine kinase
ICI	Immune checkpoint inhibition
IHC	Immunohistochemistry
IL	Interleukin
INF	Interferon
iRFP	Near-infrared fluorescent protein
JAK	Janus kinase
LAG-3	Lymphocyte activation gene 3
LFA-3	Lymphocyte function-associated antigen 3
mAb	Monoclonal antibody
MAGE-A	Melanoma-associated antigen A
MFI	Mean fluorescence intensity
MPO	Myeloperoxidase
MRI	Magnetic resonance imaging
Nb	Nanobody
Ni-NTA	Nickel-nitrilotriacetic acid
NIS	Sodium/Iodide symporter
NKT	Natural killer T cell
NOTA	1,4,7-Triazacyclononane-1,4,7-triacetic acid
PBMC	Peripheral blood mononuclear cells
PBS	Phosphate-buffered saline

PCR	Polymerase chain reaction
PD1	Programmed cell death protein 1
PDL1	Programmed cell death ligand 1
PE	Phycoerythrin
PEG	Polyethylene glycol
PET	Positron emission tomography
PFA	Paraformaldehyde
PFC	Perfluorocarbon
PTPRD/PTPRT	Protein Tyrosine Phosphatase Receptor Type D/T
REV	Reverse
RNA	Ribonucleic acid
RNP	Ribonucleoprotein
sdAb	Single domain antibody
SDS	Sodium dodecyl sulfate
SE-HPLC	Size exclusion high performance liquid chromatography
sgRNA	Single guide RNA
SPECT	Single-photon emission computed tomography
STAT	Signal Transducers and Activators of Transcription
SUV	Standardized uptake value
T7E1	T7-endonuclease-1
TCR	T cell receptor
TIL	Tumor-infiltrating lymphocyte
TIM-3	T cell immunoglobulin mucin 3
tracrRNA	Trans-activating CRISPR RNA
V_{END}	Endvolume
VHH	Variable heavy domain of heavy chain

List of Figures

List of Tables

Summary

In search for new therapy approaches in malignancies, T cells and modification of their reactivity have become the focus over the past decades, resulting in multiple treatment options which reached clinical translation. However, response patterns to immunotherapies still need to be fully understood and are highly individual. Pseudoprogression, for instance, is a phenomenon that often occurs in patients treated with immunotherapies, meaning that distinct tumor regress is seen after initial progress. Developing tools to properly evaluate response patterns is essential to avoid premature treatment discontinuation.

We developed and characterized Nanobodies targeting the clusters of differentiation (CD) 2 and 7 as pan-T cell markers for tracking their response in tumor rejection. In the first step, target-specific Nanobodies were derived from immunized llama via variable heavy domain of heavy chain (VHH) phage display library construction followed by biopanning and enzyme-linked immunosorbent assay (ELISA) by VIB Nanobody Core in Brussels. Specificity was confirmed in a dual approach using antigen-transduced tumor cells and a CRISPR/Cas9 knockout model of Jurkat cells. In the next step, possible impairment of T cell functionality was excluded in a coculture assay as targeting T cell antigens can lead to dysfunctionality and apoptosis. Therefore, we established a co-incubation assay to measure cytokine levels by ELISA which consisted of T cells transgenic for T cell receptor (TCR) 2.5D6, cell lines transduced with TCR-matching human leukocyte antigen (HLA) and Nanobodies in high concentrations. In addition, lack of impairment was confirmed in a previously established mouse model compared to $F(ab')_2$ fragments which are known to lack sufficient tumor rejection. Ex vivo analysis showed successful tagging of T cells at the tumor side without any functional impairment. As a proof-of-concept, CD2-specific Nanobody was used for a preliminary in vivo imaging experiment and hence, was labeled with Gallium-68 to track T cells by positron emission tomography (PET)/magnetic resonance imaging (MRI). 90 minutes post-injection, T cells were already specifically visualized at the tumor site which was confirmed by ex vivo analysis. In contrast, the tracer ^{89}Zr-aTCRmu-$F(ab')_2$, which was previously established in the lab showed comparable visualization 48 hours post-injection.

Altogether, the presented Nanobodies enable uncomplicated and specific tracking of in vivo T cell activity without impairing their tumor rejection. Thus, decision-making regarding immunotherapies may be based on possible prospective biomarkers after

further development. Moreover, this simple approach offers a convenient and time-saving method for direct clinical translation.

Zusammenfassung

Auf der Suche nach neuen Therapieansätzen für bösartige Erkrankungen sind T-Zellen und die Veränderung ihrer Funktion in den letzten Jahrzehnten immer mehr in den Mittelpunkt gerückt, was zu einer Vielzahl an Behandlungsmöglichkeiten geführt hat, die in die klinische Praxis umgesetzt wurden. Die Reaktionsmuster verschiedener Immuntherapien sind jedoch noch nicht vollständig geklärt und sind sehr individuell. Pseudoprogression ist zum Beispiel ein Phänomen, das insbesonders bei Patienten auftritt, die mit Immuntherapien behandelt werden. Es äußert sich dadurch, dass sich der Tumor nach anfänglichem Progress deutlich zurückbildet. Die Entwicklung von Verfahren zur angemessenen Bewertung von Ansprechmustern ist von entscheidender Bedeutung, um ein vorzeitiges Absetzen der Behandlung zu vermeiden.

Wir haben Nanobodies entwickelt und charakterisiert, die auf CD2 und CD7 als Pan-T-Zell-Marker abzielen, um das T-Zell Verhalten bei der Tumorabwehr nachverfolgen zu können. Die antigenspezifischen Nanobodies wurden aus immunisierten Lamas mittels Konstruktion einer VHH-Phagendisplay-Bibliothek und anschließendem Biopanning sowie ELISA durch das VIB Nanobody Core in Brüssel gewonnen. Die Spezifität wurde in einem dualen Ansatz mit Antigen-transduzierten Tumorzellen und einem CRISPR/Cas9-Knockout-Modell von Jurkat-Zellen bestätigt. In einem nächsten Schritt wurde eine mögliche Beeinträchtigung der T-Zell-Funktionalität in einem Kokultur-Versuch ausgeschlossen, da das Markieren von T-Zell-Antigenen zu Dysfunktionalität und Zelluntergang führen kann. Daher wurden T-Zellen, die für den TCR2.5D6 transgen sind zusammen mit Zelllinien, die mit TCR-übereinstimmendem HLA transduziert wurden, sowie Nanobodies in hohen Konzentrationen inkubiert und die Zytokinspiegel mittels ELISA gemessen. Die fehlende Beeinträchtigung wurde zusätzlich in einem zuvor etablierten Mausmodell im Vergleich zu F(ab')$_2$-Fragmenten bestätigt, die bekanntermaßen zu einer eingeschränkten Tumorabstoßung führen. Ex-vivo-Analysen zeigten eine erfolgreiche Markierung von T-Zellen im Bereich des Tumors. Als konzeptioneller Beweis wurde der CD2-spezifische Nanobody für eine vorläufige In-vivo-Bildgebung verwendet und daher mit Gadolinium-68 markiert, um T-Zellen mittels PET/MRT zu verfolgen. Die T-Zellen konnten bereits 90 Minuten nach der Injektion spezifisch am Tumor dargestellt werden, was durch Ex-vivo-Analysen bestätigt wurde. Der zuvor im Labor etablierte Tracer 89Zr-aTCRmu-F(ab')$_2$ zeigte eine vergleichbare Darstellung erst 48 Stunden nach der Injektion.

Insgesamt ermöglichen die vorgestellten Nanobodies eine unkomplizierte und spezifische Verfolgung der T-Zell-Aktivität in vivo, ohne deren Tumorabstoßung zu beeinträchtigen. Somit können Entscheidungen über Immuntherapien, nach weiterer Entwicklung, auf der Grundlage möglicher zukünftiger Biomarker getroffen werden. Darüber hinaus bietet dieser einfache Ansatz eine komfortable und zeitsparende Methode für die direkte klinische Umsetzung.

1. Introduction

1.1. Role of T cells in immune response and cancer immunotherapy

T lymphocytes are often designated as the leading player in the adaptive immune system as their regulatory function leads the immune response in different directions. Dysregulation of T cells occurs frequently and can appear in various clinical pathophysiological “phenotypes” such as autoimmunity and autoinflammation, allergies, chronic infection, or cancer. Therefore, they are often targeted by therapy approaches (Mosmann and Sad 1996, Walker and Abbas 2002, Christen and von Herrath 2004, Wherry and Ahmed 2004, Braga, Schiavone et al. 2012).

In recent years, research has focused on the capability of antigen-specific cytotoxicity of T cells and, subsequently, the redirection of their antitumor response through cancer immunotherapies (Waldman, Fritz and Lenardo 2020). Different approaches have been developed within the last years, many of which have reached clinical translation and showed superior results to conventional therapies. (O'Day, Hamid and Urba 2007, Restifo, Dudley and Rosenberg 2012, Wolchok, Kluger et al. 2013, Butterfield 2015, Postow, Callahan and Wolchok 2015, Kubli, Berger et al. 2021). A few techniques of immunotherapy, which are currently under clinical investigation, will be briefly delineated.

1.1.1. Vaccination therapy

The idea of cancer vaccines is the stimulation of immune cells towards the differentiation of antigen-specific effector cells, like vaccinations against infectious diseases. This approach could be either used as a preventive or a therapeutic method. Preventive vaccination against oncogenic viruses such as hepatitis B virus has already been performed for a long time (Chang, Shau et al. 2000). Likewise, more recent vaccines against human papillomavirus (HPV), which can cause anogenital cancer, showed an excellent preventive effect and different compounds have been approved (Joura, Giuliano et al. 2015, Huh, Joura et al. 2017). Therapeutic vaccines follow different strategies to prompt an immune response. They are tumor cell, dendritic cell, peptide or genetically based. Tumor cells transduced with granulocyte-macrophage colony-stimulating factor (GM-CSF) (GVAX) showed promising results in preclinical and phase II studies as cell-based vaccination. Yet, they failed in a phase III trial for the treatment of castrate-resistant prostate cancer (Lassi and Dawson 2010). However, a combination therapy of GVAX and cytotoxic T-lymphocyte associated protein 4 (CTLA-4) antibodies

is still being investigated and has shown superior results in clinical trials (van den Eertwegh, Versluis et al. 2012, Le, Lutz et al. 2013). Sipuleucel-T was the first dendritic cell (DC)-based vaccine approved by the Food and Drug Administration (FDA) containing antigen-presenting cells (APCs) incubated with a prostatic acid phosphatase fusion protein and GM-CSF. The intervention arm of the pivotal study showed a roughly four-month prolonged survival time (Kantoff, Higano et al. 2010). Approaches based on peptides have the advantage that specific mutations or neoantigens can be used as vaccine bases because somatic alterations within the genome of tumor cells are mainly individual. Potential neoepitopes generated by mutations can be mapped after Next Generation Sequencing, and their immunogenicity regarding patient's MHC can be predicted. Further research and improvements are still required for permanent clinical translation as manufacturing process currently takes about 4 months (Sahin and Türeci 2018). The only non-individual peptide-based vaccine which showed promising data in a phase III study with patients suffering from advanced melanoma consists of gp100, a shared antigen between normal tissue and melanoma, together with interleukin (IL) 2 (Schwartzentruber, Lawson et al. 2011). A hybrid therapy of a genetic-based vaccine and an oncolytic virus approved in 2015 by the FDA is talimogene laherparepvec (T-Vec). It consists of a genetically modified herpes simplex virus, which infects melanoma cells explicitly and introduces a coding sequence for GM-CSF into these cells. The release of tumor antigens and GM-CSF after lysis due to viral infection results in a systemic anti-tumor response. Phase III trial analysis showed far better outcomes for patients treated with talimogene laherparepvec (Andtbacka, Collichio et al. 2019).

1.1.2. Adoptive T cell transfer (ATC)

The first attempts of T cell transfer were based on extracting tumor-infiltrating lymphocytes (TILs) from the tumor tissue of melanoma patients, followed by in vitro expansion. After reinfusion of T cells together with IL-2, the overall response rate was 34% which lasted only for a median of 4 months (Rosenberg, Yannelli et al. 1994). Following studies with previous lymphodepletion showed more significant effect and longer-lasting remission (Rosenberg, Yang et al. 2011). As a recent study of a patient with metastatic breast cancer showed, current technological advances enabled specific sorting and enrichment for tumor-reactive TILs, promising adoptive therapies for tumor entities with only low somatic mutational load (Zacharakis, Chinnasamy et al. 2018). Clinical trials using this approach are still running and have already shown meaningful results in heavily pretreated patients (Chesney, Lewis et al. 2022). Challenges regarding the isolation and expansion of TILs as well as their specificity have driven the developing

field of engineered T cells as a more precise and effective alternative. With the introduction of tumor-specific TCRs or chimeric antigen receptors (CARs), every T cell may become redirected against tumor cells. TCR and CAR transduction into T cells has advantages and disadvantages. Although introducing a TCR represents a more physiological approach as the activation includes the regular intracellular signaling cascade, the recognition of an antigen is restricted to the presentation of these antigens on major histocompatibility complex (MHC) molecules. Consequently, TCR transgenic T cells are affected by common cancer escape mechanisms such as the downregulation of MHC molecules (Khong and Restifo 2002, Lee, Shklovskaya et al. 2020). However, clinical trials with TCR-engineered T cells specific for viral oncogenes, or germline antigens showed encouraging results in different tumor entities (Louis, Straathof et al. 2010, Robbins, Morgan et al. 2011, Rapoport, Stadtmauer et al. 2015).

By contrast, CARs can target regular surface antigens overcoming MHC restriction and can be linked to the signaling domain of the TCR or various intra- and extracellular costimulatory domains, increasing the opportunities to achieve high therapy efficiencies (Waldman, Fritz and Lenardo 2020). So far, the FDA has approved 6 CARs for treating refractory B cell leukemia, lymphoma, mantle-cell lymphoma, and multiple myeloma. The respective CARs target the B cell antigen CD19 or B-cell maturation antigen (BCMA) and showed durable remission in the majority of patients (Maude, Pulsipher et al. 2016, Neelapu, Locke et al. 2017, Schuster, Bishop et al. 2019, Wang, Munoz et al. 2020, Martin, Usmani et al. 2021, Munshi, Anderson et al. 2021). The present approval of CARs restricted to CD19 and BCMA emphasizes the difficulty in finding target antigens only expressed by the tumor cells, reducing off-target toxicity and severe side effects. Nevertheless, there have been advances regarding other target antigens as CD7-specific CARs in T cell malignancies and a current trial with anti-GD2 CAR natural killer T cells in patients with neuroblastoma showed (Gomes-Silva, Srinivasan et al. 2017, Lu, Liu et al. 2022, Heczey, Xu et al. 2023). Developing effective therapies to the same extent as in hematologic malignancies is still limited for solid malignancies due to unsolved problems such as immunosuppressive microenvironment, on-target off-tumor toxicity, and aggravated T cell trafficking (Li, Li et al. 2018, Flugel, Majzner et al. 2023).

1.1.3. Immune checkpoint inhibition

Immune response is regulated by numerous inhibitory and costimulatory markers, whose direct function in the regulatory loops is often not completely understood. Two well-characterized and well-known receptors are CTLA4 and programmed cell death protein 1 (PD1), which mediate T cell inhibition. PDL1, the ligand to PD1, is commonly

overexpressed on tumor cells as an escape mechanism in the immunosuppressive environment of cancer (Iwai, Ishida et al. 2002). Thus, inhibiting these regulatory markers is a preferable option for reinducing anti-tumoral activity. The first checkpoint inhibitor approved by the FDA was Ipilimumab, an anti-CTLA4 mAb, as it showed prolonged survival for patients with metastatic melanoma (Hodi, O'Day et al. 2010). Currently, six other checkpoint inhibitors are approved by the FDA for a variety of cancer entities targeting either PD1 or PDL1, showing prolonged survival or equal survival to conventional therapy methods with fewer side effects in clinical trials (Robert, Schachter et al. 2015, Weber, D'Angelo et al. 2015, Rosenberg, Hoffman-Censits et al. 2016, Powles, O'Donnell et al. 2017). Many other targets for checkpoint inhibition are under investigation, and some already showed convincing results in initial trials. One of them, lymphocyte-activation gene 3 (LAG3), also seems to have a negative regulatory effect on T cells, but the actual mechanism remains unclear. Nevertheless, first studies of combination therapy with a soluble form of LAG3 and conventional chemotherapy detected in over 90% of patients suffering from metastatic breast carcinoma benefit from this treatment (Brignone, Gutierrez et al. 2010). Relatlimab, a LAG-3-blocking antibody, has currently even been approved in a fix combination with Nivolumab for treatment of advanced melanoma (Tawbi, Schadendorf et al. 2022). Patients with TILs expressing T cell immunoglobulin and mucin domain containing protein 3 (TIM3) as another negative regulatory molecule are known to have a poor prognosis. Hence, investigation of TIM3 as a possible target of checkpoint inhibition is also highly interesting (Gao, Zhu et al. 2012, Yang, Grote et al. 2012). A current clinical trial, which investigates the combination of an anti-TIM3 antibody and decitabine in acute myeloid leukemia, showed promising results in preliminary data (Borate, Esteve et al. 2019).

The combination of different checkpoint inhibitors showed even better outcomes as they have a complementary effect in regulating immune response, and single-use seems to cause upregulation of other immune checkpoints (Koyama, Akbay et al. 2016, Patel and Minn 2018). Nivolumab and Ipilimumab together showed synergistic effects in clinical trials and subsequent prolonged survival in advanced melanoma, renal-cell carcinoma and non-small-cell lung cancer (Wolchok, Chiarion-Sileni et al. 2017, Motzer, Tannir et al. 2018). Further combination of dual checkpoint inhibition and radiation therapy increases the abscopal effect and seems to improve immune response. However, this combination is still under investigation in clinical trials (Twyman-Saint Victor, Rech et al. 2015, Ngwa, Irabor et al. 2018).

1.2. Non-invasive imaging of T cells

In recent years, immunotherapies have made impressive advances and have provided superior therapy for millions of patients. Nevertheless, the full potential of immunotherapies has yet to be exploited. Further understanding of T cell behavior and interaction within the tumor microenvironment after immunomodulating therapy in vivo is essential for ongoing development. T cells directed against neoepitopes expressed on tumor cells are an attractive target for further investigation as they may be responsible for the success of immunotherapies (Gros, Parkhurst et al. 2016, Verdegaal, de Miranda et al. 2016). Translation of immunotherapies into clinical studies and daily clinical routine entailed new challenges regarding the evaluation of therapy efficiency as their response pattern significantly differs from conventional therapies. For up to 10% of the patients treated with immunotherapies, pseudoprogression occurred, meaning after an initial progression of the tumor, lesions showed later distinct regression (Borcoman, Kanjanapan et al. 2019). Clinical studies have detected pseudoprogression in various tumor entities after immune checkpoint inhibition (Wolchok, Hamid et al. 2015, Long, Weber et al. 2017, Gandara, von Pawel et al. 2018, Katz, Hammer et al. 2018, Parseghian, Patnana et al. 2018). However, mechanisms for this phenomenon remain unclear. Two possible explanations are the delayed efficient anti-tumor response and immune cell infiltration causing an inflammatory reaction (Borcoman, Kanjanapan et al. 2019). Tumor biopsies of melanoma patients after treatment with Ipilimumab gave evidence for the second hypothesis (Di Giacomo, Danielli et al. 2009). Considering that 1 in 10 patients could benefit from treatment beyond progression, conventional RESIST criteria for clinical trials have been revised for the treatment with immunotherapies (Seymour, Bogaerts et al. 2017, Tazdait, Mezquita et al. 2018).

Nevertheless, patients with definite progression could benefit from alternative treatment strategies. Thus, sensitive imaging methods for evaluating anti-tumor immune activity are crucial for distinguishing between actual progress and pseudoprogression, preventing belayed diagnosis, and offering every patient the most effective therapy. Response patterns of immunotherapies cannot be fully captured by current imaging methods such as MRI, single photon emission tomography (SPECT) and PET, which will be outlined in the following.

1.2.1. Magnetic resonance imaging

MRI is commonly used in today's medicine because of its high resolution, superior contrast for soft tissue and no ionizing radiation. Different contrast agents for direct and indirect labeling of cells are available such as gadolinium complexes, iron oxide nanoparticles, chemical exchange saturation transfer (CEST) agents and perfluorocarbon (PFC) (Ahrens and Bulte 2013). For imaging of T cells, iron oxide nanoparticles and PFC-based approaches were used. They showed auspicious results in preclinical in vivo studies but were not further translated into human studies so far (Kircher, Allport et al. 2003, Liu, Ye et al. 2012, Li, Wu et al. 2016, Saini, Korf et al. 2019). Indirect labeling by introducing receptor and surface marker, kinases, or binding protein genes have the potential to specifically track transferred T cells without loss of signal by cell division (Genove, DeMarco et al. 2005, Tannous, Grimm et al. 2006, Iordanova and Ahrens 2012, Bar-Shir, Liu et al. 2014, Liu and Li 2014). However, indirect labeling of T cells for MRI imaging is barely reported and further investigation is necessary regarding genetic manipulation and cell function.

1.2.2. Nuclear imaging

Imaging methods such as SPECT and PET have the advantage that they can provide functional imaging and anatomical imaging in combination with CT or MRI. Almost every structure can be targeted and imaged in nuclear imaging methods by labeling different agents, substrates, or antibodies with radioactive isotopes and still offering outstanding depth penetration as well as absolute quantification (Nagy, Tóth et al. 2013).

For imaging of adoptively transferred T cells, direct or indirect labeling methods exist as described above. As a direct labeling agent, ^{111}In-oxine has been used for SPECT imaging of T cells in different tumor entities (Griffith, Read et al. 1989, Grimfors, Schnell et al. 1989). This method could display lymphocytes specific for hemagglutinin for up to 120h post-injection (Pittet, Grimm et al. 2007). Clinical trials investigating tumor infiltration of ex vivo ^{111}In-oxine-labeled CD8+ T cells are still ongoing. Due to its higher sensitivity in detecting only small numbers of cells and the possibility of direct quantification, PET is more attractive for clinical applications (Krekorian, Fruhwirth et al. 2019). Moreover, PET tracers such as ^{89}Zr showed superior characteristics to ^{111}In (Charoenphun, Meszaros et al. 2015). Direct labeling of cytotoxic T-lymphocytes (CTLs) and CAR T cells with ^{89}Zr-oxine allowed cell tracking for several days (Sato, Wu et al. 2015, Weist, Starr et al. 2018). Indirect labeling methods introduce reporter genes and avoid "dilution" of signal after cell division enabling consecutive imaging with multiple tracer applications. Conventional reporter genes like the herpes simplex virus 1

thymidine kinase showed promising results using 9-[4-[^{18}F]fluoro-3-(hydroxymethyl)butyl]guanine ([^{18}F]FHBG) as tracer in patients with glioma after CTL administration (Keu, Witney et al. 2017). However, as a viral protein, the kinase causes immunogenic reactions, which influence the persistence of transgenic cells (Berger, Flowers et al. 2006). Thus, human reporter genes have become the focus and were investigated. The sodium/iodide symporter (NIS), as one of them, was successfully used in preclinical studies for tracking CAR cells (Emami-Shahri, Foster et al. 2018, Kurtys, Lim et al. 2018). Another approach for imaging engineered T cells used the constant murine TCR beta domain as a target. Thus, F(ab')$_2$ fragments of a mouse IgG were produced and labeled with ^{89}Zr. Intravenous tracer injection after adoptive T cell transfer followed by PET imaging showed susceptible detection of small cell numbers and was confirmed by correlation of ex vivo quantification (Mall, Yusufi et al. 2016, Yusufi, Mall et al. 2017).

Nevertheless, other labeling strategies for imaging need to be used to image non-modified T cells in vivo. Targeting surface markers using antigen-binding tracers like antibodies or peptides is an attractive option as they can label T cells without genetical manipulation and can be used for imaging purposes in already developed therapeutic approaches, such as checkpoint inhibitors (Niemeijer, Leung et al. 2018). Moreover, specific subpopulations or activated cells can be differentiated if respective markers are targeted. Current approaches in imaging early-stage T cell activation use ^{18}F-labelled IL-2, which binds to the upregulated IL-2 receptor on activated T cells. Specific accumulation was detected in tumor-bearing mice receiving antitumor therapy compared to control mice (Hartimath, Draghiciu et al. 2017). Clinical trials using N-(4-[^{18}F]fluorobenzoyl)-interleukin-2 ([^{18}F]FB-IL-2) are still ongoing. Another target currently being investigated in clinical trials is the T cell activation marker OX40. Preclinical studies with the labeled murine antibody ^{64}Cu-DOTA-AbOX40 already showed good prediction of antitumor response after cancer vaccination in a murine model (Alam, Mayer et al. 2018). Other tracers directed against differentiation markers like OX40 have been developed for imaging specific cell populations and are presently investigated in clinical trials. As a general T cell marker, CD3 was used to predict immune response to anti-CTLA-4 immunotherapy in a murine model of colon cancer. Therefore, ^{89}Zr-p-isothiocyanatobenzyl-deferoxamine-CD3 was applied to mice bearing colon cancer and receiving immunotherapy. Imaging was performed on day 14 and showed two groups, although tumor sizes were similar. Mice with high tracer accumulation later showed smaller tumor sizes than the low-uptake and control groups, suggesting better response

to immunotherapy (Larimer, Wehrenberg-Klee et al. 2016). CD4 and CD8, as distinction markers of the two main subpopulations, have also been used as a target for imaging with cys-diabodies and Minibodies in clinical trials. Imaging performed with labeled cys-diabodies enabled visualization of immune response and T cell distribution after application of immunotherapy in mice. Only low doses were necessary to get high-contrast PET images. Nevertheless, application of these tracer resulted in adverse effects concerning T cell functionality, such as decrease of CD4 expression, inhibition of proliferation and inhibition of INFy secretion (Tavaré, Escuin-Ordinas et al. 2016, Freise, Zettlitz et al. 2017, Seo, Tavaré et al. 2018). An anti-CD8 Minibody has completed phase I clinical trial, showing successful imaging of CD8-positive tissue and lesions of different entities but not in all entities tested. Analysis of biodistribution and pharmacokinetics favored imaging after 4h to 24h and showed quick clearance of the tracer. However, further evaluation of this tracer regarding prediction of immunotherapy success as well as reliable detection of different entities is still necessary (Pandit-Taskar, Postow et al. 2020, Farwell, Gamache et al. 2022). Another CD8-specific antibody labeled with ^{89}Zr was successfully used to visualize the body distribution of $CD8^+$ T cells in patients before and after treatment with immune checkpoint inhibitors. Analysis showed not only that expression of CD8 is highly individual but also huge heterogeneity between lesions in patients who responded and even between lesions within the same patient (Kist de Ruijter, van de Donk et al. 2022).

Most approaches, still in murine preclinical investigation, showed adverse effects on T cells or are unsuitable for imaging non-transferred T cells. Thus, imaging strategies based on labeled antigen-binding proteins or peptides should be favored as they can be applied and modified for different purposes. Current approaches that reach clinical investigation still need late imaging time points and validation for reliable detection.

1.2.3. Antigen-binding proteins

Antigen-binding proteins offer many target structures and function as highly customizable and specific vectors for different purposes. Either used as therapeutic drugs with their cytotoxic effect or as delivery agents linked to other medications and radioactive agents, monoclonal antibodies and their derivates are on the rise (Buss, Henderson et al. 2012, Scott, Wolchok and Old 2012, Carter and Rajpal 2022).

Over time, antibody engineering has become increasingly important to overcome side effects, disadvantages, and limitations of immense antibody structures, such as the most commonly used IgG, especially regarding the usage for nuclear imaging. (Kenanova and

Wu 2006, Lugat, Bailly et al. 2022). Due to its function in the immune system, immunoglobulins like IgG have high immunogenic potential and it is often even higher because of the murine or chimeric origin. As a result of the high molecular weight (~150 kDa), there are other unfavorable characteristics such as long plasma half-life and low tissue penetration capacity resulting in the need for long-lived radionuclides and longer waiting time for the ideal imaging point (Hansel, Kropshofer et al. 2010, Manafi-Farid, Ataeinia et al. 2022).

On that account, modifications and smaller constructs of antigen-binding proteins have been developed to improve their in vivo behavior towards more suitable tracers for everyday clinical practice (Kenanova and Wu 2006) (Table 1).

Table 1: Antibodies and derivates

Name	Size	Valence	Immunogenicity	PK half-life	Elimination
IgG	150 kDa	Divalent	Mouse > Chimeric > Humanized	Days to weeks	Liver
F(ab')2	110 kDa	Divalent	Low	24h	Liver
F(ab)	50 kDa	Monovalent	Low	4h	Kidney
Minibody	75 kDa	Divalent	Low	Few hours	Liver
ScFv	25 kDa	Monovalent	Low	1h	Kidney
Nanobody	15 kDa	Monovalent	Low	1h	Kidney
Affibody	<14 kDa	Monovalent	Low	<1h	Kidney

Modified from (Lugat, Bailly et al. 2022)

After reducing immunogenicity of IgG by designing chimeric and humanized constructs, $F(ab')_2$ and F(ab) fragments were developed by digestion of IgG, thereby removing the Fc fragment. In preclinical studies, these fragments showed faster uptake within the tumor region and blood clearance with subsequent lower body radiation (Kenanova and Wu 2006, Chan, Scollard et al. 2011, Kang, Li et al. 2021). Nevertheless, production of $F(ab')_2$ and F(ab) fragments is difficult and expensive due to large amounts of initial antibodies needed and cannot be gained from all antibody subtypes (Fu, Carroll et al. 2018).

In further developments, synthetically modified small proteins, like single-chain fragment variable (ScFv), were generated, leaving only an antibody's light and heavy variable chains. These modifications result in even higher tumor penetration and easy production but instability in its single form (Manafi-Farid, Ataeinia et al. 2022). Thus, multiple

combinations and further adjustments have been performed, leading to more extensive, multivalent, or bi-specific molecules, which can partly improve stability issues (Weisser and Hall 2009, Fu, Carroll et al. 2018). One of the subsequent developments is the Minibody, which consists of two ScFvs linked to a constant heavy chain (Hu, Shively et al. 1996). Designed to bypass the slow renal clearance of ScFvs, Minibodies showed excellent results in preclinical imaging studies, for example of CD8+ T cells and prostatic cancer and a successful first clinical study as mentioned above (Olafsen and Wu 2010, Knowles, Zettlitz et al. 2014, Tavaré, McCracken et al. 2014, Tsai, Zettlitz et al. 2018) (Pandit-Taskar, Postow et al. 2020).

The smallest known natural antibodies are Nanobodies and are also called single domain antibodies as they consist only of the variable domain derived from camelid heavy chain-only antibodies (VHH) (Hamers-Casterman, Atarhouch et al. 1993, Jafari, Maali et al. 2023). Their numerous advantages, such as very low molecular weight (~15kD) therefore, efficient penetration of tumor tissue, high stability, low immunogenicity, and easy, low-cost production compared to other antigen-binding proteins make them a perfect platform for development of new approaches in immunotherapy and imaging (Orcutt, Adams et al. 2017, Ingram, Schmidt and Ploegh 2018, Lecocq, De Vlaeminck et al. 2019, Verhaar, Woodham and Ploegh 2021). They have been successfully used in different preclinical settings. For example, they were already used to detect CD8+ T cells after CTLA-4 blockage in mice (Rashidian, Ingram et al. 2017). In addition, as mentioned above, first clinical trials have been completed and showed that in vivo Nanobody imaging is feasible (Keyaerts, Xavier et al. 2016). The first Nanobody-based drug, Caplacizumab, has even been approved by the European Union in 2018 and by the FDA in 2019 for treatment of acquired thrombotic thrombocytopenic purpura (aTTP) in adults. The bivalent Nanobody inhibits interaction between platelets and the von Willebrand factor and showed great outcome in the phase III HERCULES trial (Scully, Cataland et al. 2019, Peyvandi, Cataland et al. 2021).

The smallest commonly used antigen-binding proteins, so-called affibodies, are synthetical derivates from the protein A of staphylococcus aureus with an average molecular weight of 7kD (Nord, Gunneriusson et al. 1997). Although their properties seem ideal for imaging and first preclinical studies showed successful imaging, for instance, of HER2 and PDL1, reduced target-avidity and fast clearance are challenging in practice (Frejd and Kim 2017, González Trotter, Meng et al. 2017, Fu, Carroll et al. 2018, Oroujeni, Rinne et al. 2021).

2. Aim of this study

Research focusing on redirecting the immune system toward an anti-tumor activity has made significant progress over the last years. It showed promising results in preclinical studies as well as clinical trials. Nevertheless, not all patients treated with immunotherapy respond immediately, and predictive biomarkers for response are still lacking. Imaging of T cells and their activity is highly relevant to further understand their function in different stages of tumor rejection and to evaluate response patterns of T cells invading the tumor site after treatment with immunotherapies. Therefore, we developed and characterized two Nanobodies, which should function as possible tracers directed against pan-T cell markers CD2 and CD7 as a foundation for subsequent investigation of image-based biomarkers.

In cooperation with the VIB Nanobody Core in Brussels, Nanobodies targeting CD2 and CD7 have been generated. In a characterization process, two candidates have been selected for further investigation by former lab members. In the first step, characterization of Nanobodies was completed, especially regarding target specificity and thermal stability of Nanobodies, as it is crucial for later conjugation and labeling in the imaging process. Targeting T cell antigens sometimes induces overstimulation, dysfunctionality, and apoptosis, reducing anti-tumor activity. Thus, the possible impact on T cell functionality by Nanobody binding was evaluated in the second step. Co-incubation assays detecting multiple cytokines with different tumor cell lines and Nanobodies were set up to exclude possible alterations. Next, results were confirmed by an in vivo tumor rejection study in which Nanobodies were compared to $F(ab')_2$ fragments known to lead to failed tumor rejection. Lastly, a preliminary in vivo imaging study compared to previously evaluated 89Zr-aTCRmu-F(ab')2 as a control and ex vivo analysis functioned a proof-of-concept for further development.

Summarized, we aimed to characterize and evaluate the potential of new tracers for T cells, which can help gain deeper insights into tumor rejection patterns to develop biomarkers of treatment response and are more suitable for clinical practice due to rapid uptake at tumor site.

3. Material

3.1. Technical equipment

Table 2: Technical equipment

Device	Company
Analytical balance SI-64	Denver Instrument / Sartorius AG, Göttingen, Germany
Autoclave Systec V75, V150	Systec GmbH, Linden, Germany
BD FACSCanto II	BD Biosciences, Franklin Lakes, USA
BD LSR II	BD Biosciences, Franklin Lakes, USA
BioDocAnalyze Gel documentation system	Biometra GmbH, Göttingen, Germany
Biometra Mitsubishi P95 Printer	Biometra GmbH, Göttingen, Germany
BIOSAFE MD sample container	Cryotherm, Kirchen/Sieg, Germany
Centrifuge 5417R	Eppendorf AG, Hamburg, Germany
Centrifuge 5810R	Eppendorf AG, Hamburg, Germany
Centrifuge with vortex 7-0040	neoLab Migge GmbH, Heidelberg, Germany
Digital microtiter shaker MTS 2/4	IKA-Werke GmbH & CO. KG, Staufen, Germany
Dynal MPC-L Magnetic Particle Concentrator	Invitrogen Dynal AS, Oslo, Norway
EcoVac Vacuum Pump	schuett-biotec GmbH, Göttingen, Germany
Envair eco safe Comfort laminar flow	CARLO ERBA Reagents GmbH, Emmendingen, Germany
Freestanding fridge 4°C	Siemens Aktiengesellschaft, München, Germany
Fume cupboard 2-453-DXNN	Köttermann GmbH & Co KG, Uetze/Hänigsen, Germany
GABI Star γ detector	Elysia-raytest GmbH, Straubenhardt, Germany
Gamma counter 2480Wizard2	PerkinElmer, Waltham, USA
GEL iX20 Imager	Intas Science Imaging Instruments GmbH, Göttingen, Germany
Gene Pulser Xcell Electroporation System	Bio-Rad Laboratories GmbH, Hercules, USA
Glomax Discover Microplate Reader	Promega GmbH, Walldorf, Germany

Growth chamber WTC	BINDER GmbH, Tuttlingen, Germany
HERAfreeze BASIC -86°C Freezer	Thermo Fisher scientific, Waltham USA
Incubator BBD 6220	Heraeus Holding GmbH, Hanau, Germany
Incubator CB 150	BINDER GmbH, Tuttlingen, Germany
Infors HT shaker	Infors AG, Bottmingen, Switzerland
Innova 40 shaker	Eppendorf AG, Hamburg, Germany
Irradiation Cabinet	Gulmay, Byfleet, UK
LS6000 sample container	Tec-lab GmbH, Taunusstein, Germany
MACSmix Tube Rotator	Miltenyi Biotec GmbH, Bergisch Gladbach, Germany
Magnetic stirrer RH basic 2	IKA®-Werke GmbH & CO. KG, Staufen, Germay
Megafuge 1.0R	DJB Labcare Ltd, Buckinghamshire, UK
Microscope Axiovert 40 C	Carl Zeiss AG, Feldbach, Schweiz
Mini-PROTEAN Tetra Vertical Electrophoresis Cell	Bio-Rad Laboratories GmbH, Hercules, USA
Minishaker MS2	IKA®-Werke GmbH & CO. KG, Staufen, Germay
Multichannel pipets	Eppendorf AG, Hamburg, Germany
Multifuge 3 S-R	Heraeus Holding GmbH, Hanau, Germany
NALGENE Cryo 1°C Freezing Container	Thermo Fisher scientific, Waltham, USA
NanoDrop Spectrophotometer ND1000	PeqLab / VWR International GmbH, Darmstadt, Germany
Nanophotometer	Implen GmbH, Munich, Germany
nanoScan PET/MR	Mediso GmbH, Münster, Germany
Neubauer improved counting chamber	Karl Hecht GmbH & Co KG, Sondheim/Röhn, Deutschland
Pipets	Eppendorf AG, Hamburg, Germany
Pipette controller	INTEGRA Biosciences GmbH, Biebertal, Germany
PowerPac Universal Power Supply	Bio-Rad Laboratories GmbH, Hercules, USA
Precision balance 440	KERN & SOHN GmbH, Balingen, Germany
Premium -20°C Freezer	Liebherr-International Deutschland GmbH, Biberach an der Riß, Germany

Prominence HPLC system with a Photo Diode Array detector	Shimadzu, Kyoto, Japan
Refrigerator Profi line	Liebherr-International Deutschland GmbH, Biberach an der Riß, Germany
Rotina 420R	Andreas Hettich GmbH & Co.KG, Tuttlingen, Germany
SEC column Yarra 3µm SEC-3000	Phenomenex, Aschaffenburg, Germany
Sub-Cell GT horizontal gel electrophoresis cell	Bio-Rad Laboratories GmbH, Hercules, USA
TGradient	Biometra GmbH, Göttingen, Germany
Thermomixer Compact	Eppendorf AG, Hamburg, Germany
TProfessional Thermocycler	Biometra GmbH, Göttingen, Germany
Vortex Mixer 7-2020	neoLab Migge GmbH, Heidelberg, Germany
Vortexer Reax top	Heidolph Instruments GmbH & Co.KG, Schwabach, Germany
Vortex-Genie 2	Scientific Industries, Inc., New York, USA
VWR Power Source 300V	VWR International GmbH, Darmstadt, Germany
Waterbath	Memmert GmbH + Co. KG, Schwabach, Germany
Ziegra Ice machine	ZIEGRA Eismaschinen GmbH, Isernhagen, Germany

3.2. Consumables

Table 3: Consumables

Consumable	Company
Amicon Ultra – 15 Centrifugal Filter Device	Merck KGaA, Darmstadt, Germany
Cell culture flask (T25, T75, T175)	Greiner Bio-One Gmbh, Frickenhausen, Germany
Cell strainer (40, 70, 100µm)	BD bioscience, Franklin Lakes, USA
Cryopure tubes	Sarstedt AG & Co., Nümbrecht, Germany
EIA/RIA plates	Corning, New York, USA
Falcons (15ml, 50ml)	BD Biosciences, Franklin Lakes, USA

Gene PulserR Electroporation Cuvettes 0.2 cm gap	Bio-Rad Laboratories GmbH, Hercules, USA
Gloves Dermatril P	KCL GmbH, Eichenzell, Germany
Inoculating loops	VWR, Darmstadt, Germany
Microtubes (1.2 ml)	Alpha Laboratories, Hampshire, UK
Nitrile gloves	Abena A/Sm Aabenraa, Denmark
Non-tissue culture treated plates (6-/24-well)	BD Biosciences, Franklin Lakes, USA
Parafilm MR laboratory film	Pechiney Plastic Packaging, Chicago, USA
PCR reaction tubes (0.5 ml)	VWR International GmbH, Darmstadt, Germany
Petri dishes	Greiner Bio-One, Frickenhausen, Germany
Pipet tips (10/20/300/1250 µl)	Sarstedt AG & Co., Nümbrecht, Germany
Reaction tubes (1.5, 2 ml)	Sarstedt AG & Co., Nümbrecht, Germany
Round bottom flow cytometry tubes	BD bioscience, Franklin Lakes, USA
Screw Cap Micro Tubes	Sarstedt AG & Co., Nümbrecht, Germany
Sealing foil (ELISA)	Alpha Laboratories, Hampshire, UK
Serological Pipets (5 ml, 10 ml, 25 ml, 50ml)	Sarstedt AG & Co., Nümbrecht, Germany
Stericup/Steritop 0.22 µm filters	Merck KGaA, Darmstadt, Germany
Sub-Q syringes (1ml)	BD bioscience, Franklin Lakes, USA
Syringe filters (0.2, 0.45 µm)	TPP Techno Plastic Products AG, Trasadingen, Schweiz
Syringes (2ml, 5ml, 10ml, 50ml)	BD bioscience, Franklin Lakes, USA
Tissue culture-treated plates (48-well)	BD Biosciences, Franklin Lakes, USA
Tissue culture-treated plates (6-/12-/24-well, round/flat bottom 96-well)	TPP Techno Plastic Products AG, Trasadingen, Schweiz

3.3. Reagents and chemicals

Table 4: Reagents and chemicals

Reagent/chemical	Company

100bp, 1kb DNA ladder	Thermo Fisher scientific, Waltham, USA
6X loading buffer	Thermo Fisher scientific, Waltham, USA
7-Aminoactinomycin D (7-AAD)	Merck KGaA, Darmstadt, Germany
Acetic acid	Roth, Karlsruhe, Germany
Agar-Agar	Roth, Karlsruhe, Germany
Agarose	Roth, Karlsruhe, Germany
Ampicillin	Merck KGaA, Darmstadt, Germany
Bacto Tryptone	BD Biosciences, Franklin Lakes, USA
Bacto Yeast Extract	BD Biosciences, Franklin Lakes, USA
Bovine serum albumin	Merck KGaA, Darmstadt, Germany
Brilliant blue R 250	Roth, Karlsruhe, Germany
DEPC-H_2O	Thermo Fisher scientific, Waltham, USA
Desferrioxamine	Macrocyclics, Inc, Dallas, USA
DMEM	Thermo Fisher scientific, Waltham, USA
DMSO	Merck, KGaA, Darmstadt, Germany
EDTA	Thermo Fisher scientific, Waltham, USA
Ethanol	Merck KGaA, Darmstadt, Germany
Fetal bovine serum	Thermo Fisher scientific, Waltham, USA
Ficoll-Paque	Cytiva, Marlborough, USA
Gentamycin	Thermo Fisher scientific, Waltham, USA
Glucose	Roth, Karlsruhe, Germany
Glycerol	Merck KGaA, Darmstadt, Germany
HEPES	Thermo Fisher scientific, Waltham, USA
Human serum (HS)	Technische Universität München, Germany
Isofluran	CP Pharma, Burgendorf, Germany
Isopropanol	Merck KGaA, Darmstadt, Germany

LDS Sample Buffer (4X)	Thermo Fisher scientific, Waltham, USA
L-Glutamine	Thermo Fisher scientific, Waltham, USA
Lipofectamine CRISPRMAX	Thermo Fisher scientific, Waltham, USA
Methanol	Roth, Karlsruhe, Germany
$MgCl_2$	Roth, Karlsruhe, Germany
NaCl	Roth, Karlsruhe, Germany
Non-essential amino acids	Thermo Fisher scientific, Waltham, USA
Opti-MEM I	Thermo Fisher scientific, Waltham, USA
PageRuler Prestained Protein Ladder	Thermo Fisher scientific, Waltham, USA
Paraformaldehyde (PFA)	Merck KGaA, Darmstadt, Germany
PBS	Thermo Fisher scientific, Waltham, USA
PBS powder	Merck KGaA, Darmstadt, Germany
Penicilline/Streptomycine	Thermo Fisher scientific, Waltham, USA
Protamine sulfate	MP Biomedicals, Illkirch, France
Restriction enzymes	New England Biolabs, Ipewich, UK
RetroNectin	Takara Bio, Japan
RPMI 1640	Thermo Fisher scientific, Waltham, USA
S.O.C. Medium	New England Biolabs, Ipewich, UK
Skim milk powder	Merck KGaA, Darmstadt, Germany
Sodium carbonate (Na_2CO_3)	Merck KGaA, Darmstadt, Germany
Sodium hydrogen carbonate ($NaHCO_3$)	Merck KGaA, Darmstadt, Germany
Sodium pyruvate	Thermo Fisher scientific, Waltham, USA
Sucrose	Roth, Karlsruhe, Germany
Sulfuric acid (1M)	Roth, Karlsruhe, Germany
SYBR Safe	Thermo Fisher scientific, Waltham, USA
Terrific Broth medium	Thermo Fisher scientific, Waltham, USA

TransIT transfection reagent	Mirus Bio LLC, Madison, USA
Trypane blue	Thermo Fisher scientific, Waltham, USA
Trypsine EDTA (0.5%)	Thermo Fisher scientific, Waltham, USA
Tween 20	Merck KGaA, Darmstadt, Germany
Zombie Green, Zombie Yellow	BioLegend, San Diego, USA

3.4. Kits

Table 5: Kits

Reagent	Company
Alt-R Genome Editing Detection Kit	Integrated DNA Technologies, Coralville, USA
Alt-R HPRT PCR Primer Mix, Human, 2nmol	Integrated DNA Technologies, Coralville, USA
BD OptEIA Human GM-GSF ELISA Set	BD Biosciences, Franklin Lakes, USA
BD OptEIA Human IL-2 ELISA Set	BD Biosciences, Franklin Lakes, USA
BD OptEIA Human IL-6 ELISA Set	BD Biosciences, Franklin Lakes, USA
BD OptEIA Human INFy ELISA Set	BD Biosciences, Franklin Lakes, USA
BD OptEIA TMB Substrate Reagent Set	BD Biosciences, Franklin Lakes, USA
DNA blood and tissue kit	QIAGEN GmbH, Hilden, Germany
DreamTaq Green PCR Master Mix (2X)	Thermo Fisher scientific, Waltham, USA
Dynabeads Human T-Activator CD3/CD28	Thermo Fisher scientific, Waltham, USA
Dynabeads Untouched Human CD8 T Cells Kit	Thermo Fisher scientific, Waltham, USA
FOXP3 Fix/Perm buffer set	BioLegend, San Diego, USA
HisPur Ni-NTA Spin Purification Kit, 3ml	Thermo Fisher scientific, Waltham, USA
NEB 5-alpha Competent E.coli	New England Biolabs, Ipewich, UK
NucleoBond Xtra Maxi EF	MACHEREY-NAGEL GmbH & Co. KG, Düren, Germany

Nucleospin Gel and PCR Cleanup kit	MACHEREY-NAGEL GmbH & Co. KG, Düren, Germany
NucleoSpin Plasmid EasyPure	MACHEREY-NAGEL GmbH & Co. KG, Düren, Germany
PlasmoTest Mycoplasma Detection Kit	InvivoGen, Toulouse, France
Quick Ligation Kit	New England Biolabs, Ipewich, UK

3.5. Buffers

Table 6: Buffers

Buffer	Ingredients	Application
25 mM wash buffer	PBS + 25mM imidazole	Nanobody purification
50 mM wash buffer	PBS + 50mM imidazole	Nanobody purification
Blocking buffer	PBS + 1% (w/v) skim milk powder	ELISA
Coating buffer	100mM $NaHCO_3$ and 30mM Na_2CO_3 in H_2O, pH 9.5	ELISA
Coomassie solution	1g/l Brilliant blue, 50% ethanol, 10 % acetic acid in H_2O	SDS-PAGE
Destain buffer	50% methanol, 10 % acetic acid in H_2O	SDS-PAGE
Elution buffer	PBS + 250mM imidazole	Nanobody purification
Equilibration buffer	PBS + 10mM imidazole	Nanobody purification
FACS buffer	PBS + 1% ΔFCS	Flow Cytometry
Fix solution	PBS + 25% FOXP3 Fix/Perm buffer (4X)	Intracellular staining
IDTE buffer	10 mM Tris, 0.1 mM EDTA in H_2O	RNP production
Isolation buffer	PBS + 2 % ΔFCS, 2mM EDTA	T cell isolation
MES buffer (1X)	H_2O + 5% MES SDS Running Buffer (20X) (Thermo Fisher scientific)	SDS-PAGE
Perm buffer	PBS + 10% FOXP3 Perm buffer 10X (BioLegend)	Intracellular staining
TAE buffer (1X)	H2O + 10% TAE buffer 10X (Thermo Fisher scientific)	Gel electrophoresis

TES buffer	0.2M Tris, 0.5 mM EDTA, 0.5M sucrose in H_2O, pH 8.0	Nanobody purification
Washing buffer	PBS + 0.05% (v/v) Tween 20	ELISA
ΔFCS	FCS, heat-inactivated for 20 min at 58°C	various
ΔHS	HS, heat-inactivated for 20 min at 58°C	various

3.6. Media

Table 7: Media

Medium	Ingredients
cDMEM	DMEM supplemented with 10% ΔFCS, 100 U/ml Penicilline/Streptomycine
cRPMI	RPMI supplemented with 10% ΔFCS, 2 mM L-Glutamine, 100 U/ml Penicilline/Streptomycine, 1mM sodium pyruvate, 10 mM non-essential amino acids
Freezing medium	ΔFCS supplemented with 10% DMSO
LB medium	10g/l Bacto-Tryptone, 5g/l Bacto-Yeast extract, 10g/l NaCl and optional 20g/l Agar-Agar for Agar plates dissolved in H_2O and autoclaved
OptiMEM	OptiMEM (Thermo Fisher scientific), no supplements
S.O.C. medium	S.O.C. medium (New England Biolabs), no supplements
T cell medium (TCM)	RPMI supplemented with 5% ΔFCS, 5% ΔHS, 10 mM HEPES, 2mM L-Glutamine, 1mM sodium pyruvate, 10mM non-essential amino acids, 100 U/ml Penicilline/Streptomycine, 16µg/ml Gentamycine
Terrific broth medium (TB medium)	Terrific broth (Thermo Fisher scientific) supplemented with 2 nM $MgCl_2$, 0.1% Glucose

3.7. Cytokines

Table 8: Cytokines

Cytokine	Company
IL-2, Human	PeproTech, London, UK

IL-7, Human	PeproTech, London, UK
IL-15, Human	PeproTech, London, UK

3.8. Antibodies

Table 9: Antibodies

Target	Clone	Fluorophore	Company/Origin
Polyhistidine-tag	AD1.1.10	AF 647	Bio-Rad Laboratories GmbH, Hercules, USA
Human CD2	HIK27	unconjugated	
Human CD2	RPA-2.10, OKT11	PE, APC and unconjugated	BioLegend, San Diego, USA
Human CD2	Nanobody 10563 (Nb 563)	unconjugated	VIB Nanobody Core, Brussels, Belgium
Human CD3	UCHT1	V500, APC	BD Biosciences, Franklin Lakes, USA
Human CD4	SK3	V450	BD Biosciences, Franklin Lakes, USA
Human CD7	M-T701	PerCP-Cy5.5.	BD Biosciences, Franklin Lakes, USA
Human CD7	Nanobody 10215 (Nb 215)	unconjugated	VIB Nanobody Core, Brussels, Belgium
Human CD8	SK1	BV605, PE	BioLegend, San Diego, USA
Human HLA-B7	BB7.1	APC	Novus Biologicals, Centennial, USA
Isotype control	MOPC-21, G155-228	FITC, PE, V450, BV605, APC, PerCP-Cy5.5.	BD Biosciences, Franklin Lakes, USA
Isotype control	Control Nanobody	unconjugated	VIB Nanobody Core, Brussels, Belgium
MPO	5B8	FITC	BD Biosciences, Franklin Lakes, USA
Murine TCR (TCRmu)	H57-597	FITC and unconjugated	BD Biosciences, Franklin Lakes, USA

3.9. Vektors, primers and crRNAs

Table 10: Vektors

Vektor	Description
pMP71	Retroviral vector with Ampicillin resistance, containing MPSV-LTR promoter and PRE element from woodchuck Hepatitis Virus (Engels, Cam et al. 2003).

Primers were dissolved to a concentration of 100µM in DEPC-H_2O and were ordered at Eurofins Genomics, Ebersberg, Germany.

Table 11: Primers

Primer	Sequence	Purpose
MP71 FWD	5'-TGAAAATTAGCTCGACAAAG-3'	Sequencing of MP71 insert
MP71 REV	5'-GTAAATGATTGCCCCACCA-3'	Sequencing of MP71 insert
CD2 FWD	5'-TCAGAATCAAAAGAGGAAACCAAC-3'	PCR and Sequencing of edited CD2 locus
CD2 REV	5'-ATAGCACCCACACTGAAATAAAGC-3'	PCR and Sequencing of edited CD2 locus

The crRNAs and related tracrRNA were purchased from Integrated DNA Technologies, Coralville, USA.

Table 12: Sequences of crRNAs

crRNA	Sequence
CD2-M	5'-CAAGGCAUUCGUAAUCUCUUGUUUUAGAGCUAUGCU-3'
CD2-N	5'-CUUGGGUCAGGACAUCAACUGUUUUAGAGCUAUGCU-3'
CD2-O	5'-ACGAAUGCCUUGGAAACCUGGUUUUAGAGCUAUGCU-3'

3.10. Cell lines

Table 13: Cell lines

Cell line	Characteristics	Origin
293Vec-RD114	Retroviral packaging cell line based on HEK 293	BioVec Pharma inc., Québec, Canada
Jurkat E6.1	Human acute T cell leukemia	AG Ruland, Technische Universität München, Germany
ML2	Human acute myelomonocytic leukemia	The Cabri consortium
ML2-B15	ML2, transduced with HLA-B*15:01-P2A-GFP	Retrovirally transduced by former lab members
ML2-B7	ML2, transduced with HLA-B*07:02-P2A-eGFP	Retrovirally transduced by former lab members
NB4	Human acute promyelocytic leukemia	CLS, Eppelheim, Germany
NB4-B15	NB4, transduced with HLA-B*15:01-P2A-GFP	Retrovirally transduced by former lab members
NB4-B7	NB4, transduced with HLA-B*07:02-P2A-eGFP	Retrovirally transduced by former lab members
U698M	Human B cell lymphoma	DSMZ, Braunschweig, Germany
U698M-CD2	U698M, transduced with human CD2-P2A-DsRed	Retrovirally transduced by former lab members

3.11. Software and webtools

Table 14: Software

Software	Company
Microsoft Office 365	Microsoft Corporation, Redmond, USA
FlowJo v10.7.1	Tree Star, Ashland, USA
Graphpad Prism v7	GraphPad Software, Inc., La Jolla, USA
SerialCloner v2.6	Freeware

EndNote X20	Thomson Reuters, New York City, USA

Table 15: Web-based tools

Tool	Homepage
BLAST – Basic Local Alignment Search Tool	https://blast.ncbi.nlm.nih.gov/Blast.cgi
CHOPCHOP	https://chopchop.cbu.uib.no (Labun, Montague et al. 2019)

4. Methods

All centrifugation steps were performed for 5 min at 500g if not indicated differently.

4.1. Molecular biology

4.1.1. Gel electrophoresis

1-2% agarose gels were prepared by melting the respective amount of agarose in 1x TAE buffer. SYBR Safe stain was added to the solution (c_{END} = 1µl/ml) after agarose was completely dissolved. For hardening, the solution was poured into a tray with proper combs. Samples were prepared by adding 6x loading buffer before loading them on the solid gel. Also, 7µl of appropriate DNA ladder was loaded on the gel. The gel was run for 30-60 min at 100V in 1X TAE buffer.

4.1.2. Purification of DNA fragments

Gel was checked for appropriate fragments, which were cut out and purified using NucleoSpin Gel and PCR clean-up Kit as stated in manufacturer's instructions. DNA was eluted with 20µl of DEPC-H_2O, followed by checking the concentration on the NanoDrop ND-1000.

4.1.3. Restriction digest

For cloning purposes, backbone vector and the purified DNA fragment of interest were digested with the restriction enzymes NotI and SalI. The following amounts in the table (Table 17) were used for the set-up.

Table 16: Reaction mix for restriction digest

Component	Volume / Amount
DNA	1µg
10x CutSmart buffer	5µl
NotI	1µl (10 units)
SalI	1µl (10 units)
DEPC-H_2O	to 50µl

The mix was incubated for 2 h at 37°C. After digestion, backbone was separated by gel electrophoresis (4.1.1) and purified as described above (4.1.2).

4.1.4. Ligation of DNA fragments

The purified DNA fragments from restriction digestion were ligated with the backbone vector in a 3:1 ratio using Quick ligase in the following reaction mixture.

Table 17: Reaction mix for ligation

Component	Volume / Amount
Backbone vector	0.05pmol
Insert DNA	0.15pmol
Quick Ligase reaction buffer (2x)	10µl
Quick Ligase	1µl
DEPC-H_2O	to 20µl

For calculation of molar ratios, the ensuing approximation formula was used.

$$\boldsymbol{n\big(DNA\ (mol)\big) = \frac{m(DNA\ (g))}{length\ of\ DNA\ (bp) \times \frac{618\ g}{mol \times bp} + 36\frac{g}{mol}}}$$

The mix was incubated for 5 minutes at room temperature and then used for subsequent transformation or stored at -20°C for later use.

4.1.5. Chemical transformation of E.coli

For transformation of vectors, chemically competent E.coli (NEB5α) were used. Therefore, bacteria were thawed on ice, and 2µl of the ligation mixture were directly added to 25µl of bacteria and incubated for 30 minutes on ice after pipetting up and down. The suspension was heat shocked at 42°C for 30 seconds, and then 475µl of SOC media was added to the tube. After shaking the bacteria for 60 minutes at 37°C, 100µl of the mixture were spread on prewarmed agar plates with Ampicillin (c_{END} = 100µg/ml) and incubated overnight at 37°C.

4.1.6. Plasmid purification from bacterial culture

Single colonies of previously transformed and plated E.coli were picked and transferred to 3ml of LB-medium containing Ampicillin (c_{END} = 100µg/ml). After overnight culture at 37°C in a shaker, 2ml of bacterial culture were purified using NucleoSpin Plasmid EasyPure (Macherey-Nagel) as stated in manufacturer's instructions. Gel electrophoresis was used for analysis of purified vectors. Vectors with correct length were then sent for Sanger sequencing. When large-scale amplification was needed, re-

transformation was performed with vectors containing the confirmed sequence as described above (4.1.5). Single colonies were picked and inoculated in 300ml of LB-medium overnight. Vector was purified from culture using NucleoBond Xtra Maxi EF (Macherey-Nagel) according to manufacturer's recommendations.

4.1.7. Polymerase chain reaction (PCR)

Amplification of gene sections was performed with DreamTaq Green PCR Master Mix 2X (Thermo Fisher scientific).

Table 18: Reaction mix for PCR

Component	Volume / Amount
DreamTaq Green PCR Master Mix (2X)	25µl
Forward primer (10µM)	1µl
Reverse primer (10µM)	1µl
DNA template	100ng
DEPC-H_2O	to 50µl

Reaction mix was set up as described in the table above and transferred into 0.5ml PCR tubes. Polymerization was performed in a T-Gradient Thermocycler with the following settings depending on the individual primer melting temperature (T_M).

Table 19: Thermocycler settings for PCR

Step	Temperature	Time	Number of cycles
Initial Denaturation	95°C	1min	1
Denaturation	95°C	30s	30
Annealing	T_M-5°C	30s	
Extension	72°C	1min	
Final extension	72°C	5min	1

4.1.8. Isolation of genomic DNA

For Isolation, approximately 2 million cells were harvested and washed with PBS. The extraction was performed using DNA blood and tissue kit (Qiagen) as stated in manufacturer's instructions. For Elution, 50µl of DEPC-H2O was used, and concentration was determined on NanoDrop ND-1000.

4.2. Cell culture

Cell culture work was performed under sterile conditions and regularly checked for mycoplasma contamination using PlasmoTest Mycoplasma Detection Kit according to manufacturer's recommendations.

4.2.1. Cultivation of cell lines

For cultivating suspension cell lines, cRPMI was used, and cDMEM was used for adherent cell lines. Every 3 to 4 days, cells were split regularly unless color of medium signaled change in pH and depleted medium. For splitting adherent cell lines, cells were washed once with PBS and incubated with Trypsine/EDTA for 4-5 minutes at 37°C. Cells were then resuspended with additional medium and centrifuged. After discarding the supernatant, cells were resuspended in respective medium. RD114, as semi-adherent cell line, was mechanically detached either by clapping the flask or by rinsing the bottom multiple times with medium.

4.2.2. Counting of cells

Cells were counted weekly in a Neubauer chamber. Before counting, cells were checked in the flask under the light microscope. For counting, 20µl of cell suspension was mixed with 80µl of Trypane blue solution and carefully pipetted on the Neubauer chamber. Each corner was counted under the light microscope, and cell density was calculated using the following formula:

$$C_{cells}\left(\frac{cells}{ml}\right) = \frac{(number\ of\ counted\ cells)}{4} \times 5\ (dilution\ factor) \times 10000$$

4.2.3. Freezing and thawing of cells

Before freezing, cells were checked for good viability. Afterwards, cells were centrifuged and resuspended in 1ml of freezing medium. Cell suspension was then transferred to a cryovial and placed in a freezing container containing isopropyl alcohol. After keeping them overnight at -80°C, cryovials were transferred in liquid nitrogen to provide high recovery under long-term storage.

Frozen cell suspensions were quickly thawed in the cryovials using a water bath at 37°C. When cell suspension was melted, it was transferred into 10ml of medium. After centrifugation and discarding the supernatant, cells were resuspended in appropriate medium.

4.2.4. Isolation of primary cells

For purification of peripheral blood mononuclear cells (PBMC), blood was drawn from healthy donors according to safety and ethical requirements from local authorities. Syringes were previously prepared with EDTA for anticoagulation of blood. The PBMC were isolated by density gradient centrifugation. Thus, the blood was diluted 1:1 with RPMI and carefully overlaid on 15ml of Ficoll solution in a 50ml falcon. Any disturbance of the two layers was avoided. The leukocyte interphase was delicately collected after a centrifugation step for 25 minutes with no brake at 880g. Cells were washed twice with RPMI to remove residual Ficoll and used for subsequent experiments.

4.3. Gene transfer and gene editing techniques

Safety regulations according to S2 guidelines were respected during gene transfer and gene editing.

4.3.1. Isolation of untouched CD8+ T cells

The isolation was done by negative selection of CD8+ cells with the Dynabeads Untouched Human CD8 T cell Kit (Thermo Fisher) according to manufacturer's recommendations. Therefore, 1 x 10^8 PBMC were resuspended in 1ml of isolation buffer. After adding 200µl of FBS and antibody mix each, the cells were incubated in the fridge for 20 min at 4°C. Then the cells were washed once and centrifuged for 8 min at 350g. After the supernatant had been discarded, the cells were resuspended in 1ml of isolation buffer and 1ml of Dynabeads, which had been washed previously according to manufacturer's recommendations. The cells were then incubated on a rotator for 15 min at room temperature. 8ml of isolation buffer was added to the cell suspension and mixed gently by pipetting up and down several times. The tube containing the cell suspension was placed in a magnet for 2 min until all of the cell-bound Dynabeads were attached to the wall of the tube. The supernatant with the CD8+ cells was transferred to a new tube, and the residual beads were resuspended in 8ml of isolation buffer for a second round of separation in the magnet. Both supernatants, including the CD8+ T cells, were combined and used for downstream applications.

4.3.2. Activation of CD8+ T cells

Freshly isolated CD8+ T cells were seeded at 1 x 10^6 cells/ml in TCM. CD3/CD28 beads (Thermo Fisher) were used for activation after being washed according to manufacturer's recommendations and resuspended in TCM. Thus, 25µl of beads per 1 x 10^6 cells were mixed with the cell suspension, and hIL-2 was added to a concentration of 30 U/ml. After

incubating for 2 to 3 days in a flask at 37°C, suspension was mixed thoroughly, and beads were removed via magnetic separation. Cells were then used for retroviral transduction.

4.3.3. Production of retroviral particles

RD114, as a packaging cell line, was used to synthesize the retrovirus. 75 x 10^4 cells were seeded in a treated 6-well plate in 3 ml cDMEM. The confluency was checked under the light microscope after 3 days and aimed at roughly 60%. For the transfection, 3µl of the transfection reagent TransIT was added to 200µl of DMEM and incubated for 20 minutes at room temperature. Afterwards, 1µg of the retroviral plasmid with the gene of interest was added. The solution was mixed carefully and incubated at room temperature for 30 min. The medium of the RD114 was changed without letting the cells detach, and then the transfection solution was added dropwise on the adherent cells and incubated at 37°C for at least 2 days.

4.3.4. Transduction of CD8+ T cells and cell lines

RetroNectin-coated 24-well plates were used for the transduction as an enhancer of gene transfer. The final concentration of RetroNectin was 12,5µg/ml, of which 400 µl were added to each well for coating non-tissue culture treated 24-well plates. After sealing plates with Parafilm, they were incubated overnight at 4°C. RetroNectin solution was removed, and the plates were blocked with 500µl of filtered PBS + 2% BSA at 37°C for 30 min. For washing of plates, PBS with 2.5% of HEPES was used. After 2 steps of washing with 1ml of the solution, the plates were sealed and stored at 4°C until needed for transduction.

1ml of supernatant containing the retrovirus per 1 Mio of cells was carefully harvested as the remaining supernatant was used for a second round of transduction. After filtering through a 0.45 µm filter, the supernatant was supplemented with HEPES (c_{END} = 5mM), hIL-2 (c_{END} = 100 U/ml), and Protamine sulfate (c_{END} = 4 µg/ml). These concentrations refer to the final volume V_{END} = 2ml/well. 1ml of activated CD8+ T cells (see above 4.3.2) with 1 x 10^6 cells/ml density with 1ml of supplemented retroviral supernatant were added to the RetroNectin-coated plates. Plates were then centrifuged at 820g and at 32°C for 90 minutes without break.

Plates were incubated overnight at 37°C. Cells were harvested, washed, and split into two wells of a new coated plate. Retroviral supernatant was prepared similarly as described for round one and was added to the cells. Transduction was equally

performed. After overnight incubation, cells were harvested from wells, centrifuged, and expanded in TCM, supplemented with hIL-7 and hIL-15, each diluted to a final concentration of 5ng/ml.

Transduction was performed similarly for suspension cell lines. As indicated, 1 million of cells were seeded in a 24-well plate coated with RetroNectin in 1ml of cRPMI supplemented with HEPES and Protamine sulfate.

4.3.5. Preparation of ribonucleoproteins (RNP) for CRISPR/Cas9 knockout

Preparation and transfection methods are based on manufacturer's instructions. Therefore, crRNA and tracrRNA were resuspended and diluted in IDTE buffer to a final concentration of 200µM. gRNA was produced by mixing crRNA and tracrRNA in an equimolar ratio to a duplex concentration of 100µM. Mixture was incubated for 5 min at 95°C and was then allowed to cool down at room temperature. According to the following table, previously produced gRNA was mixed with Cas9 enzyme in PBS to form the ribonucleoprotein complex.

Table 20: Reaction mix for RNP complex

Component	Volume / Amount
gRNA (100µM)	12µl
Cas9 enzyme (62µM)	16.7µl
PBS	to 50µl

After incubation for 20 minutes at room temperature, complex was kept on ice until use.

4.3.6. Electroporation of Jurkat E6.1 cells

1 million cells for each electroporation were washed twice with PBS, resuspended in 75µl of PBS, and kept on ice. 20µl of RNP complex (see 4.3.5) were mixed with the cell suspension and immediately transferred to pre-cooled cuvettes. Electroporation was performed with a single pulse at 250V and 2ms of pulse width. Cells were transferred into 2ml of cRPMI medium in a 12-well tissue culture plate and checked for knockout rates after 3 days.

4.3.7. Lipofection of Jurkat E6.1 cells

Lipofectamine CRISPRMAX Cas9 Transfection Reagent (Thermo Fisher scientific) was used for lipofection. 3 different gRNAs were used for preparation of RNPs. The preformed RNP complexes (4.3.5) were diluted with IDTE buffer in a ratio of 1:20. For

lipofection RNPs were used in the transfection mix according to the following table for each well.

Table 21: RNP mixture for lipofection

Component	Volume / Amount
RNP	1.5µl each
Cas9 PLUS Reagent	0.6µl
Opti-MEM media	to 25µl

Mix was incubated for 5 min at room temperature. 1.2µl of CRISPRMAX transfection reagent was diluted in 23.8µl of Opti-MEM media and combined with the RNP mixture (Table 6). Transfection complex was then incubated for 20 min at room temperature, and 50µl of transfection complex were added into each well in a 96-well plate. Cells were diluted in cRPMI to a concentration of 0.4 x 10^6 cells/ml, then 100µl of cell suspension were added to transfection complex in the 96-well plate. After 2 days of incubation, cells were checked for knockout rates.

4.3.8. T7EI endonuclease assay

T7EI endonuclease assay was performed using Alt-R Genome Editing Detection Kit (Integrated DNA Technologies) to detect on-target genome editing events according to manufacturer's instructions. Genomic DNA of transfected cells (see 4.3.7. and 4.3.8) was isolated as described in section 4.1.8. and the region of interest was amplified via PCR (4.1.7.). Reaction mix for forming heteroduplexes was set up according to the following table.

Table 22: Reaction mix for heteroduplex formation

Component	Volume / Amount
PCR product	10µl
T7EI Reaction Buffer (10X)	2µl
DEPC-H_2O	6µl

Formation was then performed in a thermocycler using a ramp protocol following the settings in the table (Table 23).

Table 23: Thermocycler settings for heteroduplex formation

Step	Temperature	Time	Ramp rates
Denaturation	95°C	10min	-
Ramp 1	95°C-85°C	-	-2°C/s
Ramp 2	85°C-25°C	-	-0.3°C/s

Heteroduplexes were mixed with 2µl of T7 endonuclease I (c= 1U/µl) and incubated for 60 min at 37°C. Digested products were analyzed by gel electrophoresis (4.1.1.).

4.3.9. Generation of stable cell lines by limiting dilution

After gene editing or transduction, stable cell lines containing the desired modifications were generated by limiting dilution. Thus, cells were diluted to a final concentration of 2.5 cells/ml in appropriate medium, and 200µl of cell suspension per well were transferred to a 96-well U-bottom plate. Cells were regularly checked under light microscope for proliferation, and clones were harvested after 10 to 14 days. Clones were checked for modifications by flow cytometry analysis and Sanger sequencing after PCR amplification (4.1.7.) of genomic DNA.

4.4. Flow Cytometry techniques

LSRII or BD FACSCanto II (BD Bioscience) was used for sample acquisition. Analysis of data was done using FlowJo software (TreeStar).

4.4.1. Staining of surface markers

0.2 to 0.5 million cells were washed and resuspended in FACS buffer. For staining, 1µl of each antibody was added to samples, as well as 0.5µl of 7AAD (c_{END}= 0.5 mg/ml) when separation of dead cells was wished. After 20 min of incubation at 4°C, cells were washed with FACS buffer and stored at 4°C in the dark until use.

4.4.2. Staining of CD2 and CD7 with Nanobodies

For staining, 0.5 million cells were washed and resuspended in FACS buffer. Then respective Nanobody was added (c_{END}= 10 µg/ml) to the suspension. The cells were incubated for 60 minutes at 4°C, washed 3 times, and resuspended in FACS buffer. 1µl of histidine-tag antibody was added and incubated for 60 minutes in the dark at 4°C. After washing the cells, samples were kept at 4°C until analysis.

4.4.3. Intracellular staining

The FOXP3 Fix/Perm buffer set (Biolegend) was used to stain the intracellular marker myeloperoxidase for quantification of its expression. Therefore, Fix solution and Perm buffer were prepared according to manufacturer's recommendations. Before the intracellular staining, staining of surface molecules was done if needed. Cells were then resuspended in 200µl of Fix solution and incubated for 45 minutes in the dark at room temperature. After two steps of washing using 200µl of Perm buffer for each step, 1µl of antibody was added to cells and incubated for 40 minutes in the dark at room temperature. Cells were washed with Perm buffer, resuspended in FACS buffer, and kept at 4°C in the dark until acquisition.

4.4.4. Evaluating thermal stability of Nanobodies

Nanobodies were tested for heat resistance by incubating them at different temperatures for several periods, followed by analysis of residual binding capacity using Flow Cytometry. Thus, Nanobody was incubated at 37°C, 60°C, and 90°C for 0.5h, 1h, 2h, 4h, and 6h. Nanobody kept at 4°C, was used as a reference. After incubation, Nanobody was held at 4°C until used for staining. 0,2 million of Jurkat E6.1 per well were washed and seeded in a 96-well plate using FACS buffer. Then Nanobody was added to the cell suspension (c_{END} = 5nM) and incubated for 60 min at 4°C. Cells were washed 3 times with FACS buffer. Afterwards, 1µl of histidine-tag antibody was added into each well. After incubation for 60 minutes at 4°C in the dark, cells were washed and resuspended in FACS buffer for analysis by Flow Cytometry.

4.4.5. Specificity analysis via epitope blocking

Nanobody 563 was checked for target specificity by epitope blocking. Therefore, CD8+ T cells were washed and incubated with different CD2-specific antibodies for 60 minutes at 4°C. After washing, the different conditions were stained with Nanobody 563 as described above and analyzed in Flow Cytometer.

4.5. Analysis of T cell functionality

4.5.1. Co-incubation of tumor and T cells

CD8+ T cells were transduced with respective TCR as described above (4.3.4). 20,000 T cells were cocultured with tumor cells in a 96-well round bottom plate with an effector to target ratio of 1:1 and 3:1 in 200µl of TCM in triplicates. After 4h or 24h of co-incubation, plates were centrifuged, and 150µl of supernatant was harvested without

disturbing the pellet. Supernatant was either used for immediate analysis or frozen at -20°C for later use.

4.5.2. Determination of cytokine levels by ELISA

Previously harvested supernatant from coculture (4.5.1) was used to analyze cytokine levels. BD OptEIA Human IFN-γ, GM-CSF, IL-2, or IL-6 Elisa Set (BD Bioscience) were used according to manufacturer's recommendations with slight adjustments. ELISA plates were coated with respective capture antibody in a 1:250 dilution with Coating buffer. After incubation overnight at 4°C, plates were washed 3 times with washing buffer, and blocking buffer was added, followed by 1h of incubation at room temperature. Plates were washed 3 times, then 50µl of supernatant in an appropriate dilution, and 50 µl of standard solutions were added to each plate. For standards, a starting solution with a concentration of 1000 pg/ml in TCM was prepared, and a serial 1:1 dilution was performed until a final concentration of 31.25 pg/ml was reached. Also, a blank control was set. Plates were incubated for 1h at room temperature and then washed 5 times before detection antibody and enzyme conjugate were added in a 1:250 dilution in blocking buffer. After incubation for 1h at room temperature, plates were washed 7 times. Solutions from BD OptEIA TMB Substrate Reagent Set (BD Biosciences) were mixed in equal amounts, and 100µl per well were added to plates, followed by incubation for 15 to 30 minutes at room temperature in the dark. Substrate reaction was ended by adding 50µl of sulfuric acid when standard dilutions were entirely visible. Glomax Discover Microplate Reader was used at 450nm with 560nm as a reference for readout.

4.6. Production, purification, and labeling of Nanobodies

4.6.1. SDS-PAGE

For evaluation of protein purity, SDS-PAGE was performed using NuPAGE Bis-Tris Mini Gel (Thermo Fisher scientific). Electrophoresis cell was set up with gel and filled with 1X MES buffer. 30µl of each sample was mixed with 10µl of 4X Dye Agent and incubated for 5 min at 95°C. Then 20µl of sample mix and 7µl of prestained protein ladder were loaded into the gel pockets. After running for 30min at 200V, gel was stained for 1h in Coomassie solution. Gel was then kept in Destaining buffer overnight and scanned the next day.

4.6.2. Production of Nanobodies in bacterial culture

Nanobody 10215 and 10563 sequences containing a polyhistidine-tag were cloned into pHEN6c vector and transformed into WK6 E.coli strain by previous lab members.

Respective glycerol stocks were used for preparing bacterial culture. Therefore, bacteria were scraped carefully with a pipette tip from glycerol stock and spread on agar plates with ampicillin (c_{END} = 100µg/ml) and 1% glucose. Plates were incubated overnight at 37°C. Then a single colony was picked and transferred into 10ml of LB medium with ampicillin (c_{END} = 100µg/ml) and 1% glucose. Pre-culture was incubated overnight at 37°C and 250rpm. TB medium was supplemented with Ampicillin (c_{END} = 100µg/ml) for large-scale culture. 660ml of supplemented TB medium was added to a 2l baffled shaker flask and mixed with 2ml of the pre-culture. Culture was shaken at 37°C and 250rpm until OD_{600} was between 0.6 and 0.9. Then expression of Nanobody was induced by adding IPTG (c_{END} = 1mM). Culture was incubated overnight in a shaker at 28°C and 250 rpm until OD_{600} was between 25 and 30.

For extraction of Nanobody from periplasm, culture was centrifuged for 8min at 800g, and the supernatant was discarded. The pellet from 200ml of culture was then resuspended with 8ml of TES and shaken on ice for 1h. 12ml of TES diluted in a 1:4 ratio with DEPC-H_2O was added to the solution. After shaking for 1h on ice, solution was centrifuged at 4000g for 30min at 4°C, and the clear supernatant was carefully removed. The supernatant was used immediately for his-tag purification or frozen at -20°C.

4.6.3. His-tag purification of Nanobodies

For purification of Nanobodies HisPur Ni-NTA Kit, 3ml (Thermo Fisher scientific) was used following the manufacturer's recommendations with minor modifications. Briefly, necessary buffers (Equilibration buffer, 25mM and 50mM Wash buffer, and Elution buffer) were prepared by diluting Imidazole in PBS to different concentrations. Columns were centrifuged to remove storage buffer and then primed by adding 6ml of equilibration buffer. After centrifugation, supernatant from bacterial culture (see 4.1.10) was added to columns and incubated for 30 mins at 4°C on a rotator. Columns were centrifuged and then washed 3 times. Every washing step was performed with 6ml of Wash buffer, and columns were centrifuged after every step. The first 2 washing steps were performed with 25mM Wash buffer and the last with 50mM Wash buffer. Afterwards, Nanobodies were eluted from resin by adding 3ml of Elution buffer and centrifugation of columns. This step was repeated 3 more times, keeping each flowthrough fraction in a separate tube. Purity was analyzed via SDS-PAGE as described above (4.1.9), and SE-HPLC was kindly done by our partner Dr. Lisa Russeli from nuclear medicine.

4.6.4. Concentration and buffer exchange

When purity of each elution fraction was confirmed, fractions were pooled. Amicon Ultra – 15 Centrifugal Filter Device (Merck) was used for concentration and buffer exchange of Nanobodies according to manufacturer's instructions. Thus, devices were rinsed with PBS once, and samples were added to the reservoirs. Columns were centrifuged for 60min at 4000g at 8°C. 15ml of PBS were pipetted to the reservoir of the devices and again centrifuged as described before. The remaining solution in the reservoir containing the concentrated Nanobody in PBS was removed. Prior to downstream applications or freezing at -80°C for long-term storage, concentration was measured on the NanoDrop ND-1000.

4.6.5. Conjugation and labeling of Nanobodies

Nanobodies were conjugated with NOTA (1,4,7-Triazacyclononane-1,4,7-triacetic acid), which was used as a chelator for Gallium-68 (^{68}GA). Conjugation and labeling were kindly performed by our partner Dr. Lisa Russeli from nuclear medicine according to the protocol of Cleeren and colleagues (Cleeren, Lecina et al. 2018).

4.7. Production and labeling of F(ab')$_2$ fragments

4.7.1. Digestion of aTCRmu-IgG

According to manufacturer's recommendations, unconjugated IgG antibodies were digested with Pepsin ensuing Protein-A purification using Pierce F(ab')$_2$ Preparation Kit (Thermo Fisher scientific). Purity and fragmentation were confirmed by SDS-PAGE (4.6.1). After determination of concentration on NanoDrop ND-1000, F(ab')$_2$ was stored at 4°C until use.

4.7.2. Conjugation and labeling of aTCRmu-F(ab')$_2$

Our partner from nuclear medicine Dr. Lisa Russeli performed conjugation and labeling of F(ab')$_2$. Therefore, a derivate of DFO (p-isothiocanatobenzyl of desferrioxamine B) was used as a chelator for Zirconium-89 (^{89}Zr). Buffer of the F(ab')$_2$ solution was exchanged against sodium bicarbonate (pH 9) (4.6.2.). DFO, dissolved in DSMO (c_{END}= 5mM), was added in a 3:1 ratio to the protein solution, containing at least 2mg of antibody, in a total volume of 500µl. The mixture was incubated for 30min at 37°C, and the conjugated antibody was purified via size exclusion chromatography. Elution was done with 2.5mM sodium acetate (pH 4.9-5.5). Labeling procedure was based on the protocol of (Perk, Vosjan et al. 2010). 100µg of the previously conjugated F(ab')$_2$ was added to 37MBq ^{89}Zr in 1M oxalic acid, adjusted with 0.5M HEPES and 2M sodium

carbonate in a total volume of 1ml. The F(ab')$_2$ was then incubated and purified by size exclusion chromatography in 25mM sodium acetate/5mg/ml gentisic acid (pH 5.5).

4.8. Mice experiments

Mice were kept in the institutional facilities following the guidelines and requirements of local authorities. For the experiments, mice were between 8 and 12 weeks old.

4.8.1. ML2 tumor model

For mice experiment, ML2-B7 and ML2-B15 cells were used. Therefore, cells were washed and resuspended in PBS. 20 million cells in 200µl of PBS were injected subcutaneously into the flanks for rejection studies or into the scapular regions for imaging purposes. ML2-B7 were injected into the right side, and ML2-B15 into the left flank. Tumor size was determined via caliper measurement and indicated as length x width of tumor.

4.8.2. T-cell transfer

Transgenic T cells were injected intravenously for rejection studies or intratumorally for imaging purposes. For intravenous injection, cells were washed and resuspended in PBS at 5x10^7 cells/ml. 200µl of cell suspension were injected after 7 days of tumor cell injection (4.8.1.) into tail veins of mice. For intratumoral injection, T cells were washed and resuspended in PBS. 20µl of suspension containing 20 million T cells were then injected intratumorally.

4.8.3. Tracer application

For rejection study, respective unconjugated tracers were diluted in PBS at 100µg/ml. 3 days after T cell injection (4.8.2.), 200µl of tracer solution were injected into tail veins of mice.

For imaging purposes, either 1.6MBq of ^{89}Zr-aTCRmu-F(ab')$_2$ or 10.5MBq of ^{68}Ga-aCD2/aCD7-Nb in 200µl of PBS were injected intravenously 2 days after T cell injection.

4.8.4. PET/MRI imaging

Imaging was kindly performed by the nuclear medicine department's preclinical imaging team (Markus Mittelhäuser, Sybille Reder, Hannes Rolbieski). The Mediso PET/MRI was used for imaging, and the mice were anesthetized using 1.5% isoflurane. The mice were imaged 48h after ^{89}Zr-aTCRmu-F(ab')$_2$ injection or 1h after ^{68}Ga-aCD2/aCD7-Nb injection. First, coronal MRI was acquired for 10 minutes, then a static PET scan was

performed for 20 minutes in the same bed position. Images were fused, and acquired data were normalized for decay.

4.8.5. Analysis of biodistribution

Mice were sacrificed after imaging for biodistribution analysis. Thus, organs, tumors, and blood samples were removed and weighed separately. Residual activity of models and standard (injected activity diluted 1:100) was measured with a gamma counter. The uptake was calculated as injected dose per gram and expressed as a percentage (%ID/g) for comparison.

4.8.6. Flow cytometry analysis of mouse samples

Tumors and organs were mashed using a 40µm cell strainer. Blood samples were centrifuged, and cells were then resuspended in ACK lysis buffer for removal of erythrocytes. After 5min of incubation, cells were centrifuged and resuspended in FACS buffer. Single cells were stained as described above (4.4.1).

4.9. Statistics

Results were checked for statistical significance with a Mann-Whitney test (two-tailed, non-parametric test) using Graphpad Prism v7. If possible, results are indicated as a mean with standard deviation.

All data were acquired in collaboration with Dr. Dario Gosmann, data from in vivo tumor rejection study were additionally acquired with Theresa Käsbauer. Data concerning the purity of Nanobody and imaging experiments were gained additionally in cooperation with Dr. Lisa Russeli.

5. Results

5.1. Characterizing transgenic T cells and respective tumor cells

As a TCR/antigen model, the TCR2.5D6 recognizing the MPO_5 peptide derived from the myeloperoxidase (MPO) characterized by former lab members (Klar, Schober et al. 2014) was used. The TCR2.5D6 contains a constant murine beta chain and is restricted to the HLA-B7. CD8+ T cells were isolated from PBMC of healthy donors. Afterwards, the construct TCR2.5D6-T2A-iRFP was retrovirally transferred into T cells. To evaluate transduction rates and expression of the transferred TCR, T cells were analyzed by flow cytometry with an anti-TCRmu antibody targeting the constant murine beta chain and checking for iRFP signal (Figure 1).

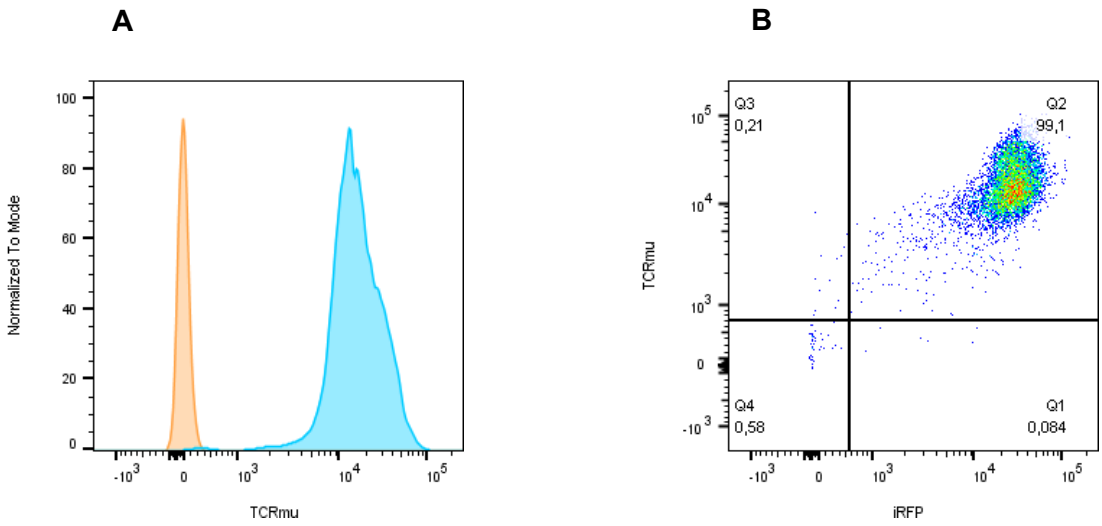

Figure 1: Characterization of TCR2.5D6 transduced T cells
Representative flow cytometry analysis of TCR2.5D6-T2A-iRFP transduced CD8+ T cells. T cells were extracellularly stained after transduction with a monoclonal anti-TCRmu antibody conjugated with FITC.
(A) TCRmu expression of transduced (blue histogram) and untransduced (orange histogram) CD8+ T cells
(B) Correlation of TCRmu and iRFP expression in transduced CD8+ cells

The acute myeloid leukemia cell line ML2 and the acute promyelocytic leukemia cell line NB4 were used as respective tumor cells. Both cell lines expressing myeloperoxidase endogenously were missing the corresponding HLA-B7 for the TCR2.5D6 (Klar, Schober et al. 2014) (Hu, Ma et al. 1993). Cells were retrovirally transduced with the construct HLA-B*07:02-P2A-eGFP. As a control and to exclude any impact of transduction procedure on T cell reactivity, cells were also transduced with a mismatched HLA construct, the HLA-B*15:01-P2A-eGFP. Former lab members performed transduction of tumor cells and generation of stable cell lines. Cell lines were analyzed for quantitative expression of antigen and HLA. Cell lines were intracellularly stained for MPO with the lymphoblastic lymphoma cell line U698M as a negative control (Figure 2A) (Hu, Ma et al. 1993). HLA expression was determined by extracellular staining (Figure 2B).

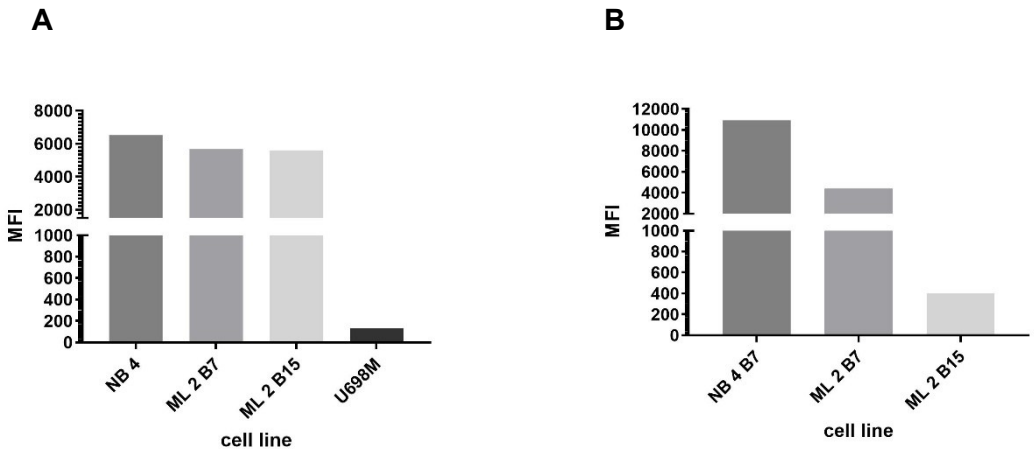

Figure 2: Quantification of antigen and HLA expression in transduced cells
Flow cytometry analysis of transduced tumor cells. Cells were intracellularly stained with an anti-MPO antibody conjugated with FITC for figure A and extracellularly stained with an anti-HLA B7 antibody conjugated with APC for figure B. Mean fluorescent intensity (MFI) was used for quantification of marker expression after gating for positive FITC or APC signal.
(A) Intracellular MPO staining of different cell lines. U698M was used as a negative control.
(B) Extracellular HLA B7 staining of retrovirally transduced tumor cells. ML2 B15 was used as a negative control.
Data and figures were generated in cooperation with Dr. Dario Gosmann

Both tumor cell lines showed high levels of MPO expression. Regarding HLA B7 expression NB4-B7 showed much higher levels than ML2-B7.

5.2. Evaluation of Nanobody purity

Target-specific Nanobodies were derived from immunized llamas by VHH phage display library construction and following biopanning done by the VIB Nanobody Core in Brussels. Cloning the Nanobody sequence into a pHEN6c vector performed by former lab members resulted in a polyhistidine-tag fusion protein. Polyhistidine-tag was used for purification via immobilized metal affinity chromatography after production of Nanobodies in bacterial culture. In the first step, purity was assessed by SDS-PAGE.

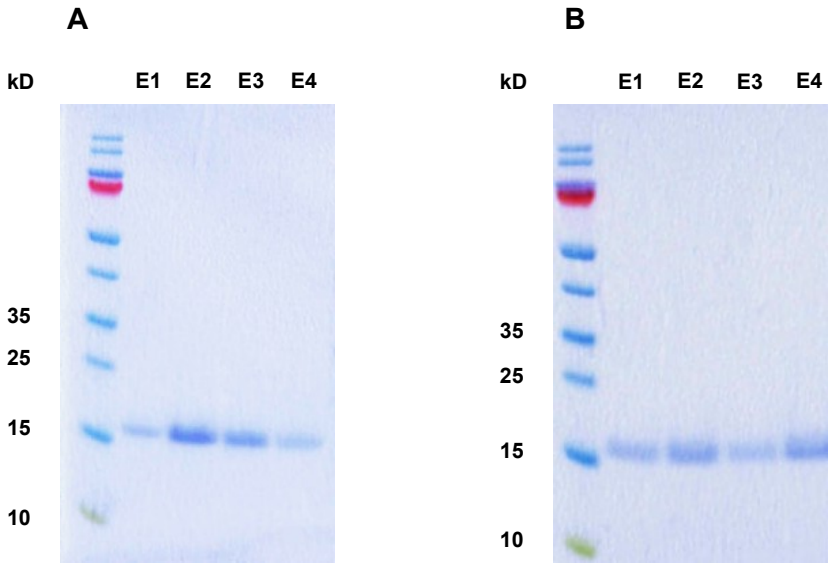

Figure 3: SDS-PAGEs of elution fractions from Nanobody purification
Representative SDS-PAGEs from Nanobody purification are shown. After production in bacterial culture Nanobodies were purified with immobilized metal affinity chromatography. The elution fractions at the end of the procedure were kept separately and loaded onto a gel for evaluation of purity in SDS-PAGE. Size of proteins in elution fractions (E1-E4) were compared to a standard protein ladder.
(A) SDS-PAGE after purification of CD2-specific Nanobody 10563
(B) SDS-PAGE after purification of CD7-specific Nanobody 10215
Data and figures were generated in cooperation with Dario Gosmann

Only one band was visible in every elution fraction with an estimated size of about 15kD. Bands correspond to the respective molecular weight of Nanobodies (15.4-15.6kD)

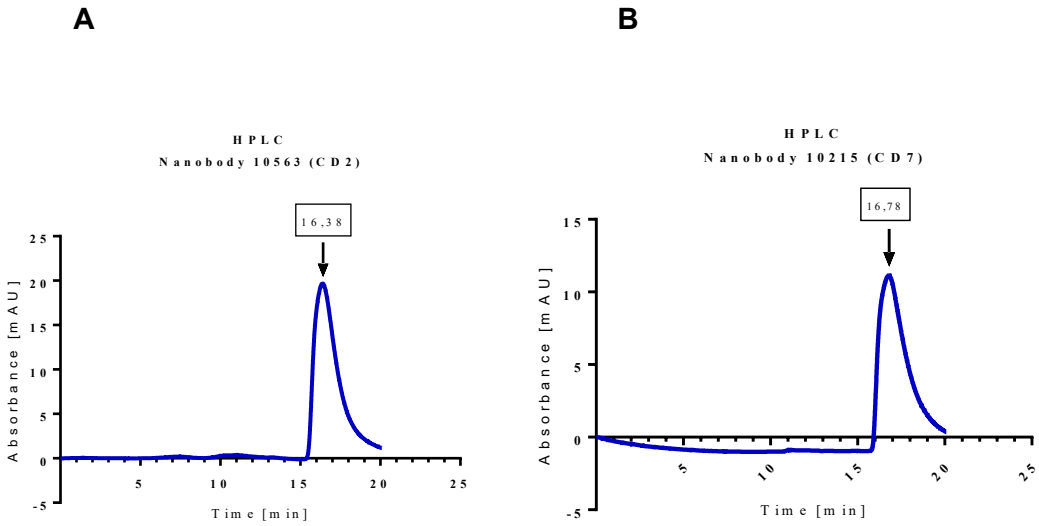

Figure 4: Size-exclusion HPLC of Nanobodies
Representative chromatograms are shown for both Nanobodies after purification. Elution fractions of immobilized metal affinity chromatography were pooled after purity confirmation in SDS-PAGE for further evaluation. Pooled elution fractions were then loaded into the HPLC column and analyzed for protein contaminations by absorbance measurement in a spectrometer over time.
(A) Chromatogram of pooled elution fractions of CD2-specific Nanobody 10563
(B) Chromatogram of pooled elution fractions of CD7-specific Nanobody 10215
Data and figures were generated together with Dr. Dario Gosmann, Theresa Käsbauer and Dr. Lisa Russeli

(Figure 3). SDS-PAGE showed high purity of each cleaned-up Nanobody.

When SDS-PAGE indicated high purity, respective fractions were pooled, and samples were used for size-exclusion HPLC. High purity after clean-up was confirmed by HPLC, excluding any protein contaminations which could interfere with following experiments (Figure 4).

5.3. Confirming target specificity of CD2-specifc Nanobody 10563

Respective Nanobodies were investigated as pan T cell markers for specificity of human CD2 and CD7 detection. Target specificity is crucial for imaging and monitoring purposes. Therefore, it was intensively evaluated. Former lab members already confirmed the specificity of our CD7-specific nanobody (CD7-Nb). For verification of target specificity for our CD2-specific Nanobody (CD2-Nb), modified assays were required compared to the process of CD7-Nb.

As a first step, the lymphoblastic lymphoma cell line U698M, missing endogenous CD2 expression, was retrovirally transduced with the construct CD2-P2A-DsRed. A stable cell line expressing the surface marker was then generated by limiting dilution.

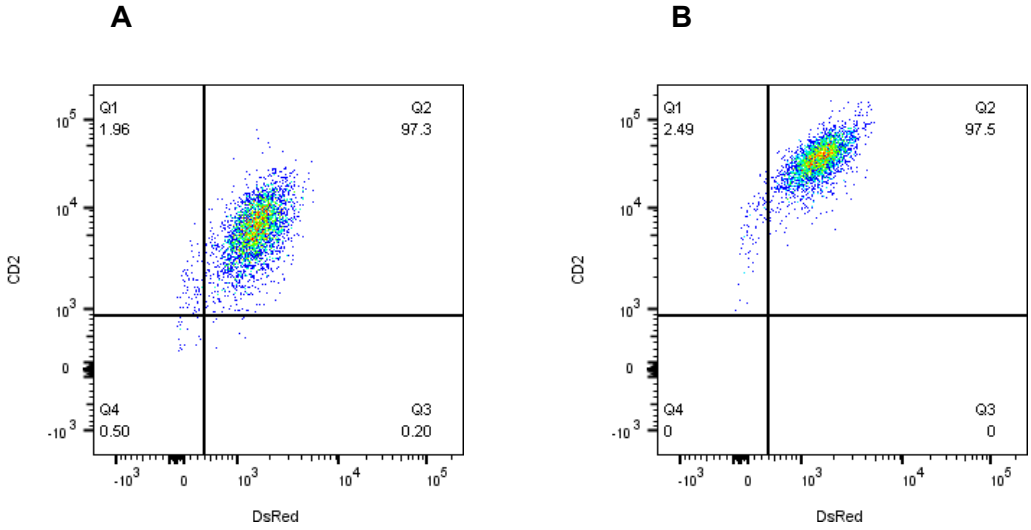

Figure 5: Specificity testing on CD2 transduced tumor cells
Binding was investigated on CD2 transduced U698M cells by flow cytometry. The non-endogenously CD2-expressing cell line U698M was therefore retrovirally transduced with CD2. Cells were then extracellularly stained for CD2 either with the control anti-CD2 antibody RPA-2.10 conjugated with APC or our unlabeled CD2-Nb followed by an anti-histidine-tag antibody targeting the polyhistidine-tag in our nanobodies conjugated with AF647.
(A) Dot plot analysis of U698M cells after CD2-specific Nanobody and subsequent histidine-tag antibody incubation
(B) Dot plot analysis of U698M cells after incubation of control anti-CD2 antibody (RPA-2.10) conjugated with APC
Data and figures were generated in cooperation with Dario Gosmann

Binding of Nanobody on transduced U698M cells was then tested by flow cytometry. As a control, a CD2 specific antibody (RPA-2.10) was used. Both nanobody and positive

control showed good binding to DsRed-positive tumor cells, first proving target specificity.

CD2 binding was tested by epitope blocking on T cells to confirm target specificity (Mayer, Mall et al. 2018). Different commercial anti-CD2 clones were tested for blocking efficiency. For most of them, inhibition of Nanobody binding was not possible. Only for the clone HIK27 a partial shift in binding efficiency was visible in flow cytometry. This clone is specific for the T11.2 epitope on the CD2 protein (van Kemenade, Tellegen et al. 1994), which is one of 3 mainly described epitopes for the CD2 antigen (Brottier, Boumsell et al. 1985, Hünig, Tiefenthaler et al. 1987, Peterson and Seed 1987).

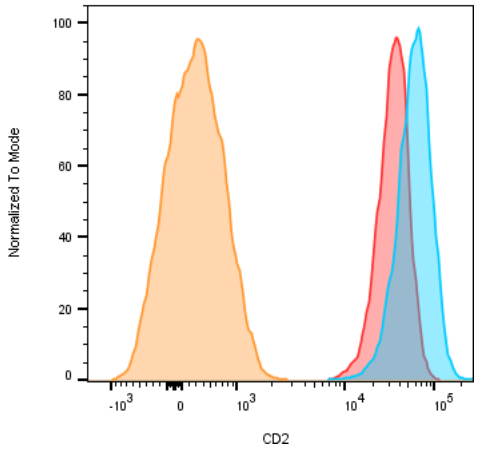

Figure 6: Epitope blocking with HIK27
CD2-Nb binding was tested on T cells before blocking (blue plot) and after blocking (red plot) was performed. For the unblocked condition T cells were stained with our unlabeled CD2-Nb followed by an anti-histidine-tag antibody targeting our nanobodies conjugated with AF647. In the blocked setting T cells were first incubated with the anti-CD2 antibody HIK27 and after washing stained with our CD2-nanobody as well as the anti-histidine-tag antibody.
Both conditions were compared to T cells stained with just anti-histidine-tag antibody for exclusion of background signal (orange plot).

Flow cytometry analysis for Nanobody showed a slight shift in intensity after previous blocking of the CD2 protein with the HIK27 clone, suggesting competition for bound epitopes (Figure 6). Hence similar specificity for the Nanobody and the HIK27 clone was assumed.

However, as only minor differences in intensities could be detected after blocking an alternative method to investigate the specificity of the nanobody was applied. CD2 knockout in a CD2 expressing T cell leukemia cell line, Jurkat E6.1, was performed. Therefore CRISPR-Cas9 method was used as it allowed precise DNA modifications. gRNAs were designed to target the first exon of the human CD2 gene, which should lead to changes by non-homologous end joining and subsequent frameshift mutations.

Jurkat cells were separately transfected with prepared RNPs, targeting CD2 and ubiquitously expressed HPRT gene as respective positive control. 3 days after transfection, DNA was isolated and investigated for modifications in HPRT genes by T7EI endonuclease assay. Thus, transfection methods could be evaluated. T7EI endonuclease assay detected only insertions or deletions with more than one base in PCR-amplified gDNA fragments by cleavage of mismatched heteroduplexes between wild-type and mutated DNA followed by gel electrophoresis. Thereby editing efficiency could be evaluated on a semi-quantitative base.

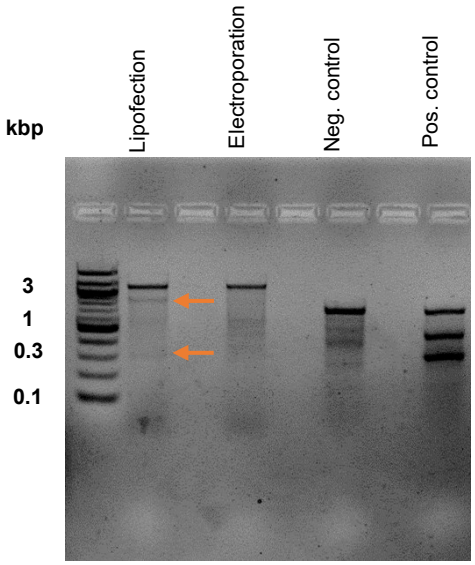

Figure 7: Gel analysis of T7EI endonuclease assay
Lipofection and electroporation as transfection methods for Jurkat E6.1 were compared in T7EI endonuclease assay regarding editing rates. After transfection gDNA was isolated from cells and CD2 locus was amplified by PCR. The amplified products were then incubated with T7E1 endonuclease. Cleavage of mismatched heteroduplexes was then investigated by gel electrophoresis. Respective controls included in manufacturer's kit were also set.
Specific bands for positive editing are highlighted (orange arrows)

Low gene editing rates could be detected for lipofection, whereas for electroporation, no editing was visible in gel electrophoresis (Figure 7). DNA fragments of lipofection correspond to the bands indicated in manufacturer's instructions, despite poor running quality of gel. As for electroporation no editing could be detected, only lipofection was used for further transfections.

3 days after lipofection of Jurkat cells with RNPs, CD2 expression of Jurkat cells was tested by flow cytometry.

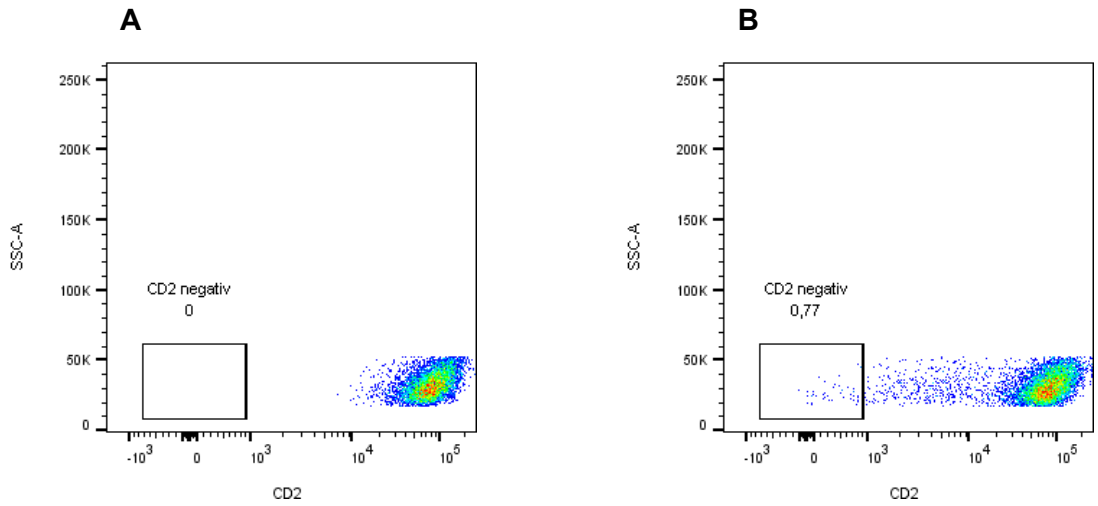

Figure 8: Flow cytometry analysis of CD2 expression in Jurkat cells
Jurkat cells were extracellularly stained with anti-CD2 antibody RPA-2.10 conjugated with APC before and after transfection with RNPs for CD2 knockout. Respective plots are shown with percentages of CD2-negative cells based on unstained Jurkat cells (Data not shown).
(A) Dot plot of Jurkat cell analysis stained with anti-CD2 antibody RPA-2.10 before transfection with RNPs
(B) Dot plot of Jurkat cell analysis stained with anti-CD2 antibody RPA-2.10 3 days after transfection with RNPs
Data and figures were generated in cooperation with Dario Gosmann

Before transfection, Jurkat cells showed high expression of CD2, resulting in an entirely positive population, whereas transfected cells showed partly reduced expression of CD2. Only 0.77 percent of transfected population showed no expression gated in reference to unstained Jurkat cells (Figure 8). Cells with only reduced intensity were excluded because of possible heterozygote genotype.

Single-cell clones were then derived from transfected population by limiting dilution and screened for CD2 expression in flow cytometry. After selecting several clones based on negative CD2 expression, genomic DNA was isolated from respective clones. Target locus of gRNAs was amplified by PCR and sent for Sanger sequencing. Sequences of selected clones were compared to wild-type sequence, and only clones with deletions or insertions resulting in frameshift mutations were further selected.

Selected clones and wild-type population were then screened for T cell markers to ensure that clones chosen were not derived from contaminations or dedifferentiated cells. Pan T cell markers CD3, CD2, CD7, and CD4 for the T helper subset, as Jurkat cell line is derived from a CD4+ T cell leukemia, were analyzed.

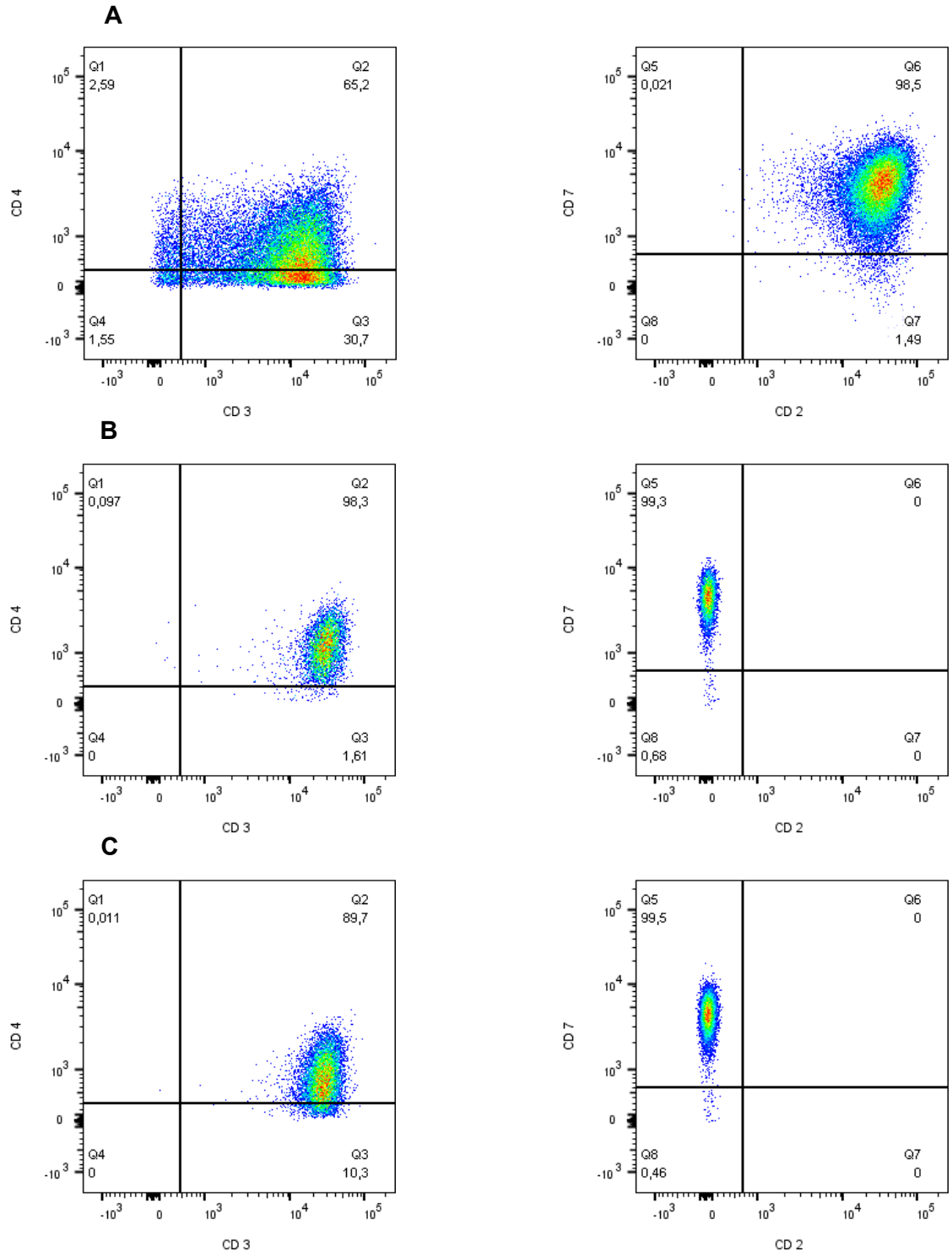

Figure 9: Flow cytometry analysis of T cell surface markers after CD2 knockout and subsequent clone selection in Jurkat cells.

Dot plots after analysis in flow cytometer are shown. Gates were set based on the wild-type population with isotype controls. Cells were extracellularly stained for CD2 (RPA-2.10), CD3 (UCHT1), CD4 (SK3) and CD7 (M-T701). Wild-type population (A) and two representative knockout clones (B, C) after limiting dilution and knockout confirmation by Sanger sequencing are shown.

Data and figures were generated in cooperation with Dario Gosmann

Wild-type clones showed the typical expression of T cell surface markers, as cells were mainly positive for all selected markers. Marker expression for selected knockout clones

corresponded to the wild-type population except for CD2, which was not detectable (Figure 9). Summarized, we assumed that the lack of CD2 expression of the selected clones resulted from successful knockout. The shown procedure allowed the generation, selection, and validation of CD2 knockout clones to further investigate target specificity.

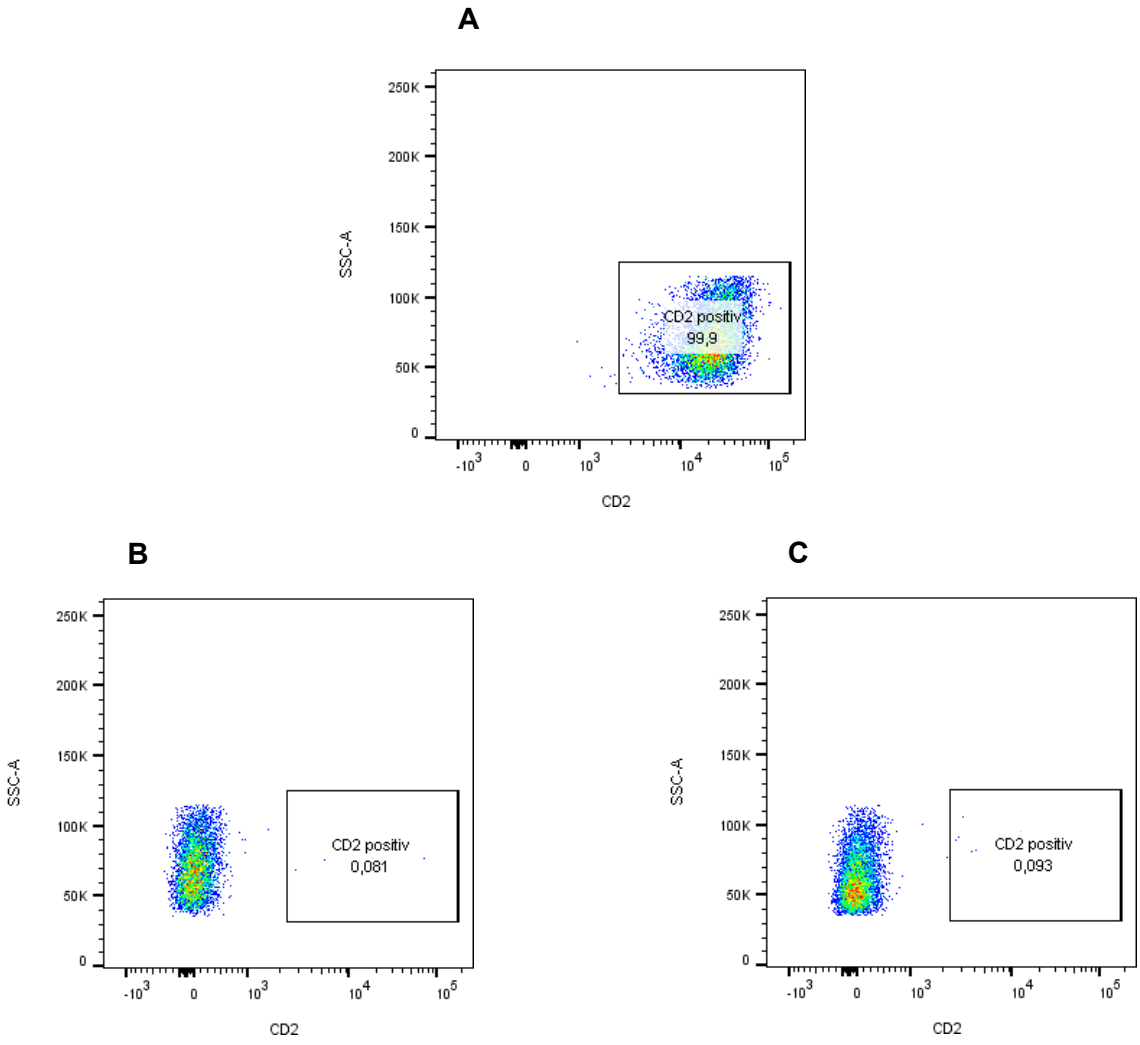

Figure 10: Flow cytometry analysis of CD2-Nb binding on Jurkat wild-type and knockout clones.
Jurkat cells were incubated for 1h with nanobodies and subsequently stained with anti-polyhistidine-tag antibody targeting the nanobody. Cells were then analyzed in flow cytometer. Respective dot plots are shown for Jurkat wild-type (A) and for representative selected knockout clones after Sanger sequencing (B, C).

Nanobody binding was tested on Jurkat knockout clones compared to Jurkat wild-type for final evaluation of target specificity. Strong signal of polyhistidine-tag antibody was visible for Jurkat wild-type, whereas for knockout clones, no specific binding was detectable (Figure 10). The three approaches suggested high target-specific binding of the Nanobody and was thereby confirmed.

5.4. Thermal stability assessment

For conjugation of proteins to chelators and the following labeling with radionuclides in conventional methods, often high temperatures are required due to slow reaction kinetics and low radiochemical yields at room temperature (Breeman, De Jong et al. 2003, Sosabowski and Mather 2006, Ebenhan, Chadwick et al. 2014). Therefore, heat resistance regarding the binding capacity of Nanobodies was tested. Nanobodies were incubated for 0.5h, 1h, 2h, 4h, and 6h at 37°C, 60°C and 90°C. Afterwards, they were used for staining of surface markers of Jurkat cells with subsequent polyhistidine-tag antibody incubation. Cells were then analyzed in flow cytometer to check if Nanobodies could maintain antigen binding after thermal stress. Flow cytometry was a more physiological approach than other methods commonly used (Yan, Wang et al. 2015, Kunz, Zinner et al. 2018).

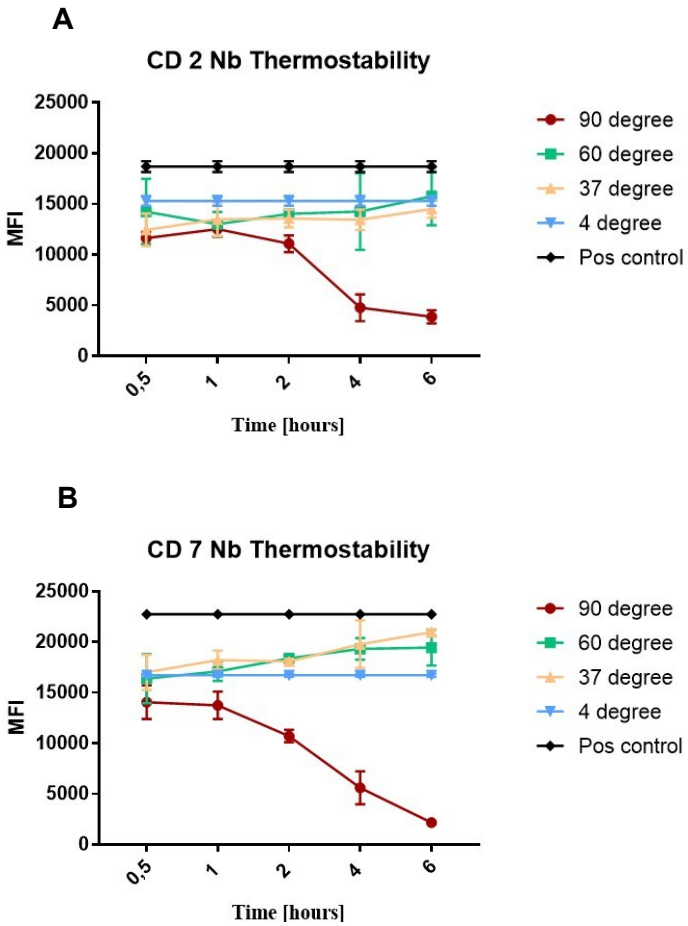

Figure 11: Analysis of remaining binding capacity of Nanobodies after heat incubation.
MFI was used as an indicator for binding capacity and was plotted over time and for different temperatures. Nanobodies were incubated for overall 6h at 37, 60 and 90 degrees and samples were taken after different time periods for staining of Jurkat cells followed by staining with polyhistidine-tag antibody. Respective Nanobodies kept at 4°C were used as a reference and as positive control Nanobody in excess was used. Negative control consisting of Jurkat cells stained with polyhistidine-tag antibody was already subtracted as background noise from other values. Graphs for CD2-Nb (A) and CD7-Nb (B) are shown and values are indicated as mean with standard deviation calculated from triplicates.
Data and figures were generated together with Dario Gosmann

Nanobodies were used at a concentration of 5nM close to the K_D value of the Nanobodies so that changes in concentrations of “functional” Nanobody could be detected very sensitively by flow cytometry. Minor differences in concentrations close to the K_D resulted in significant variance in flow cytometry signal (Benedict, MacKrell and Anderson 1997, Benmebarek, Cadilha et al. 2021).

Nanobodies incubated at 37°C and 60°C showed, compared to the reference Nanobody kept at 4°C, no significant loss in binding capacity independently regarding the incubation time. At 90°C, Nanobodies were stable for 1h without substantial loss of binding capacity. After 1h signal decreased rapidly so that after 6h, almost no binding was detectable. Nanobodies showed good heat resistance for at least until 60°C. Even 90°C was tolerable for a short incubation time, sufficient for our method used (Cleeren, Lecina et al. 2018) and for most common conjugation and labeling procedures (Gainkam, Huang et al. 2008, Vosjan, Perk et al. 2010, Vosjan, Perk et al. 2011).

5.5. Functionality testing of T cells in vitro

Targeting of T cell antigens by antibodies can lead to overstimulation, T cell dysfunctionality, and apoptosis (Griessinger, Maurer et al. 2015, Mall, Yusufi et al. 2016, Freise, Zettlitz et al. 2017, Mayer, Mall et al. 2018). Thus, T cell functionality was assessed by analysis of cytokine levels after Co-incubation with tumor cells and tracers in different conditions. For coculture, the acute promyelocytic leukemia cell line NB4 and the acute myelomonocytic leukemia cell line ML2 transduced with the corresponding HLA-B7 to the TCR2.5D6 and transduced with a mismatched HLA construct HLA-B15 were used. Nanobodies 10563, 10215 and an unspecific isotype Nanobody were added to a final 100nM concentration, which is much higher than commonly used doses for imaging purposes (Vosjan, Vercammen et al. 2012, Xavier, Vaneycken et al. 2013). High concentrations were used to saturate antigen binding excluding any impact on T cell functionality.

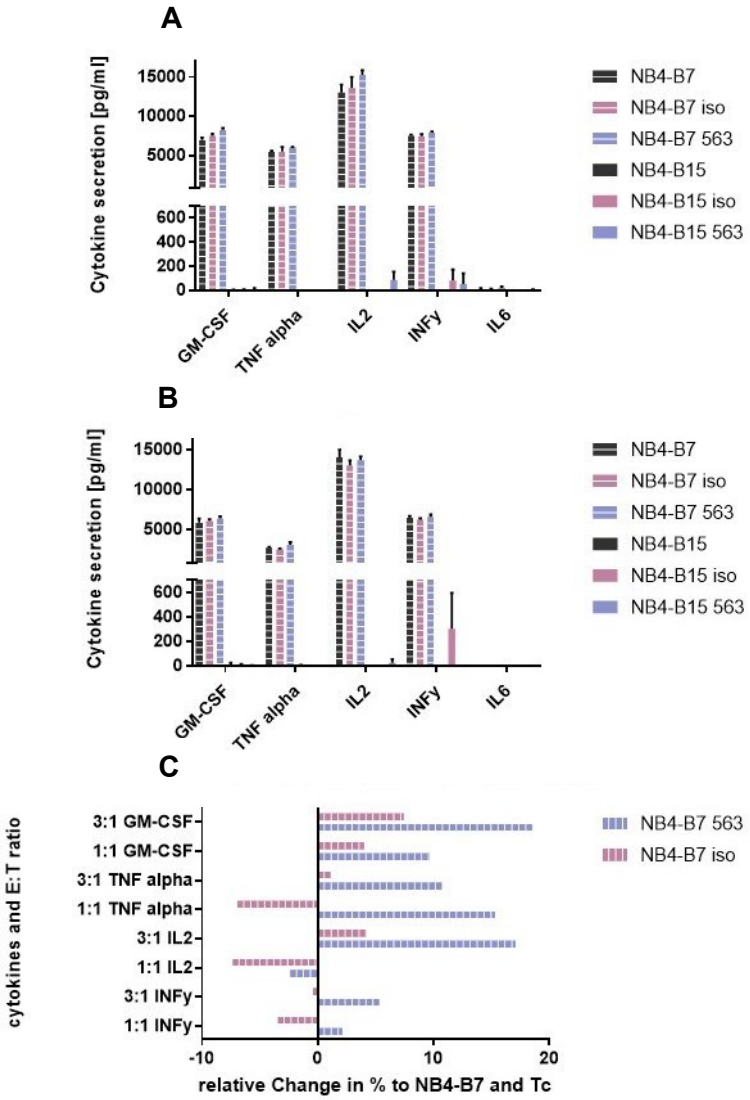

Figure 12: Cytokine analysis of CD2-Nb with NB4 and T cells.
TCR-transgenic T cells and HLA-transduced tumor cells were cocultured for 4h, afterwards supernatant was removed and used for ELISA. In total 6 different conditions were analyzed, 3 for matched HLA/TCR (NB4-B7) and 3 for mismatched HLA/TCR (NB4-B15). CD2-specific Nanobody 10563 (563) or isotype (iso) were added as indicated to a final 100nM concentration. Transduction efficiency of T cells was approximately 100% (Figure 1). Triplicates were set for all conditions and values are indicated as mean with standard deviation (A, B) or as percentages (C).
(A) Cytokine analysis of coculture with an effector to target ratio of 3:1
(B) Cytokine analysis of coculture with an effector to target ratio of 1:1
(C) Relative changes in cytokine secretion in comparison to control condition with just T cells and NB4-B7 cells.
Data and figures were generated in cooperation with Dario Gosmann

After 4h of incubation, T cells showed high cytokine secretion, except for IL-6, which suggested non-restricted tumor reactivity (Figure 12). IL-6 was measured as a primary indicator for cytokine release syndrome, which frequently occurred after transmission of transgenic T cells (Lee, Gardner et al. 2014, Maude, Frey et al. 2014, Porter, Hwang et al. 2015). Overall, conditions of T cells and tumor cells incubated in the presence of CD2-specific Nanobody 10563 showed a slight increase in cytokine secretion compared to control conditions.

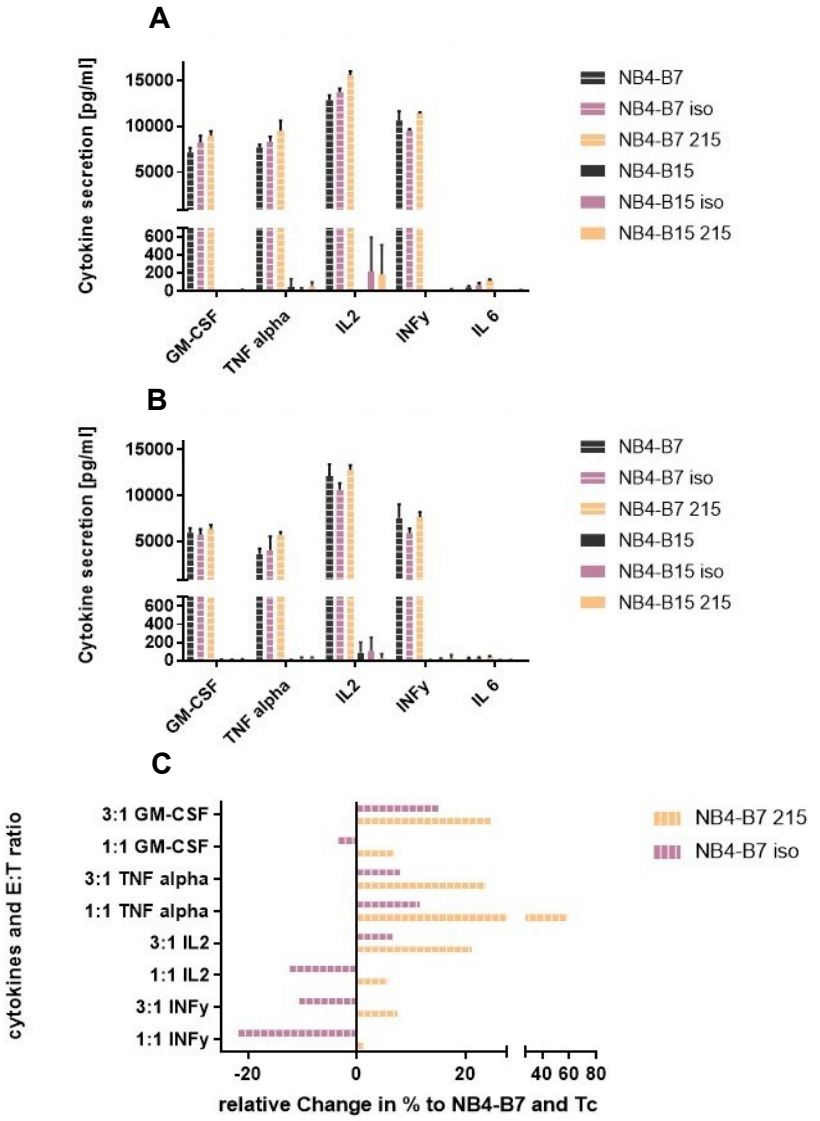

Figure 13: Cytokine analysis of CD7-Nb with NB4 and T cells.
TCR-transgenic T cells and HLA-transduced tumor cells were cocultured for 4h, afterwards supernatant was removed and used for ELISA. In total 6 different conditions were analyzed, 3 for matched HLA/TCR (NB4-B7) and 3 for mismatched HLA/TCR (NB4-B15). CD7-specific Nanobody 10215 (215) or isotype (iso) were added as indicated to a final 100nM concentration. Transduction efficiency of T cells was approximately 100% (Figure 1). Triplicates were set for all conditions and values are indicated as mean with standard deviation (A, B) or as percentages (C).
(A) Cytokine analysis of coculture with an effector to target ratio of 3:1
(B) Cytokine analysis of coculture with an effector to target ratio of 1:1
(C) Relative changes in cytokine secretion in comparison to control condition with just T cells and NB4-B7 cells.
Data and figures were generated in cooperation with Dario Gosmann

Conditions cocultured with isotype Nanobody also showed a slight increase in cytokine secretion but remained under the level of CD2-Nb (Figure 12 C). Similar effects were generally observed for CD7-specific Nanobody 10215 (Figure 13). Increase of cytokine levels was higher than for CD2-Nb but also showed higher variances for cytokine levels of isotype Nanobody. Effector to target ratio had no relevant effect on differences in cytokine secretion. Differences were tested for significance by Mann-Whitney Test and showed no significant results for Nanobody 10563 nor Nanobody 10215. Absent cytokine secretion in conditions with the mismatched HLA/TCR suggested missing unspecific or

general stimulatory effects of Nanobodies on T cells. No relevant impact on T cell functionality based on cytokine secretion could be detected in this short-term assay.

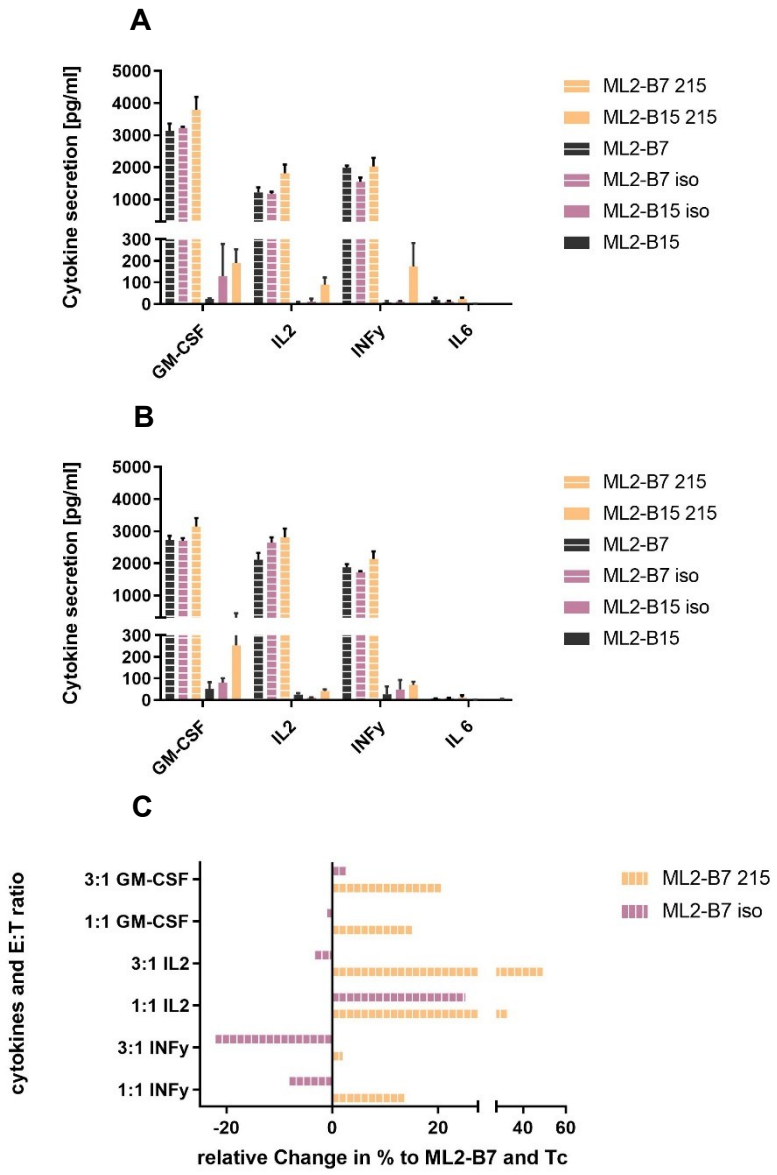

Figure 14: Cytokine analysis of CD7-Nb with ML2 and T cells.
TCR-transgenic T cells and HLA-transduced tumor cells were cocultured for 24h, afterwards supernatant was removed and used for ELISA. In total 6 different conditions were analyzed, 3 for matched HLA/TCR (ML2-B7) and 3 for mismatched HLA/TCR (ML2-B15). CD7-specific Nanobody 10215 (215) or isotype (iso) were added as indicated to a final 100nM concentration. Transduction efficiency of T cells was approximately 100% (Figure 1). Triplicates were set for all conditions and values are indicated as mean with standard deviation (A, B) or as percentages (C).
(A) Cytokine analysis of coculture with an effector to target ratio of 3:1
(B) Cytokine analysis of coculture with an effector to target ratio of 1:1
(C) Relative changes in cytokine secretion in comparison to control condition with just T cells and NB4-B7 cells.
Data and figures were generated in cooperation with Dario Gosmann

For long-term analysis in vitro, the ML2 cell line was used as T cells showed lower reactivity in general, and thus lower cytokine levels were detected. This lower cytokine secretion evoked by the ML2 reduced the risk of any saturation effects on the system. T cells and ML2 cells were cocultured under the same conditions as shown above for 24h.

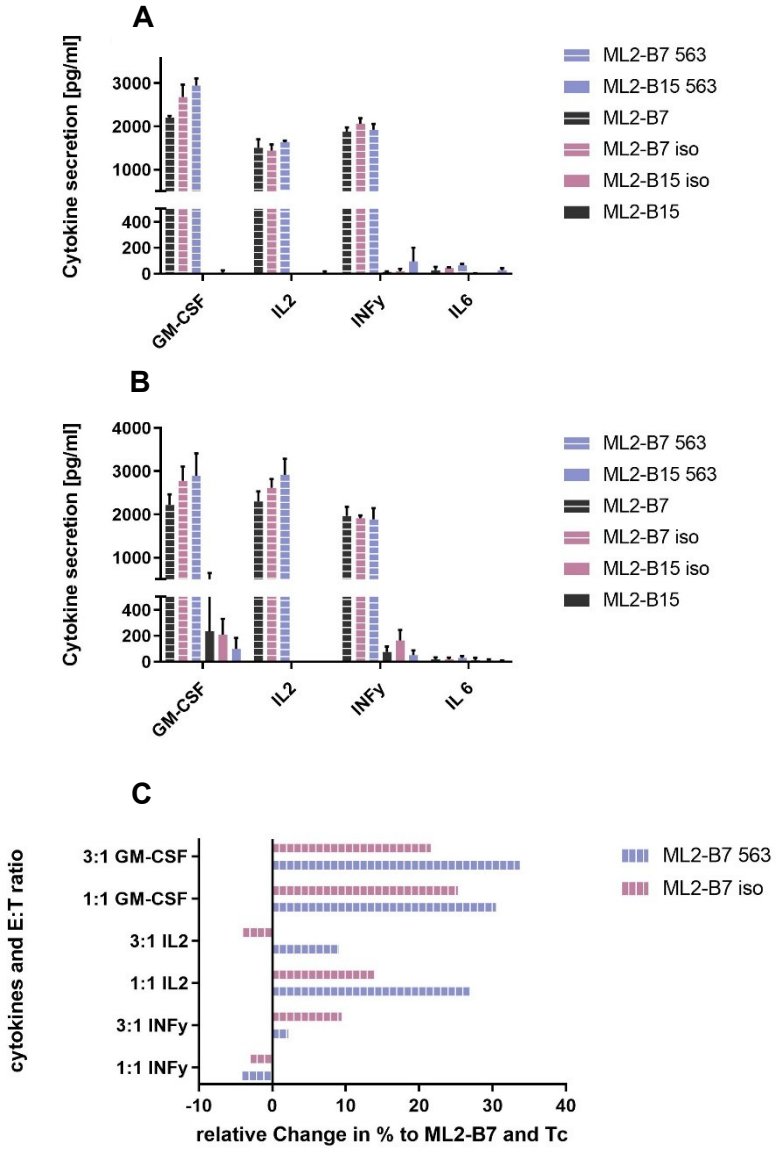

Figure 15: Cytokine analysis of CD2-Nb with ML2 and T cells.
TCR-transgenic T cells and HLA-transduced tumor cells were cocultured for 24h, afterwards supernatant was removed and used for ELISA. In total 6 different conditions were analyzed, 3 for matched HLA/TCR (ML2-B7) and 3 for mismatched HLA/TCR (ML2-B15). CD2-specific Nanobody 10563 (563) or isotype (iso) were added as indicated to a final 100nM concentration. Transduction efficiency of T cells was approximately 100% (Figure 1). Triplicates were set for all conditions and values are indicated as mean with standard deviation (A, B) or as percentages (C).
(A) Cytokine analysis of coculture with an effector to target ratio of 3:1
(B) Cytokine analysis of coculture with an effector to target ratio of 1:1
(C) Relative changes in cytokine secretion in comparison to control condition with just T cells and NB4-B7 cells.
Data and figures were generated in cooperation with Dario Gosmann

ELISAs of ML2 cocultures showed higher background signals than the NB4 cocultures because of longer incubation time, but absolute cytokine production was distinctly lower

than NB4 despite longer incubation time. One of the reasons could be lower expression of relevant HLA-B7, as shown previously (Figure 2). Overall, cytokine ratios are similar to NB4 cells (Figure 12, Figure 13). ML2 cells incubated with T cells and CD7-Nb (Figure 14) showed slightly increased cytokine secretion, as did the condition with CD2-Nb (Figure 15). IL-2 secretion seemed to depend on effector to target ratio in ML2 cells as 1:1 ratios showed higher levels than 3:1 ratios (Figure 14, Figure 15). Neither relevant differences between CD2-Nb and CD7-Nb nor significant increase in cytokine secretion by Mann-Whitney test could be detected in ELISA cytokine analysis.

Resumed, targeting surface antigens of T cells with CD2-Nb and CD7-Nb showed no unspecific stimulatory effect in mismatched HLA/TCR conditions or significant differences in cytokine secretion between control and Nanobody conditions. However, Nanobodies seemed to have a costimulatory impact on T cells. Tendency to higher levels of cytokines in conditions containing Nanobody was detected, which could only partly be explained by purification process. To which extent it impacts T cell functionality needs to be further investigated.

5.6. Tumor rejection study

As we detected minimal changes in T cell functionality in vitro, we complemented an in vivo study. Previous studies already detected significant lack of T cell killing in vivo, although in vitro data showed no or minor dysfunctionality after targeting surface markers with antibodies (Mayer, Mall et al. 2018).

Thus, T cell functionality was evaluated in a mouse experiment by measurement of tumor size after tracer application. The ML2 cell line, either transduced with HLA-B7 or with HLA-B15, was used in mouse model as described previously (Mall, Yusufi et al. 2016, Mayer, Mall et al. 2018). ML2-B7 cells were injected subcutaneously into the right flank, and ML2-B15 cells were injected into the left side as a negative control for exclusion of unspecific interaction between T cell and tumor. Six experimental groups were set and injected with different antibodies and PBS as reference. The antibodies included the CD2-Nb and the CD7-Nb, the Nanobody isotype used in previous experiments, and two $F(ab')_2$ clones (RPA-2.10, OKT11) directed against CD2. The isotype was used to exclude any unspecific impact of the Nanobody itself. As positive controls, the two $F(ab')_2$ clones were used to detect impairment of T cell functionality as previously observed (Mayer, Mall et al. 2018).

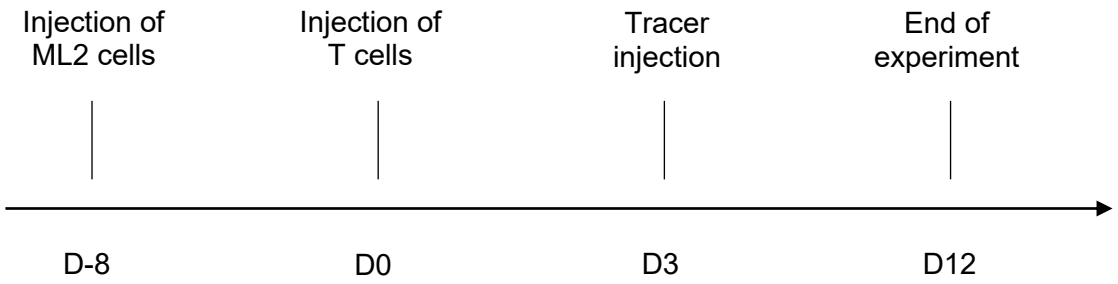

Figure 16: Experimental timeline of tumor rejection study
Timeline of rejection study is shown. T cells were injected after 8 days following tumor engraftment. Tracer injection was subsequently performed 3 days later. Mice were sacrificed after 12 days.

Chronological procedure of experiment as performed is shown above (Figure 16). Tumor sizes were measured every day to evaluate tumor rejection by T cells. 60 minutes after tracer application on day 3, one mouse of PBS and each Nanobody group were taken out of experiment for flow cytometry analysis.

After 8 days tumors engrafted well in all experimental groups (Figure 17). After T cell injection, changes in growth kinetics of ML2-B7 tumors were visible as slope was decreasing. Tumor sizes began to decline after tracer application for all groups except the $F(ab')_2$ groups, in which tumor sizes were stable for few days after application before rejection failed. $F(ab')_2$ fragments distinctly impacted T cell functionality as tumor sizes increased exponentially after application as described previously. Significant differences compared to the PBS group could be detected at the end of experiment only for $F(ab')_2$ fragments, clone RPA-2.10 ($p<0.05$) as well as for clone OKT11 ($p<0.001$) (Figure 17 B).

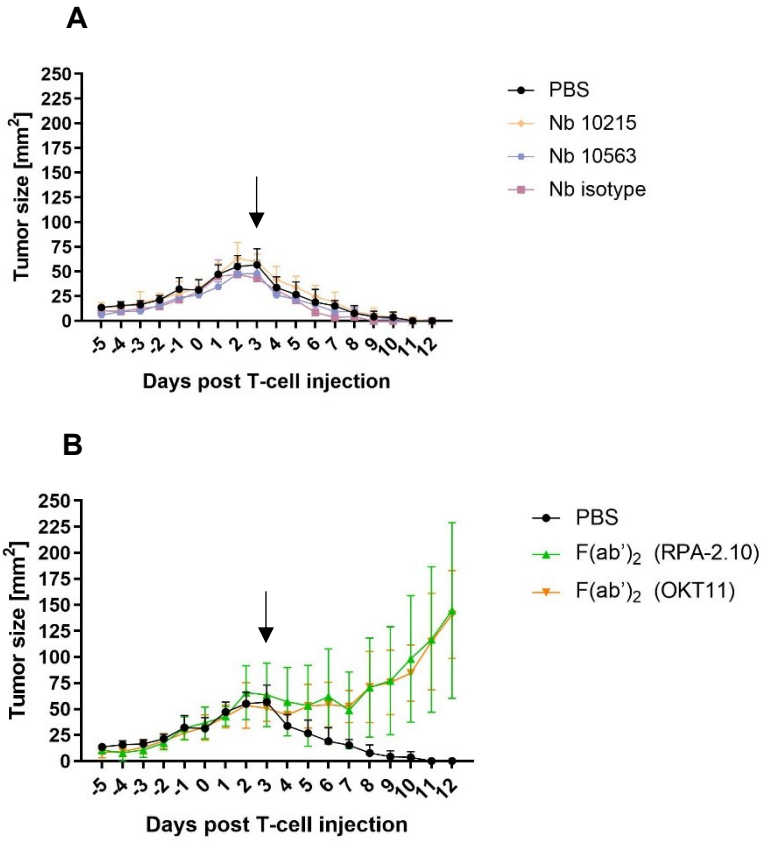

Figure 17: ML2-B7 tumor sizes of Nanobodies and F(ab')$_2$ groups in rejection study
ML2-B7 tumor sizes of Nanobody and F(ab')$_2$ groups are plotted with the PBS group as a mean with standard deviation and were determined by caliper measurement. Black arrows indicate day of tracer application. Only data for mice, which stayed in experiment until day 12 post T cell injection are shown.
(A) Data for CD7-specific Nanobody 10215 (n=5), CD2-specific Nanobody 10563 (n=5) and Nanobody isotype (n=3) are shown in comparison to PBS control (n=4)
(B) Data for F(ab')$_2$ fragment of clone RPA-2.10 (n=5) and of clone OKT11 (n=6) are shown in comparison to PBS control (n=4)
Data and figures were generated in cooperation with Dario Gosmann and Theresa Käsbauer

No significant difference in tumor sizes or growth kinetics compared to the PBS group could be detected for Nanobody groups (Figure 17 A). At the end of the experiment, tumors could no longer be seen and measured in the Nanobody and PBS groups as indicated by a size of 0.

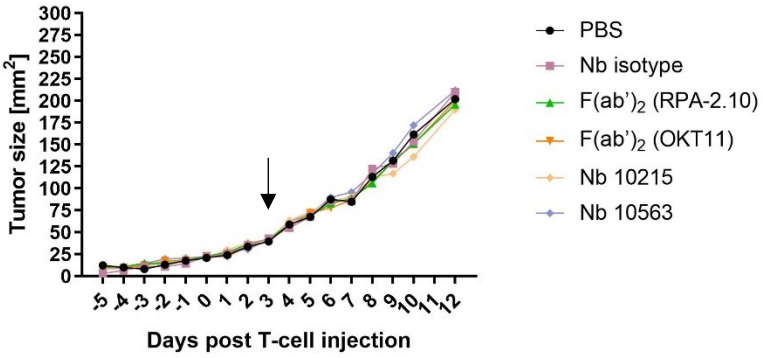

Figure 18: ML2-B15 tumor sizes of all experimental groups in rejection study
ML2-B15 tumor sizes of all experimental groups were plotted as a mean without standard deviation for reasons of clarity and were determined by caliper measurement. Black arrow indicates day of tracer application. Only data for mice, which stayed in experiment until day 12 post T cell injection are shown.
Data and figures were generated in cooperation with Dario Gosmann and Theresa Käsbauer

ML2-B15 tumors as a negative control kept constantly growing in all experimental groups without any relevant differences between the groups, showing no general impact of tracer application on tumor growth kinetics.

Taken together, Nanobodies showed no impact on tumor rejection of T cells, whereas F(ab')$_2$ fragments directed against CD2 showed highly significant differences compared to PBS regarding the tumor sizes.

However, the presence of Nanobodies bound to T cells in tumors needed to be verified. Thus, 60 minutes after tracer injection, mice were sacrificed, and organs and tumors were used for flow cytometry analysis.

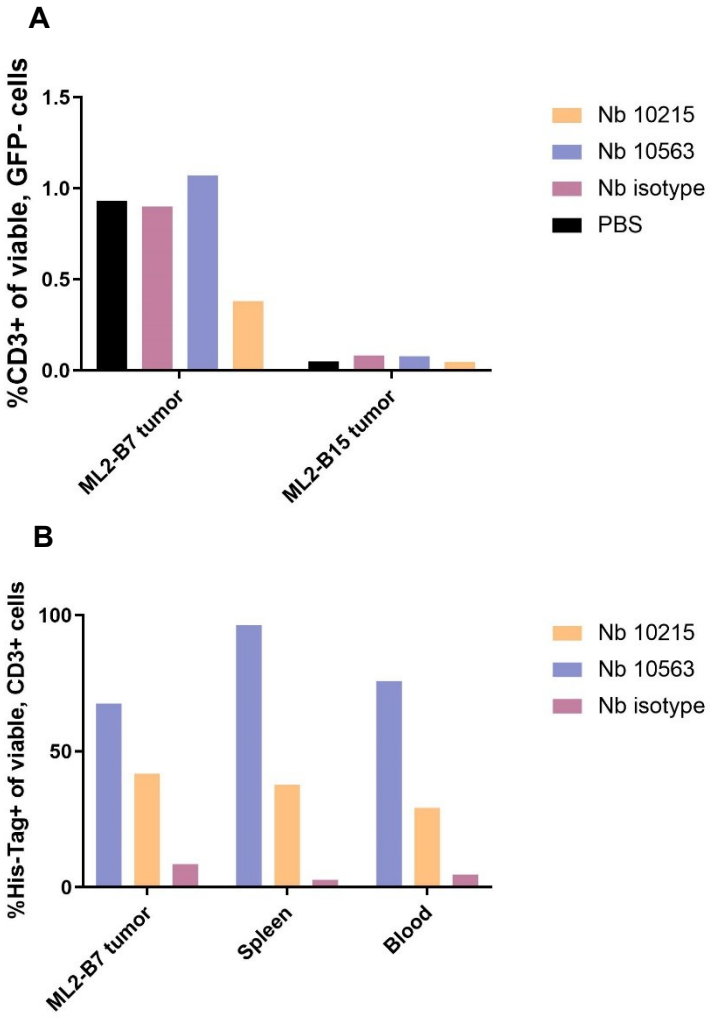

Figure 19: Ex vivo flow cytometry analysis of mice from tumor rejection study
Single cell suspensions were produced from organs, blood and tumors, then washed with PBS for flow cytometry analysis. Representative plots are shown for each experimental group.
(A) Single cell suspensions of ML2-B7 and ML2- B15 tumors were extracellularly stained for CD3. Fraction of CD3+ of viable and GFP- cells are shown in percentages.
(B) Single cell suspensions derived from ML2-B7 tumors, spleens and blood were stained for CD3 and polyhistidine-tag. Fraction of polyhistidine-tag+ of viable, CD3+ cells are shown as percentages.
Data and figures were generated in cooperation with Dario Gosmann and Theresa Käsbauer

First specific invasion of human T cells into HLA-matched tumor was analyzed. Therefore, single-cell suspensions of tumors were stained for the ubiquitous T cell marker CD3 and subsequently gated for CD3+ of viable, GFP- cells. Gating should exclude tumor cells as HLA expression was linked to GFP. Human T cells showed specific invasion of HLA-B7 expressing tumors as fractions were multiple times higher compared to HLA-B15 expressing tumors (Figure 19 A). A difference for CD7-Nb could be detected among the respective experimental groups. Fraction of T cells in ML2-B7 tumors was lower compared to PBS and the other Nanobody groups.

T cells were then analyzed for successful Nanobody binding in vivo. Thus, single-cell suspensions were stained for CD3 and polyhistidine-tag and gated for polyhistidine-tag+

of viable, CD3+ cells. CD2-Nb and CD7-Nb could be specifically detected in all tissues analyzed. Compared to isotype Nanobody, control percentages of polyhistidine-tag+ cells in groups of CD2-Nb and CD7-Nb were distinctly higher (Figure 19 B). However, binding of CD7-Nb to T cells remained under the level of CD2-Nb.

Taken together, Nanobodies bound already after 60 minutes specifically to T cells in vivo, which showed no dysfunctionality after targeting CD2 and CD7 in vivo. These characteristics are desirable for a diagnostical tracer. Consequently, Nanobodies were used for an imaging experiment.

5.7. Preliminary imaging experiment

The previously acquired data suggested that the Nanobodies could be used as tracers for T cell imaging as they fulfill the following desirable characteristics for a tracer. Nanobodies showed high specificity for target structures without major impact on specific functionality. Moreover, quick enrichment after application at the target structure as seen in the rejection study suggested favorable pharmacokinetics.

For proof of concept, the CD2-Nb was used in a small experiment to evaluate imaging capabilities; therefore, a similar set-up as for the rejection study was used (Figure 20).

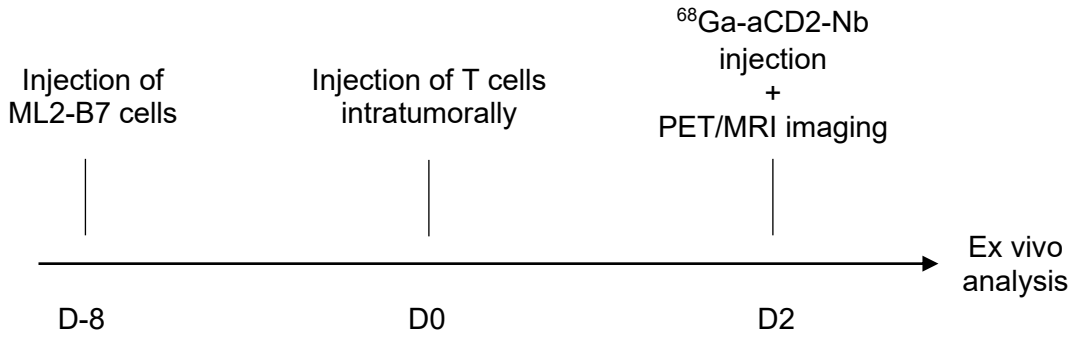

Figure 20: Experimental timeline of preliminary imaging
Timeline of preliminary imaging experiment is shown. T cells were injected after 8 days of tumor engraftment followed by tracer injection 2 days later. Mice were imaged 90 minutes after tracer injection and were sacrificed after imaging for ex vivo analysis.

For imaging purposes, ML2-B7 cells were not injected into the flank but into the scapular region, as kidneys and bladder typically have high background signals because of tracer elimination. After tumor engraftment, T cells transduced with TCR2.5D6 were injected intratumorally, two days later tracer was injected. Because of short biological half-life and quick accumulation of Nanobodies in target structures, imaging was already performed after 90 minutes (Hoefman, Ottevaere et al. 2015, Keyaerts, Xavier et al. 2016). As an internal control, one mouse received ^{89}Zr-aTCRmu-F(ab')$_2$ as established previously in the lab (Mall, Yusufi et al. 2016).

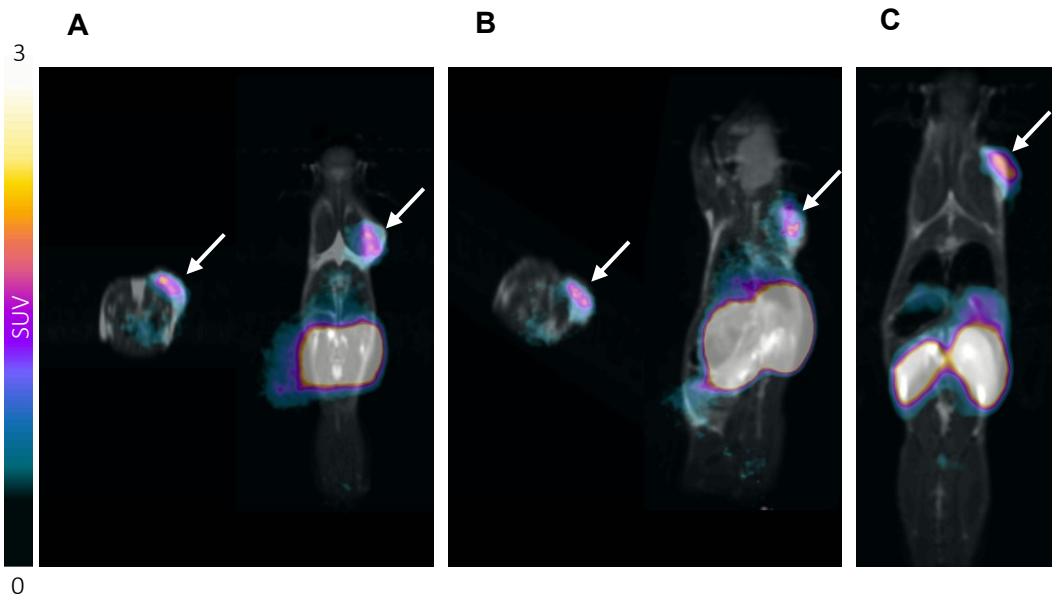

Figure 21: Preliminary PET/MRI images
PET/MRI images in axial and coronal planes after tracer injection are shown. Scalebar = SUV from 0% to 3%. White arrows indicate tumor site.
(A/B) Representative images in axial and coronal planes of mice, which received ^{68}Ga-aCD2-Nb 90 minutes post injection (n=2).
(C) Representative image in coronal plane of control mouse which received ^{89}Zr-aTCRmu-F(ab')$_2$ 48 h post injection (n=1).
Data and figures were generated in cooperation with Dario Gosmann and Lisa Russeli

Respective PET/MRI images of mice that received the ^{68}Ga-aCD2-Nb showed good tracer accumulation at the tumor site after 90 minutes post-injection with low background signal. Only kidneys and bladder showed high signal intensity (Figure 21). Tracer uptake at tumor site could also be confirmed by the images of the mouse which received the ^{89}Zr-aTCRmu-F(ab')$_2$. Tracer uptake of tumor in percent of injected dose per gram (%ID/g) was in the mice which received the Nanobody 0.33%ID/g and in the control mouse 2.9%ID/g.

After imaging, mice were sacrificed, and biodistribution analysis was performed in a gamma counter to confirm tracer distribution within the different organs.

Biodistribution confirmed tracer uptake derived from PET images. Nanobody uptake in tumor was higher compared to most other tissues excluding kidney, bladder, and bones.

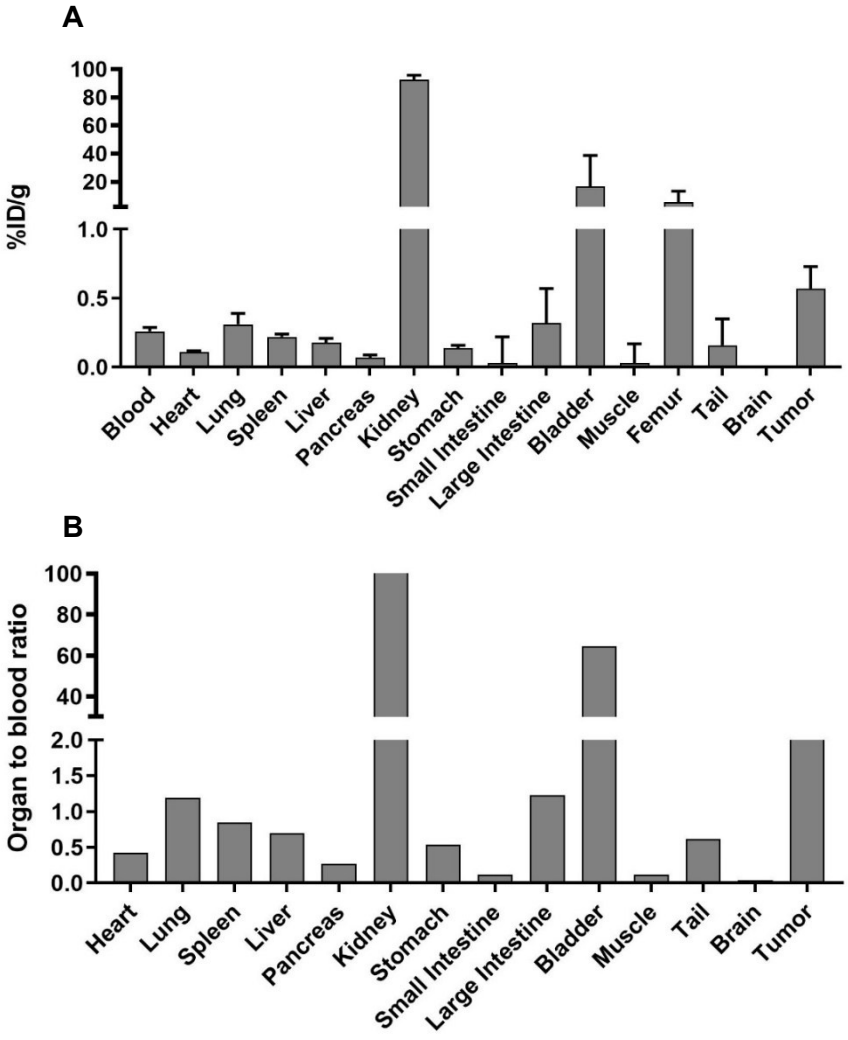

Figure 22: Biodistribution analysis after imaging
Quantitative analysis in indicated organs is shown 90 minutes after Nanobody injection. Mice were sacrificed and organs were separately analyzed in a gamma counter. Data are depicted for the Nanobody mice (n=2).
(A) Mean and standard deviation of %ID/g are shown
(B) Organ to blood ratio is shown and was calculated directly from previously shown means.
Data and figures were generated in cooperation with Dario Gosmann and Lisa Russeli

Calculation of organ-to-blood ratio fortified this observation, as tumor showed specific accumulation to a doubled level. Due to the early imaging time point after application, kidneys and bladder showed very high tracer accumulation as Nanobodies were mainly eliminated by renal secretion.

Organs were then prepared for flow cytometry analysis, and single-cell suspensions were stained for CD3 and polyhistidine-tag to validate previous observations. Data were then gated for CD3+ of viable and GFP- cells or His-tag+ of CD3+, viable, and GFP- cells.

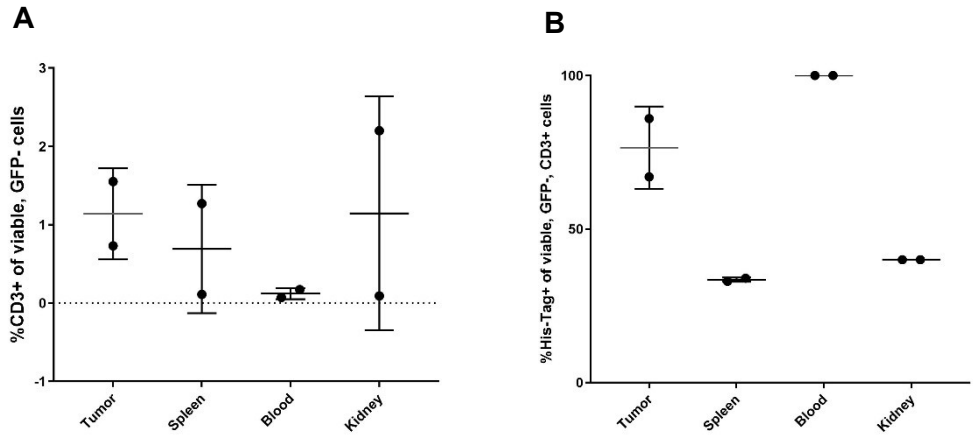

Figure 23: Flow cytometry analysis of imaging experiment
Single cell suspensions were produced from organs, blood, and tumors, then washed with PBS for flow cytometry analysis. Representative plots with mean and standard deviation are shown (n=2).
(A) Single cell suspensions of respective tissues were stained for CD3. Fraction of CD3+ of viable and GFP- cells are shown in percentages.
(B) Single cell suspensions of respective tissues were stained for CD3 and polyhistidine-tag. Fraction of His-tag+ of CD3+, viable and GFP- cells are shown in percentages.
Data and figures were generated in cooperation with Dario Gosmann and Lisa Russeli

Flow cytometry data showed homogenous distribution of T cells in respective tissues except in blood, despite intratumoral injection. Nanobodies also attached detected T cells to a significant fraction as staining for polyhistidine-tag revealed. Tumor tissue showed even higher ratios of Nanobodies attached to T cells than other solid tissue such as kidney and spleen. In the blood only very low cell counts could be detected constraining comparability.

Resumed, targeting CD2 as a pan-T cell marker showed satisfying results, as good tracer accumulation at tumor site was visible. Ex vivo biodistribution and flow cytometry analysis could also confirm specific enrichment. The high tagging efficiency of reactive T cells in the tumor prompted superior potential for tracing activated T cells. This preliminary imaging experiment with the CD2-Nb was pivotal for further investigations also concerning the CD7-Nb.

6. Discussion

6.1. Tracking T cell activity

Visualization of T cell responses has gained importance over the last years as T cells play a crucial role in tumor control. Their presence, distribution, and expressed biomarkers within tumor lesions are associated with therapy response (Tumeh, Harview et al. 2014, Topalian, Taube et al. 2016, Huang, Postow et al. 2017). Novel therapy approaches have increasingly been focussing on boosting T cell activity and have already shown promising results in clinical practice. However, many mechanisms in tumor recognition and rejection remain unclear and the Patients' response to immunotherapies is still highly individual. Therefore, influencing factors must be identified (Chen and Mellman 2017, Zhang and Zhang 2020, Finck, Blanchard et al. 2022, Oliveira and Wu 2023). Several markers can help in the selection process to identify susceptible patient subsets for immune checkpoint inhibition. Programmed death-ligand 1 (PDL1) expression, T cell marker expression profile, or mutational burden of the tumor can help but not precisely predict response to immunotherapies (Havel, Chowell and Chan 2019, Lee and Ruppin 2019, Chang, Pelosof et al. 2021).

Conventional assessment criteria for therapy response such as established RECIST are inadequate for immunotherapies. Thus, revised iRECIST were developed and have shown improved correlations regarding survival (Seymour, Bogaerts et al. 2017, Park, Kim et al. 2021). Still, clinically applicable monitoring techniques, which allow early and reliable detection of therapy response, are lacking for these therapies, although they may also help to further understand pharmacokinetics and pharmacodynamics of immunotherapies. Moreover, sensitive imaging technologies for tracking T cell activity would provide insights into T cell migration, enabling possible precise predictive biomarkers of treatment response to avoid premature termination (Masopust and Schenkel 2013). As response to immunotherapies is correlated with T cell density, it seems reasonable to link the specific signal of these biomarkers to therapy efficiency (Tumeh, Harview et al. 2014, Sommermeyer, Hudecek et al. 2016, Huang, Postow et al. 2017, Mayer, Mall et al. 2018).

Imaging of transgenic T cells such as CAR-T cells has been investigated over the last years focussing on reporter genes as they can be quickly introduced with the CAR. This solution allows longitudinal imaging as reporter genes are expressed continuously, and

probe can be repeatedly administered. A combination of reporter gene herpes simplex virus type-1 thymidine kinase (HSV1-TK) and 9-[4-[^{18}F]fluoro-3-(hydroxymethyl)butyl]guanine ([^{18}F]FHBG) showed specific enrichment in glioma patients after CAR therapy (Keu, Witney et al. 2017). HSV1-TK is a viral protein that is potentially immunogenic as other reporter genes (McCracken, Vatakis et al. 2015). Reporter genes of human origin, such as the sodium/iodide symporter, may be an alternative but have a high background in tissue with physiological expression (Emami-Shahri, Foster et al. 2018, Krebs, Ahad et al. 2018, Hu and Huang 2020). Latest developments have been trying to extend the function of the reporter gene to a suicide gene to limit adverse events, as shown with a modified HSV1-TK gene (Murty, Labanieh et al. 2020). Although reporter genes allow imaging over a long time and avoid dilution of signal through cell division, genetic modification with potential immunogenicity is not desirable. Antibody-based imaging targeting transgenic TCRs is a promising approach and showed high sensitivity allowing direct quantification of T cells with a Zirconium-89 labeled F(ab')$_2$ fragment directed against the murine TCR beta domain (Mall, Yusufi et al. 2016, Yusufi, Mall et al. 2017). However, this allows exclusive imaging of engineered T cells and is therefore unsuitable as an universal tracer for T cell activity. Direct labeling molecules for T cells such as ^{111}In-tropolonate, ^{89}Zr-oxine/^{89}Zr-DFO, or GNP-^{64}Cu/PEG2000 require ex-vivo modifications and allow only short-term observation (Parente-Pereira, Burnet et al. 2011, Bhatnagar, Li et al. 2013, Lee, Soh et al. 2020, Sta Maria, Khawli et al. 2021, Leland, Kumar et al. 2023). For a clinically feasible approach, non-invasive in vivo labeling is favored. Moreover, T cell migration and tumor rejection during immunotherapies require extended observation periods. Immuno-PET imaging strategies allow long-term monitoring which is independent from therapy regiments. The constantly evolving field of immunotherapies and an increasing number of targeting systems suggest universal target structures on T cells regarding transferability to other approaches. (Waldman, Fritz and Lenardo 2020). In this study, we developed camelid-derived Nanobodies directed against pan-T cell markers CD2 and CD7 as cross-therapy tracers. Tracers were evaluated in an adoptive T cell transfer setting, using CD8+ T cells transduced with MPO-specific TCR2.5D6 (Klar, Schober et al. 2014). The AML cell line ML2 produces MPO endogenously and was transduced with the TCR-specific HLA HLAB*07:02 to generate a suitable tumor model for in vivo and in vitro assessments (Mall, Yusufi et al. 2016, Mayer, Mall et al. 2018).

6.2. Target structures on T cells

Different targets to monitor T cell response are currently evaluated in preclinical or clinical settings. PD1 and the ligand PDL1 with over 50 individual tracers are the most used structures as their function is well-characterized. Various therapeutic antibodies are already in clinical practice (Natarajan, Mayer et al. 2017, Bensch, van der Veen et al. 2018, Natarajan, Patel et al. 2018, Niemeijer, Leung et al. 2018, Xing, Chand et al. 2019, Kramer and Dimitrakopoulou-Strauss 2022). ^{89}Zr-Nivolumab and ^{89}Zr-Atezolizumab uptake in tumor lesions correlated well with patients' response showing that patients with the highest SUV were more likely to have complete remission. ^{89}Zr-Atezolizumab showed even better discrimination of patient outcome than immunohistochemistry (Bensch, van der Veen et al. 2018, Niemeijer, Leung et al. 2018). However, both markers are also expressed on other cell populations, reducing their specificity (Chen, Crabill et al. 2019, Liu, Zugazagoitia et al. 2020). Moreover, current tracers are mainly labeled to therapeutic antibodies with modulatory effects and are restricted to monitoring in context of immune checkpoint inhibition. CD8, as a marker of effector T cells, has been identified as a predictive marker for therapy response as it indicates infiltration of cytotoxic, tumor-specific T cells (Zhang, Conejo-Garcia et al. 2003, Herbst, Soria et al. 2014, Rosenberg, Hoffman-Censits et al. 2016, Sun, Limkin et al. 2018). As a result, numerous studies targeting CD8 as an imaging marker have been published. Some of them advanced to clinical studies (Kristensen, Fröhlich et al. 2019, Pandit-Taskar, Postow et al. 2020, Kasten, Houson et al. 2021, Zhao, Wang et al. 2021, Farwell, Gamache et al. 2022, Kist de Ruijter, van de Donk et al. 2022). Visualization of CD8 positive T cells in tumors with different entities was successfully performed in human trial and matched with immunohistochemistry from biopsies. Their pretherapeutic detection correlated with overall survival, underlining the potential as a predictive biomarker in preference to invasive biopsies (Kist de Ruijter, van de Donk et al. 2022). Yet, there was considerable heterogeneity within and between patients during ICI, and it did not allow proper evaluation regarding response to therapy. Furthermore, only one imaging during ICI at day 30 was performed in this study, lacking initial stages of T cell dynamics due to tracer and radionuclide characteristics. CD8 and other targets, such as IL2 receptor and CD4, have also enabled imaging of T cells in the context of immunotherapy but are restricted to subpopulations (Kristensen, Fröhlich et al. 2019, van de Donk, Wind et al. 2021).

To include most T cell subpopulations, the pan-T cell markers CD2 and CD7 were selected as targets for our tracers. CD2 functions as a receptor protein on T cells,

thymocytes, and natural killer cells (NK), in which it undertakes different functions and regulatory effects (Howard, Ledbetter et al. 1981, Scott, Bolender et al. 1989). In the context of tumor rejection and activation of cytotoxic T cells, CD2 surface expression is upregulated (Rooney, Shukla et al. 2015, Mayer, Mall et al. 2018). Three different epitopes on CD2, which were previously named T11.1, T11.2, T11.3 seem to be the most relevant target structures for antibodies (Meuer, Hussey et al. 1984, Brottier, Boumsell et al. 1985, Peterson and Seed 1987, Moingeon, Chang et al. 1989). T11.1 plays a vital role in cell adhesion and the activation process of T cells as it interacts with the Lymphocyte function-associated antigen 3 (LFA-3) (Selvaraj, Plunkett et al. 1987, Bierer, Peterson et al. 1988). Studies showed that T11.3 is only presented on activated T cells. Antibodies targeting T11.3 together with antibodies targeting one of the other epitopes can induce further activation, whereas targeting T11.1 and T11.2 alone had no effect (Meuer, Hussey et al. 1984, Hünig, Tiefenthaler et al. 1987, Moingeon, Chang et al. 1989). However, for our CD2-specific Nanobody, epitope blocking by several commercial antibodies to evaluate target specificity was impossible. Only minor blocking had been observed using the monoclonal antibody HIK27, which seems to target T11.2 (van Kemenade, Tellegen et al. 1994). Lack of blocking by conventional monoclonal antibodies may be attributable to the small size of Nanobodies, enabling them to reach a wide range of antigens in tight or concave sections that are inaccessible for whole antibody constructs (Hamers-Casterman, Atarhouch et al. 1993, Jovčevska and Muyldermans 2020, Jin, Odongo et al. 2023). CD7 is mainly expressed on early progenitor cells of lymphoid and myeloid origin but also mature T cells and NK cells (Lobach, Hensley et al. 1985, Bárcena, Muench et al. 1995, Stillwell and Bierer 2001). Small subpopulations of T cells, especially CD4+ memory cells, can lose CD7 expression after multiple stimulations, whereas native cells have a twofold higher expression (Akbar, Salmon and Janossy 1991, Shimizu, van Seventer et al. 1992, Sperling, Auger et al. 1996). T cell-derived malignancies generally express CD7 on a high level (Lewis, Cruse et al. 2006, Cortelazzo, Ponzoni et al. 2011, Png, Vinanica et al. 2017). Its function is currently not fully elucidated but seems to play an essential role in T cell activation, and its targeting with antibodies in conjunction with CD3 can cause proliferation and cytokine production (Carrera, Rincón et al. 1988, Jung, Roy and Chakkalath 1992, Chan, Reynolds and Shimizu 1994, Lazarovits, Osman et al. 1994). A recent study investigated the consequences of CD7 knockout in mice and CD7 blockage in human T cells. Interestingly, CD7 knockout or blockage did not impair hematopoietic development in mice and did not restrain infiltration capacity of donor cells. Nevertheless, infiltration capacity of CD8+ T cells in CD7-deficient mice was significantly affected, and tumor

growth increased (Sheng, Zhang et al. 2023). Currently, CD7 is already used as a therapeutic target mainly for CAR therapy of T cell malignancies in clinical trials (Zhang, Fu et al. 2021, Chiesa, Georgiadis et al. 2023). Moreover, Alefacept, a CD2-blocking fusion protein, has been approved by the FDA for the treatment of severe psoriasis, suppressing autoimmune T cell activity (Sugiyama, McCormick et al. 2008).

The broad expression of CD2 and CD7 among T cell subpopulations and their almost exclusive appearance on T cells makes them a highly favorable target for us regarding a wide-range monitoring approach. Enhanced expression on activated T cells emphasizes their eligibility for tracing tumor-specific T cells (Mayer, Mall et al. 2018). The specificity of our Nanobodies was confirmed in vitro on antigen-transduced lymphoblastic lymphoma cell line U698M, missing endogenous CD2 and CD7 expression, and epitope blocking by monoclonal antibodies. As epitope blocking for our CD2-Nb remained challenging, we transfected the CD2 expressing T cell leukemia cell line, Jurkat E6.1, with RNPs targeting CD2 locus, and established a stable knockout cell line as negative control. In vivo tracking was then verified in our ACT mice model with intratumoral or intravenously injection of TCR2.5D6-transgenic T cells. In tumor rejection study, ex vivo flow cytometry analysis showed successful Nanobody binding on CD3+ cells. However, binding of CD7-Nb to T cells remained under the level of CD2-Nb. Lower or lost CD7 expression in effector cells, which was mainly observed in CD4+ cells so far, may be a factor that needs further investigation (Akbar, Salmon and Janossy 1991, Sperling, Auger et al. 1996). Comparability was constrained because only one mouse for each group was analyzed. In further studies, groups should be enlarged to allow statistical analyses. Our preliminary imaging experiment data could be confirmed for our labeled CD2-Nb. PET/MRI imaging detected a clear signal at the tumor side, followed by ex vivo analysis with an increased tumor-to-blood ratio.

6.3. Tracer-induced T cell impairment

The interaction between antibodies and cells can lead to multiple effects, ranging from blocking surface molecules, inducing pathways, and secretion of effector molecules to cell death. The latter is mainly used for therapeutic monoclonal antibodies, such as Trastuzumab or Rituximab commonly used in clinical practice, which can be carried out by effector cells, called antibody-dependent cell-mediated cytotoxicity (ADCC) or by humoral response, called complement-dependent cytotoxicity (CDC) (Maloney, Smith and Rose 2002, Meyer, Leusen and Boross 2014, Killock 2017, Wang, Mathieu and

Brezski 2018). However, these effects are mediated through Fc domains activating Fc gamma receptors (FcγRs), which are removed in smaller antibody fragments. T cell activation, reduced proliferation or depletion, possibly by overstimulation, has been shown for various antibodies targeting T cell antigens (Cobbold, Jayasuriya et al. 1984, Anasetti, Martin et al. 1992, Loubaki, Tremblay and Bazin 2013, Griessinger, Maurer et al. 2015, Freise, Zettlitz et al. 2017). Moreover, activation and apoptosis have also been described for targeting CD2 and CD7 (Hünig, Tiefenthaler et al. 1987, Moingeon, Chang et al. 1989, Jung, Roy and Chakkalath 1992, Mayer, Mall et al. 2018). Hence, evolution of T cell tracers must be carefully accompanied concerning their effects on T cell functionality in vitro and in vivo. No or minor effects in vitro do not exclude negative impact in vivo, and the risk for side effects such as cytokine release syndrome needs to be considered. (Mayer, Mall et al. 2018, Wang and Han 2018, Gosmann, Russelli et al. 2022). Targeting of T cells by tracer constructs in vivo has been reported to impair proliferation capacity or induce a shift in T cell subpopulations (Freise, Zettlitz et al. 2017, Beckford Vera, Smith et al. 2018, Lee, Soh et al. 2020). Intriguingly, an anti-CD3 and an anti-CD4 antibody, both labeled with ^{89}Zr, showed temporary decrease of the CD4+ T cell population and a subsequent increase of CD8+ cells after tracer administration (Freise, Zettlitz et al. 2017, Beckford Vera, Smith et al. 2018). Unfortunately, T cell functionality and tumor rejection capacity have not been assessed as it is unclear if a temporary shift of subpopulations leads to sustained impairment. Nevertheless, the role of radioactivity regarding T cell damage may be relevant and needs to be considered. T cells were exposed to different amounts of ^{89}Zr-labeled tracer monitoring the DSB-marker γH2AX regarding DNA damage by Yusufi and colleagues (Yusufi, Mall et al. 2017). Their study revealed that only considerably higher amounts than normally used led to double-strand breaks in vitro. Moreover, IHC analysis after in vivo application showed no evidence of T cell depletion, whereas high activity of γH2AX and cleaved Caspase-3 was detected in tumor cells.

As tracers for repetitive T cell monitoring in different settings should not have any impact on T cells and should not influence therapy success, we intensively investigated our tracers regarding T cell impairment. Cytotoxicity assay and dynamic, impedance-based functionality testing in the xCELLigence system were performed by other lab members. We added a multi-cytokine assay to investigate activation patterns in presence of Nanobodies and tumor cells. The coculture was set up in a Nanobody-saturated environment with the acute promyelocytic leukemia cell line NB4 and the acute myelomonocytic leukemia cell line ML2 transduced with the corresponding HLA-B7 to

the TCR2.5D6 and transduced with a mismatched HLA construct HLA-B15. The mismatched setting functioned as a negative control. It showed very low to no cytokine secretion. Thus, we assumed that Nanobodies do not lead to major unspecific stimulation of inactive T cells. In the matched settings, cytokine levels were not entirely consistent, and we observed marginal higher secretion in Nanobody presence, suggesting a costimulatory impact. Unspecific isotype control also showed increased secretion. A general increase in Nanobody conditions can be attributed to unsterile production or minimal immunogenic potential, although other determinants need to be ruled out. No specific signal could be detected for IL6, which is used as a marker for cytokine release syndrome (Maude, Frey et al. 2014, Porter, Hwang et al. 2015). Still, differences were not significant, so deeper evaluation, especially regarding the specific impact on activated T cells on tumor cells, is necessary. In our in vivo setting, we studied long-term influence on tumor rejection as in vitro data are not always fully transferable, and in vivo settings can differ substantially (Mayer, Mall et al. 2018). Analysis of tumor sizes revealed failed tumor rejection in mice receiving anti-CD2 $F(ab')_2$ fragments as described before (Mayer, Mall et al. 2018), while our Nanobodies did not affect decrease of tumor sizes after adoptive T cell transfer as compared to PBS and isotype control during our observation. Ex vivo analysis proved specific accumulation of T cells in ML2-B7 tumors and labeling of tumor-infiltrating T cells by our Nanobodies. For our CD7-specific Nanobody, labeling efficiency was lower, and less T cells could be detected at tumor site. Failed T cell transfer or apoptotic T cells could be a contributing factor as only viable cells were stained. This issue needs to be addressed in further developments and larger groups need to be analyzed. In addition, impact of whole, labeled tracer constructs 68Ga-aCD2/7-Nbs were not assessed, although chelator-introduction was not described to increase immunogenicity (Perico, Chinol et al. 2001, Ackaert, Smiejkowska et al. 2021).

6.4. Nanobody as tracer scaffold

Monoclonal antibodies are regularly used as vehicle for ImmunoPET applications (Knowles and Wu 2012, Wei, Rosenkrans et al. 2020). However, full-length antibodies suffer from disadvantages regarding their characteristics, which present significant challenges for efficient, clinically applicable imaging. Their weight of 150kD exceeds the renal clearance threshold of 60kD. Together with the interaction of neonatal Fc receptors (FcRn), which are mainly expressed on endothelial cells, they lead to prolonged serum half-life of weeks by protecting IgGs from endocytosis and lysosomal degradation in endothelial cells (Ward, Zhou et al. 2003, Suzuki, Ishii-Watabe et al. 2010, Wei,

Rosenkrans et al. 2020). High mass also reduces their ability to efficiently penetrate tumor tissue as studies suggested that only minimal percentages of total injected dose reaches the target side (Epenetos, Snook et al. 1986, Kolkman and Law 2010). In addition, the so-called binding site barrier effect impedes penetration of high-affinity mAbs, meaning that binding of first encountered antigen is strong enough to slow down further intratumoral diffusion, which leads to more substantial accumulation in peripheral areas (Weinstein and van Osdol 1992, Adams, Schier et al. 2001). This results in prolonged waiting times for imaging because of strong background signals and the usage of long-lived isotopes, both unfavorable for patients (Knowles and Wu 2012, De Vos, Devoogdt et al. 2013). The enhanced permeability and retention phenomenon, which enables large molecules (>40kD) to accumulate in tumor lesions due to leaky tumor vessels and insufficient lymph drainage, further contribute to complicated repetitive imaging and the risk of false-positive detection (Fang, Nakamura and Maeda 2011). In contrast, the microvascular structure and deviating interstitial pressure in tumor tissue limit distribution of large molecules due to missing convection, and transportation happens mainly through diffusion, which is negatively correlated to size (Jain 1990, Jain 1994, Thurber, Schmidt and Wittrup 2008). Therefore, Nanobodies showed superior penetration and homogenous distribution after few hours in tumor lesions, whereas full-length antibodies did not reach the same homogeneity after 24 hours in vivo. Moreover, higher tumor-to-background ratios could be detected for Nanobodies 6 hours after administration and already decreasing levels after 24 hours, favoring their usage for early and repetitive imaging (Oliveira, van Dongen et al. 2012, Bannas, Lenz et al. 2015, Debie, Lafont et al. 2020). On a microscopic level, Debie and colleagues showed that specific accumulation of monomeric Nanobodies in tumor lesions occurs minutes after intravenous application, and non-specific enrichment is mainly eliminated after 20 minutes. Due to slower uptake and restricted diffusion, dimeric or bivalent Nanobodies showed no overall improved characteristics. However, maximal uptake of mAbs was higher than Nanobodies but was only reached after 24 hours and showed heterogenous distribution (Debie, Lafont et al. 2020). This is supported by our study as PET/MRI imaging, and ex vivo analysis revealed specific accumulation at tumor side 90 minutes after injection, whereas larger constructs, such as our $F(ab')_2$ fragment, enabled optimal imaging at later time points (Dijkers, Oude Munnink et al. 2010, Mall, Yusufi et al. 2016, Niemeijer, Leung et al. 2018). Moreover, other studies, preclinical and clinical, using Nanobodies as tracers for nuclear imaging also suggested early time points for optimal imaging (Keyaerts, Xavier et al. 2016, Xavier, Blykers et al. 2016, Xing, Chand et al. 2019, Lv, Sun et al. 2020).

Another aspect that comes with reduced plasma half-life and rapid on-target accumulation is the possible usage of short-lived radionuclides. As radionuclide half-life should be roughly matched with antibody half-life, mAbs are commonly labeled with ^{89}Zr ($t_{1/2}$ =78.41h) due to technical advantages and comparably cheap production (Moek, Giesen et al. 2017, Boros and Holland 2018). However, the long half-life leads to higher radiation loads between 20 to 40mSv for single administration (Yoon, Park et al. 2020). Short-lived radioisotopes such as 68Ga (t1/2 = 67.71min) and 18F (t1/2 =109.77min) are favored for smaller molecules, which diminish patients' exposure to radiation. ^{68}Ga can be quickly produced in a generator, enabling highly flexible on-demand production in clinical practice. However, ^{18}F, as a "low-energy" positron emitter, allows more granular resolution of small structures as well as reducing hazard of cellular toxicity (Carter, Kesner et al. 2020, Gosmann, Russelli et al. 2022, Lepareur 2022). Nevertheless, clinical relevance of slight differences in positron energy is still questionable and needs further studies regarding tracer optimization (Yusufi, Mall et al. 2017, Carter, Kesner et al. 2020). Linking Nanobodies to a chelator or labeling procedures are facilitated due to their natural heat resistance, as for good radiochemical yields and favorable reaction kinetics, higher temperatures are required (Breeman, De Jong et al. 2003, Sosabowski and Mather 2006, Ebenhan, Chadwick et al. 2014). Compared to other antibody constructs such as conventional antibodies and scFv, studies reported superior thermal stability at 90°C and above for Nanobodies (van der Linden, Frenken et al. 1999, Goldman, Anderson et al. 2006). Their natural resistance is attributed to a refolding process after heat denaturation, which was observed for some Nanobodies (Pérez, Renisio et al. 2001, Ewert, Cambillau et al. 2002). However, Nanobody aggregation under rough conditions frequently obstructs refolding (Kunz, Zinner et al. 2018). Thus, different engineering strategies, such as disulfide bonds, have been proposed to further improve their stability (Goldman, Liu et al. 2017). Our findings support the general heat resistance of our Nanobodies, as significant alterations of binding capacity have been observed at elevated temperatures (90°C) after more than 1h in flow cytometry. For incubation at lower temperatures, no impairment could be detected. As the environment during radiochemical labeling is challenging for protein structures, stability needs to be further assessed after labeling procedure.

As camelid-derived antibodies, Nanobodies comprise a particular risk of immunogenicity, although the VHH sequence is mainly equivalent to the human VH region (Kolkman and Law 2010, Klarenbeek, El Mazouari et al. 2015). Some studies reported possible toxicity due to immunogenic response and observed anti-VH autoantibodies in human trials

(Holland, Wurthner et al. 2013, Papadopoulos, Isaacs et al. 2015). Holland and colleagues showed that the complex of autoantibodies and the respective Nanobody led to activation and cytokine release of immune cells in vitro. Moreover, after infusion of Nanobody in autoantibody-positive patients, signs of cytokine release were observed (Holland, Wurthner et al. 2013). Strategies for humanization of Nanobodies are available but do not seem to eliminate the whole risk as a human trial with a humanized anti-DR5 Nanobody showed, which was terminated after observation of significant liver toxicity in some patients (Vincke, Loris et al. 2009, Papadopoulos, Isaacs et al. 2015). However, numerous studies have been published showing no adverse effects regarding immunogenicity (Keyaerts, Xavier et al. 2016, Xing, Chand et al. 2019, Papp, Weinberg et al. 2021, Peyvandi, Cataland et al. 2021). This issue needs to be carefully observed in advancing studies and could be assessed in immunocompetent mice or first human trials (Ackaert, Smiejkowska et al. 2021).

The simple structure of Nanobodies allows a straightforward production in microbial systems with high yields, as proposed in our study. The most commonly used approach is the extraction of periplasm from E.coli following immobilized metal affinity chromatography (Salema and Fernández 2013). This is a fundamental advantage for clinical translation requiring large-scale production, as mammalian cell production is still way more cost-intensive (Kolkman and Law 2010). Nevertheless, possible engineering of Nanobodies for different purposes results in more complex structures, which could make other production systems vital (de Marco 2020).

6.5. Future challenges and developments

In the biodistribution analysis of our preliminary imaging study we observed high accumulation in kidneys and bladder due to the small size below the clearance threshold, which is commonly observed in Nanobody imaging studies (Gainkam, Huang et al. 2008, Keyaerts, Xavier et al. 2016, Krasniqi, D'Huyvetter et al. 2017). This effect is enhanced by unspecific endocytosis, leading to kidney retention. Recently, megalin and cubilin have been identified as receptors that mediate multifunctional reabsorption and seem to take part in the retention process of Nanobodies (Christensen and Birn 2002, Gainkam, Huang et al. 2008). Renal accumulation can be reduced by coadministration of competitive molecules such as succinylated gelatin or basic amino acids (Hammond, Wade et al. 1993, Pimm and Gribben 1994, Erik, Jack et al. 2006). However, side effects such as anaphylactic shock occurred in patients to a small number and need to be

considered. Other prevention strategies require tracer modifications, such as removal of polyhistidine-tag, but should be anticipated as high kidney retention may lead to renal failure and impede imaging of structures close to the urinary tract (Erik, Marion de et al. 2010). Xavier and colleagues reported that the exchange of ^{68}Ga with ^{18}F resulted in remarkably low kidney retention, attributing it to faster elimination of catabolites (Xavier, Blykers et al. 2016). These findings are supported by other studies using ^{18}F-labeled tracers (Olafsen, Sirk et al. 2012, Blykers, Schoonooghe et al. 2015). However, individual studies are necessary to assess the benefit of these approaches for our tracers.

Modifications, which reduce renal retention, also have a benefit regarding tracer uptake at tumor side and organ-to-blood ratios, allowing to address two problems at the same time as we observed low tracer uptake in lesions compared to other studies (Xavier, Vaneycken et al. 2013, Lv, Sun et al. 2020). Removing the polyhistidine-tag of an anti-HER2 Nanobody resulted in a 60% reduction of renal uptake and significantly improved biodistribution concerning tumor uptake (3.13 ± 0.06 vs. 4.34 ± 0.90 %IA/g) in a preclinical mouse model (Xavier, Vaneycken et al. 2013). Moreover, injected amount of tracer correlated with tumor uptake, meaning that increasing amounts reduced unspecific accumulation, whereas target-side uptake was improved (Xavier, Vaneycken et al. 2013). In studies, impact of different amounts and time points for imaging should be evaluated as they are crucial for successful in vivo detection with good noise-to-background ratios (Bannas, Lenz et al. 2015). Strategies like PEGylation or coupling Nanobodies with albumin may increase tumor uptake but prolong serum half-life and kidney retention, undermining their potential for early imaging (Lecocq, De Vlaeminck et al. 2019). We generally observed low accumulation in spleen assignable to intratumoral T cell injection but should be expected in further imaging studies because of T cell homing in lymphoid tissue (Williams and Butcher 1997). High uptake in lymph nodes, spleen, bone marrow, and other lymphoid organs is in accordance with observations from other studies and contributes to background signal (Mall, Yusufi et al. 2016, Pandit-Taskar, Postow et al. 2020). Therefore, differentiation of tumor-specific T cells and unspecific accumulation can be hampered, but its relevance needs to be evaluated in immunocompetent mice or patients.

To assess whether our tracers meet the requirements to predict the response to immunotherapies, further studies are necessary. Although presence of T cells in tumors after initiation of immunotherapy is associated with response, it is still of interest to analyze T cell response in depth (Sommermeyer, Hudecek et al. 2016, Huang, Postow et al. 2017). Correlation of detailed PET images with ex vivo analysis like IHC and

autoradiography to identify patterns or areas of high T cell density within tumors may allow profound insight into T cell dynamics (Mall, Yusufi et al. 2016, Kist de Ruijter, van de Donk et al. 2022). Developing a tracer-based biomarker requires additional analysis of different settings with repetitive imaging concerning tumor entity and type of immunotherapy. Kist de Ruijter and colleagues showed for their one-armed, CD8-specific antibody that response patterns differ significantly between tumor entities and within patients, revealing interlesional heterogeneity in responding patients, which underlines the variability and complexity of systemic immune response (Kist de Ruijter, van de Donk et al. 2022). They stated the lack of repetitive imaging during immunotherapy in their study as they only provided a snapshot before ICI and 30 days after therapy began due to tracer characteristics, which should be feasible with our tracers. Mutations of PTPRD and PTPRT, which are part of the JAK-STAT pathway, have been analyzed as prediction markers for immunotherapy response. While an apparent coherence could be detected for an anti-PD1/PDL1 therapy, a similar trend could not be observed for anti-CTLA4 treatment (Wang, Ji et al. 2023). Likewise, a varying relevance for different therapies was observed for the marker MAGE-A (Shukla, Bachireddy et al. 2018). Hence, our tracer should be analyzed in different immunotherapy settings, as results in an ATC approach are not fully transferable to other techniques.

Applications other than PET imaging for our tracers are conceivable, as CD2 and especially CD7 are broadly expressed on most T cell subpopulations, including T cell malignancies (Lewis, Cruse et al. 2006, Png, Vinanica et al. 2017, Mayer, Mall et al. 2018). CD7 has been successfully targeted for CAR therapy in refractory T cell malignancies in a clinical trial using a Nanobody-based recognition domain, which could also be an intriguing development option for CD2 (Zhang, Fu et al. 2021, Chiesa, Georgiadis et al. 2023). For our tracers, a theranostic approach could be taken into consideration when labeled with other radionuclides like ^{131}I or ^{177}Lu as shown for a CD20-specific Nanobody in patients who have non-Hodgkin lymphoma or an anti-HER2 Nanobody in breast cancer patients (Krasniqi, D'Huyvetter et al. 2017, D'Huyvetter, Vos et al. 2021). As a versatile platform, further engineering would allow bispecific Nanobodies targeting tumor antigen and CD2/CD7 at the same time to activate and redirect tumor response of effector cells, which has already been reported for a mAb targeting CD2 together with EGFR (Wild, Strittmatter et al. 1999). First Nanobody-based studies have also published their results on bispecific constructs targeting other tumor and T cell antigens (de Bruin, Veluchamy et al. 2017, Liu, Ao et al. 2022).

7. References

Ackaert, C., N. Smiejkowska, C. Xavier, Y. G. J. Sterckx, S. Denies, B. Stijlemans, Y. Elkrim, N. Devoogdt, V. Caveliers, T. Lahoutte, S. Muyldermans, K. Breckpot and M. Keyaerts (2021). "Immunogenicity Risk Profile of Nanobodies." Front Immunol **12**: 632687.

Adams, G. P., R. Schier, A. M. McCall, H. H. Simmons, E. M. Horak, R. K. Alpaugh, J. D. Marks and L. M. Weiner (2001). "High affinity restricts the localization and tumor penetration of single-chain fv antibody molecules." Cancer Res **61**(12): 4750-4755.

Ahrens, E. T. and J. W. Bulte (2013). "Tracking immune cells in vivo using magnetic resonance imaging." Nat Rev Immunol **13**(10): 755-763.

Akbar, A. N., M. Salmon and G. Janossy (1991). "The synergy between naive and memory T cells during activation." Immunol Today **12**(6): 184-188.

Alam, I. S., A. T. Mayer, I. Sagiv-Barfi, K. Wang, O. Vermesh, D. K. Czerwinski, E. M. Johnson, M. L. James, R. Levy and S. S. Gambhir (2018). "Imaging activated T cells predicts response to cancer vaccines." J Clin Invest **128**(6): 2569-2580.

Anasetti, C., P. J. Martin, R. Storb, F. R. Appelbaum, P. G. Beatty, J. Davis, K. Doney, H. F. Hill, P. Stewart, K. M. Sullivan and et al. (1992). "Treatment of acute graft-versus-host disease with a nonmitogenic anti-CD3 monoclonal antibody." Transplantation **54**(5): 844-851.

Andtbacka, R. H. I., F. Collichio, K. J. Harrington, M. R. Middleton, G. Downey, K. Öhrling and H. L. Kaufman (2019). "Final analyses of OPTiM: a randomized phase III trial of talimogene laherparepvec versus granulocyte-macrophage colony-stimulating factor in unresectable stage III-IV melanoma." J Immunother Cancer **7**(1): 145.

Bannas, P., A. Lenz, V. Kunick, L. Well, W. Fumey, B. Rissiek, F. Haag, J. Schmid, K. Schütze, A. Eichhoff, M. Trepel, G. Adam, H. Ittrich and F. Koch-Nolte (2015). "Molecular imaging of tumors with nanobodies and antibodies: Timing and dosage are crucial factors for improved in vivo detection." Contrast Media & Molecular Imaging **10**(5): 367-378.

Bar-Shir, A., G. Liu, K. W. Chan, N. Oskolkov, X. Song, N. N. Yadav, P. Walczak, M. T. McMahon, P. C. van Zijl, J. W. Bulte and A. A. Gilad (2014). "Human protamine-1 as an MRI reporter gene based on chemical exchange." ACS Chem Biol **9**(1): 134-138.

Bárcena, A., M. O. Muench, M. G. Roncarolo and H. Spits (1995). "Tracing the expression of CD7 and other antigens during T- and myeloid-cell differentiation in the human fetal liver and thymus." Leuk Lymphoma **17**(1-2): 1-11.

Beckford Vera, D. R., C. C. Smith, L. M. Bixby, D. M. Glatt, S. S. Dunn, R. Saito, W. Y. Kim, J. S. Serody, B. G. Vincent and M. C. Parrott (2018). "Immuno-PET imaging of tumor-infiltrating lymphocytes using zirconium-89 radiolabeled anti-CD3 antibody in immune-competent mice bearing syngeneic tumors." PLoS One **13**(3): e0193832.

Benedict, C. A., A. J. MacKrell and W. F. Anderson (1997). "Determination of the binding affinity of an anti-CD34 single-chain antibody using a novel, flow cytometry based assay." J Immunol Methods **201**(2): 223-231.

Benmebarek, M. R., B. L. Cadilha, M. Herrmann, S. Lesch, S. Schmitt, S. Stoiber, A. Darwich, C. Augsberger, B. Brauchle, L. Rohrbacher, A. Oner, M. Seifert, M. Schwerdtfeger, A. Gottschlich, F. Rataj, N. C. Fenn, C. Klein, M. Subklewe, S. Endres, K. P. Hopfner and S. Kobold (2021). "A modular and controllable T cell therapy platform for acute myeloid leukemia." Leukemia: 1-15.

Bensch, F., E. L. van der Veen, M. N. Lub-de Hooge, A. Jorritsma-Smit, R. Boellaard, I. C. Kok, S. F. Oosting, C. P. Schröder, T. J. N. Hiltermann, A. J. van der Wekken, H. J. M. Groen, T. C. Kwee, S. G. Elias, J. A. Gietema, S. S. Bohorquez, A. de Crespigny, S. P. Williams, C. Mancao, A. H. Brouwers, B. M. Fine and E. G. E. de Vries (2018). "(89)Zr-atezolizumab imaging as a non-invasive approach to assess clinical response to PD-L1 blockade in cancer." Nat Med **24**(12): 1852-1858.

Berger, C., M. E. Flowers, E. H. Warren and S. R. Riddell (2006). "Analysis of transgene-specific immune responses that limit the in vivo persistence of adoptively transferred HSV-TK-modified donor T cells after allogeneic hematopoietic cell transplantation." Blood **107**(6): 2294-2302.

Bhatnagar, P., Z. Li, Y. Choi, J. Guo, F. Li, D. Y. Lee, M. Figliola, H. Huls, D. A. Lee, T. Zal, K. C. Li and L. J. Cooper (2013). "Imaging of genetically engineered T cells by PET using gold nanoparticles complexed to Copper-64." Integr Biol (Camb) **5**(1): 231-238.

Bierer, B. E., A. Peterson, J. C. Gorga, S. H. Herrmann and S. J. Burakoff (1988). "Synergistic T cell activation via the physiological ligands for CD2 and the T cell receptor." Journal of Experimental Medicine **168**(3): 1145-1156.

Blykers, A., S. Schoonooghe, C. Xavier, K. D'Hoe, D. Laoui, M. D'Huyvetter, I. Vaneycken, F. Cleeren, G. Bormans, J. Heemskerk, G. Raes, P. De Baetselier, T. Lahoutte, N. Devoogdt, J. A. Van Ginderachter and V. Caveliers (2015). "PET Imaging of Macrophage Mannose Receptor-Expressing Macrophages in Tumor Stroma Using 18F-Radiolabeled Camelid Single-Domain Antibody Fragments." J Nucl Med **56**(8): 1265-1271.

Borate, U., J. Esteve, K. Porkka, S. Knapper, N. Vey, S. Scholl, G. Garcia-Manero, M. Wermke, J. Janssen, E. Traer, C. C. Chua, R. Narayan, N. Tovar, M. Kontro, O. Ottmann, H. Sun, T. Longmire, S. Szpakowski, S. Liao, A. Patel, M. L. Rinne, A. Brunner and A. H. Wei (2019). "Phase Ib Study of the Anti-TIM-3 Antibody MBG453 in Combination with Decitabine in Patients with High-Risk Myelodysplastic Syndrome (MDS) and Acute Myeloid Leukemia (AML)." Blood **134**(Supplement_1): 570-570.

Borcoman, E., Y. Kanjanapan, S. Champiat, S. Kato, V. Servois, R. Kurzrock, S. Goel, P. Bedard and C. Le Tourneau (2019). "Novel patterns of response under immunotherapy." Annals of Oncology **30**(3): 385-396.

Boros, E. and J. P. Holland (2018). "Chemical aspects of metal ion chelation in the synthesis and application antibody-based radiotracers." J Labelled Comp Radiopharm **61**(9): 652-671.

Breeman, W. A., M. De Jong, T. J. Visser, J. L. Erion and E. P. Krenning (2003). "Optimising conditions for radiolabelling of DOTA-peptides with 90Y, 111In and 177Lu at high specific activities." Eur J Nucl Med Mol Imaging **30**(6): 917-920.

Brignone, C., M. Gutierrez, F. Mefti, E. Brain, R. Jarcau, F. Cvitkovic, N. Bousetta, J. Medioni, J. Gligorov, C. Grygar, M. Marcu and F. Triebel (2010). "First-line chemoimmunotherapy in metastatic breast carcinoma: combination of paclitaxel and IMP321 (LAG-3Ig) enhances immune responses and antitumor activity." J Transl Med **8**: 71.

Brottier, P., L. Boumsell, C. Gelin and A. Bernard (1985). "T cell activation via CD2 [T, gp50] molecules: accessory cells are required to trigger T cell activation via CD2-D66 plus CD2-9.6/T11(1) epitopes." J Immunol **135**(3): 1624-1631.

Buss, N. A., S. J. Henderson, M. McFarlane, J. M. Shenton and L. de Haan (2012). "Monoclonal antibody therapeutics: history and future." Curr Opin Pharmacol **12**(5): 615-622.

Butterfield, L. H. (2015). "Cancer vaccines." Bmj **350**: h988.

Carrera, A. C., M. Rincón, F. Sánchez-Madrid, M. López-Botet and M. O. de Landaźuri (1988). "Triggering of co-mitogenic signals in T cell proliferation by anti-LFA-1 (CD18, CD11a), LFA-3, and CD7 monoclonal antibodies." J Immunol **141**(6): 1919-1924.

Carter, L. M., A. L. Kesner, E. C. Pratt, V. A. Sanders, A. V. F. Massicano, C. S. Cutler, S. E. Lapi and J. S. Lewis (2020). "The Impact of Positron Range on PET Resolution, Evaluated with Phantoms and PHITS Monte Carlo Simulations for Conventional and Non-conventional Radionuclides." Mol Imaging Biol **22**(1): 73-84.

Carter, P. J. and A. Rajpal (2022). "Designing antibodies as therapeutics." Cell **185**(15): 2789-2805.

Chan, A. S., P. J. Reynolds and Y. Shimizu (1994). "Tyrosine kinase activity associated with the CD7 antigen: correlation with regulation of T cell integrin function." Eur J Immunol **24**(11): 2602-2608.

Chan, C., D. A. Scollard, K. McLarty, S. Smith and R. M. Reilly (2011). "A comparison of 111In- or 64Cu-DOTA-trastuzumab Fab fragments for imaging subcutaneous HER2-positive tumor xenografts in athymic mice using microSPECT/CT or microPET/CT." EJNMMI Res **1**(1): 15.

Chang, E., L. Pelosof, S. Lemery, Y. Gong, K. B. Goldberg, A. T. Farrell, P. Keegan, J. Veeraraghavan, G. Wei, G. M. Blumenthal, L. Amiri-Kordestani, H. Singh, L. Fashoyin-Aje, N. Gormley, P. G. Kluetz, R. Pazdur, J. A. Beaver and M. R. Theoret (2021). "Systematic Review of PD-1/PD-L1 Inhibitors in Oncology: From Personalized Medicine to Public Health." The Oncologist **26**(10): e1786-e1799.

Chang, M. H., W. Y. Shau, C. J. Chen, T. C. Wu, M. S. Kong, D. C. Liang, H. M. Hsu, H. L. Chen, H. Y. Hsu and D. S. Chen (2000). "Hepatitis B vaccination and hepatocellular carcinoma rates in boys and girls." Jama **284**(23): 3040-3042.

Charoenphun, P., L. K. Meszaros, K. Chuamsaamarkkee, E. Sharif-Paghaleh, J. R. Ballinger, T. J. Ferris, M. J. Went, G. E. Mullen and P. J. Blower (2015).

"[(89)Zr]oxinate4 for long-term in vivo cell tracking by positron emission tomography." Eur J Nucl Med Mol Imaging **42**(2): 278-287.

Chen, D. S. and I. Mellman (2017). "Elements of cancer immunity and the cancer–immune set point." Nature **541**(7637): 321-330.

Chen, S., G. A. Crabill, T. S. Pritchard, T. L. McMiller, P. Wei, D. M. Pardoll, F. Pan and S. L. Topalian (2019). "Mechanisms regulating PD-L1 expression on tumor and immune cells." J Immunother Cancer **7**(1): 305.

Chesney, J., K. D. Lewis, H. Kluger, O. Hamid, E. Whitman, S. Thomas, M. Wermke, M. Cusnir, E. Domingo-Musibay, G. Q. Phan, J. M. Kirkwood, J. C. Hassel, M. Orloff, J. Larkin, J. Weber, A. J. S. Furness, N. I. Khushalani, T. Medina, M. E. Egger, F. Graf Finckenstein, M. Jagasia, P. Hari, G. Sulur, W. Shi, X. Wu and A. Sarnaik (2022). "Efficacy and safety of lifileucel, a one-time autologous tumor-infiltrating lymphocyte (TIL) cell therapy, in patients with advanced melanoma after progression on immune checkpoint inhibitors and targeted therapies: pooled analysis of consecutive cohorts of the C-144-01 study." J Immunother Cancer **10**(12).

Chiesa, R., C. Georgiadis, F. Syed, H. Zhan, A. Etuk, S. A. Gkazi, R. Preece, G. Ottaviano, T. Braybrook, J. Chu, A. Kubat, S. Adams, R. Thomas, K. Gilmour, D. O'Connor, A. Vora and W. Qasim (2023). "Base-Edited CAR7 T Cells for Relapsed T-Cell Acute Lymphoblastic Leukemia." N Engl J Med **389**(10): 899-910.

Christensen, E. I. and H. Birn (2002). "Megalin and cubilin: multifunctional endocytic receptors." Nat Rev Mol Cell Biol **3**(4): 256-266.

Cleeren, F., J. Lecina, J. Bridoux, N. Devoogdt, T. Tshibangu, C. Xavier and G. Bormans (2018). "Direct fluorine-18 labeling of heat-sensitive biomolecules for positron emission tomography imaging using the Al(18)F-RESCA method." Nat Protoc **13**(10): 2330-2347.

Cobbold, S. P., A. Jayasuriya, A. Nash, T. D. Prospero and H. Waldmann (1984). "Therapy with monoclonal antibodies by elimination of T-cell subsets in vivo." Nature **312**(5994): 548-551.

Cortelazzo, S., M. Ponzoni, A. J. Ferreri and D. Hoelzer (2011). "Lymphoblastic lymphoma." Crit Rev Oncol Hematol **79**(3): 330-343.

D'Huyvetter, M., J. Vos, V. Caveliers, I. Vaneycken, J. Heemskerk, F. P. Duhoux, C. Fontaine, M. Vanhoeij, A. D. Windhorst, F. V. Aa, N. H. Hendrikse, J. L. E. Eersels, H. Everaert, P. Gykiere, N. Devoogdt, G. Raes, T. Lahoutte and M. Keyaerts (2021). "Phase I Trial of (131)I-GMIB-Anti-HER2-VHH1, a New Promising Candidate for HER2-Targeted Radionuclide Therapy in Breast Cancer Patients." J Nucl Med **62**(8): 1097-1105.

de Bruin, R. C. G., J. P. Veluchamy, S. M. Lougheed, F. L. Schneiders, S. Lopez-Lastra, R. Lameris, A. G. Stam, Z. Sebestyen, J. Kuball, C. F. M. Molthoff, E. Hooijberg, R. C. Roovers, J. P. D. Santo, P. M. P. van Bergen En Henegouwen, H. M. W. Verheul, T. D. de Gruijl and H. J. van der Vliet (2017). "A bispecific nanobody approach to leverage the potent and widely applicable tumor cytolytic capacity of Vγ9Vδ2-T cells." Oncoimmunology **7**(1): e1375641.

de Marco, A. (2020). "Recombinant expression of nanobodies and nanobody-derived immunoreagents." Protein Expr Purif **172**: 105645.

De Vos, J., N. Devoogdt, T. Lahoutte and S. Muyldermans (2013). "Camelid single-domain antibody-fragment engineering for (pre)clinical in vivo molecular imaging applications: adjusting the bullet to its target." Expert Opin Biol Ther **13**(8): 1149-1160.

Debie, P., C. Lafont, M. Defrise, I. Hansen, D. M. van Willigen, F. W. B. van Leeuwen, R. Gijsbers, M. D'Huyvetter, N. Devoogdt, T. Lahoutte, P. Mollard and S. Hernot (2020). "Size and affinity kinetics of nanobodies influence targeting and penetration of solid tumours." Journal of Controlled Release **317**: 34-42.

Di Giacomo, A. M., R. Danielli, M. Guidoboni, L. Calabrò, D. Carlucci, C. Miracco, L. Volterrani, M. A. Mazzei, M. Biagioli, M. Altomonte and M. Maio (2009). "Therapeutic efficacy of ipilimumab, an anti-CTLA-4 monoclonal antibody, in patients with metastatic melanoma unresponsive to prior systemic treatments: clinical and immunological evidence from three patient cases." Cancer Immunol Immunother **58**(8): 1297-1306.

Dijkers, E. C., T. H. Oude Munnink, J. G. Kosterink, A. H. Brouwers, P. L. Jager, J. R. de Jong, G. A. van Dongen, C. P. Schröder, M. N. Lub-de Hooge and E. G. de Vries (2010). "Biodistribution of 89Zr-trastuzumab and PET imaging of HER2-positive lesions in patients with metastatic breast cancer." Clin Pharmacol Ther **87**(5): 586-592.

Ebenhan, T., N. Chadwick, M. M. Sathekge, P. Govender, T. Govender, H. G. Kruger, B. Marjanovic-Painter and J. R. Zeevaart (2014). "Peptide synthesis, characterization and ^{68}Ga-radiolabeling of NOTA-conjugated ubiquicidin fragments for prospective infection imaging with PET/CT." Nucl Med Biol **41**(5): 390-400.

Emami-Shahri, N., J. Foster, R. Kashani, P. Gazinska, C. Cook, J. Sosabowski, J. Maher and S. Papa (2018). "Clinically compliant spatial and temporal imaging of chimeric antigen receptor T-cells." Nat Commun **9**(1): 1081.

Engels, B., H. Cam, T. Schüler, S. Indraccolo, M. Gladow, C. Baum, T. Blankenstein and W. Uckert (2003). "Retroviral vectors for high-level transgene expression in T lymphocytes." Hum Gene Ther **14**(12): 1155-1168.

Epenetos, A. A., D. Snook, H. Durbin, P. M. Johnson and J. Taylor-Papadimitriou (1986). "Limitations of radiolabeled monoclonal antibodies for localization of human neoplasms." Cancer Res **46**(6): 3183-3191.

Erik, V., F. M. W. Jack, G. M. R. Frans, M. Rosalinde, C. B. Otto, E. v. E. Juliette, H. M. C. Frans and J. G. O. Wim (2006). "Renal Uptake of Radiolabeled Octreotide in Human Subjects Is Efficiently Inhibited by Succinylated Gelatin." Journal of Nuclear Medicine **47**(3): 432.

Erik, V., J. Marion de, F. M. W. Jack, M. Rosalinde, M. Marleen, J. G. O. Wim, G. Martin and C. B. Otto (2010). "Renal Toxicity of Radiolabeled Peptides and Antibody Fragments: Mechanisms, Impact on Radionuclide Therapy, and Strategies for Prevention." Journal of Nuclear Medicine **51**(7): 1049.

Ewert, S., C. Cambillau, K. Conrath and A. Plückthun (2002). "Biophysical properties of camelid V(HH) domains compared to those of human V(H)3 domains." Biochemistry **41**(11): 3628-3636.

Fang, J., H. Nakamura and H. Maeda (2011). "The EPR effect: Unique features of tumor blood vessels for drug delivery, factors involved, and limitations and augmentation of the effect." Adv Drug Deliv Rev **63**(3): 136-151.

Farwell, M. D., R. F. Gamache, H. Babazada, M. D. Hellmann, J. J. Harding, R. Korn, A. Mascioni, W. Le, I. Wilson, M. S. Gordon, A. M. Wu, G. A. Ulaner, J. D. Wolchok, M. A. Postow and N. Pandit-Taskar (2022). "CD8-Targeted PET Imaging of Tumor-Infiltrating T Cells in Patients with Cancer: A Phase I First-in-Humans Study of (89)Zr-Df-IAB22M2C, a Radiolabeled Anti-CD8 Minibody." J Nucl Med **63**(5): 720-726.

Finck, A. V., T. Blanchard, C. P. Roselle, G. Golinelli and C. H. June (2022). "Engineered cellular immunotherapies in cancer and beyond." Nat Med **28**(4): 678-689.

Flugel, C. L., R. G. Majzner, G. Krenciute, G. Dotti, S. R. Riddell, D. L. Wagner and M. Abou-El-Enein (2023). "Overcoming on-target, off-tumour toxicity of CAR T cell therapy for solid tumours." Nat Rev Clin Oncol **20**(1): 49-62.

Freise, A. C., K. A. Zettlitz, F. B. Salazar, X. Lu, R. Tavaré and A. M. Wu (2017). "ImmunoPET Imaging of Murine CD4(+) T Cells Using Anti-CD4 Cys-Diabody: Effects of Protein Dose on T Cell Function and Imaging." Mol Imaging Biol **19**(4): 599-609.

Frejd, F. Y. and K. T. Kim (2017). "Affibody molecules as engineered protein drugs." Exp Mol Med **49**(3): e306.

Fu, R., L. Carroll, G. Yahioglu, E. O. Aboagye and P. W. Miller (2018). "Antibody Fragment and Affibody ImmunoPET Imaging Agents: Radiolabelling Strategies and Applications." ChemMedChem **13**(23): 2466-2478.

Gainkam, L. O., L. Huang, V. Caveliers, M. Keyaerts, S. Hernot, I. Vaneycken, C. Vanhove, H. Revets, P. De Baetselier and T. Lahoutte (2008). "Comparison of the biodistribution and tumor targeting of two 99mTc-labeled anti-EGFR nanobodies in mice, using pinhole SPECT/micro-CT." J Nucl Med **49**(5): 788-795.

Gandara, D. R., J. von Pawel, J. Mazieres, R. Sullivan, Å. Helland, J. Y. Han, S. Ponce Aix, A. Rittmeyer, F. Barlesi, T. Kubo, K. Park, J. Goldschmidt, M. Gandhi, C. Yun, W. Yu, C. Matheny, P. He, A. Sandler, M. Ballinger and L. Fehrenbacher (2018). "Atezolizumab Treatment Beyond Progression in Advanced NSCLC: Results From the Randomized, Phase III OAK Study." J Thorac Oncol **13**(12): 1906-1918.

Gao, X., Y. Zhu, G. Li, H. Huang, G. Zhang, F. Wang, J. Sun, Q. Yang, X. Zhang and B. Lu (2012). "TIM-3 expression characterizes regulatory T cells in tumor tissues and is associated with lung cancer progression." PLoS One **7**(2): e30676.

Genove, G., U. DeMarco, H. Xu, W. F. Goins and E. T. Ahrens (2005). "A new transgene reporter for in vivo magnetic resonance imaging." Nat Med **11**(4): 450-454.

Goldman, E. R., G. P. Anderson, J. L. Liu, J. B. Delehanty, L. J. Sherwood, L. E. Osborn, L. B. Cummins and A. Hayhurst (2006). "Facile generation of heat-stable antiviral and antitoxin single domain antibodies from a semisynthetic llama library." Anal Chem **78**(24): 8245-8255.

Goldman, E. R., J. L. Liu, D. Zabetakis and G. P. Anderson (2017). "Enhancing Stability of Camelid and Shark Single Domain Antibodies: An Overview." Front Immunol **8**: 865.

Gomes-Silva, D., M. Srinivasan, S. Sharma, C. M. Lee, D. L. Wagner, T. H. Davis, R. H. Rouce, G. Bao, M. K. Brenner and M. Mamonkin (2017). "CD7-edited T cells expressing a CD7-specific CAR for the therapy of T-cell malignancies." Blood **130**(3): 285-296.

González Trotter, D. E., X. Meng, P. McQuade, D. Rubins, M. Klimas, Z. Zeng, B. M. Connolly, P. J. Miller, S. S. O'Malley, S. A. Lin, K. L. Getty, L. Fayadat-Dilman, L. Liang, E. Wahlberg, O. Widmark, C. Ekblad, F. Y. Frejd, E. D. Hostetler and J. L. Evelhoch (2017). "In Vivo Imaging of the Programmed Death Ligand 1 by (18)F PET." J Nucl Med **58**(11): 1852-1857.

Gosmann, D., L. Russelli, W. A. Weber, M. Schwaiger, A. M. Krackhardt and C. D'Alessandria (2022). "Promise and challenges of clinical non-invasive T-cell tracking in the era of cancer immunotherapy." EJNMMI Res **12**(1): 5.

Griessinger, C. M., A. Maurer, C. Kesenheimer, R. Kehlbach, G. Reischl, W. Ehrlichmann, D. Bukala, M. Harant, F. Cay, J. Brück, R. Nordin, U. Kohlhofer, H. G. Rammensee, L. Quintanilla-Martinez, M. Schaller, M. Röcken, B. J. Pichler and M. Kneilling (2015). "64Cu antibody-targeting of the T-cell receptor and subsequent internalization enables in vivo tracking of lymphocytes by PET." Proc Natl Acad Sci U S A **112**(4): 1161-1166.

Griffith, K. D., E. J. Read, J. A. Carrasquillo, C. S. Carter, J. C. Yang, B. Fisher, P. Aebersold, B. S. Packard, M. Y. Yu and S. A. Rosenberg (1989). "In vivo distribution of adoptively transferred indium-111-labeled tumor infiltrating lymphocytes and peripheral blood lymphocytes in patients with metastatic melanoma." J Natl Cancer Inst **81**(22): 1709-1717.

Grimfors, G., P. O. Schnell, G. Holm, B. Johansson, H. Mellstedt, P. Pihlstedt and M. Björkholm (1989). "Tumour imaging of indium-111 oxine-labelled autologous lymphocytes as a staging method in Hodgkin's disease." Eur J Haematol **42**(3): 276-283.

Gros, A., M. R. Parkhurst, E. Tran, A. Pasetto, P. F. Robbins, S. Ilyas, T. D. Prickett, J. J. Gartner, J. S. Crystal, I. M. Roberts, K. Trebska-McGowan, J. R. Wunderlich, J. C. Yang and S. A. Rosenberg (2016). "Prospective identification of neoantigen-specific lymphocytes in the peripheral blood of melanoma patients." Nat Med **22**(4): 433-438.

Hamers-Casterman, C., T. Atarhouch, S. Muyldermans, G. Robinson, C. Hamers, E. B. Songa, N. Bendahman and R. Hamers (1993). "Naturally occurring antibodies devoid of light chains." Nature **363**(6428): 446-448.

Hamers-Casterman, C., T. Atarhouch, S. Muyldermans, G. Robinson, C. Hammers, E. B. Songa, N. Bendahman and R. Hammers (1993). "Naturally occurring antibodies devoid of light chains." Nature **363**(6428): 446-448.

Hammond, P. J., A. F. Wade, M. E. Gwilliam, A. M. Peters, M. J. Myers, S. G. Gilbey, S. R. Bloom and J. Calam (1993). "Amino acid infusion blocks renal tubular uptake of an indium-labelled somatostatin analogue." Br J Cancer **67**(6): 1437-1439.

Hansel, T. T., H. Kropshofer, T. Singer, J. A. Mitchell and A. J. George (2010). "The safety and side effects of monoclonal antibodies." Nat Rev Drug Discov **9**(4): 325-338.

Hartimath, S. V., O. Draghiciu, S. van de Wall, V. Manuelli, R. A. Dierckx, H. W. Nijman, T. Daemen and E. F. de Vries (2017). "Noninvasive monitoring of cancer therapy induced activated T cells using [(18)F]FB-IL-2 PET imaging." Oncoimmunology **6**(1): e1248014.

Havel, J. J., D. Chowell and T. A. Chan (2019). "The evolving landscape of biomarkers for checkpoint inhibitor immunotherapy." Nature Reviews Cancer **19**(3): 133-150.

Heczey, A., X. Xu, A. N. Courtney, G. Tian, G. A. Barragan, L. Guo, C. M. Amador, N. Ghatwai, P. Rathi, M. S. Wood, Y. Li, C. Zhang, T. Demberg, E. J. Di Pierro, A. C. Sher, H. Zhang, B. Mehta, S. G. Thakkar, B. Grilley, T. Wang, B. D. Weiss, A. Montalbano, M. Subramaniam, C. Xu, C. Sachar, D. K. Wells, G. Dotti and L. S. Metelitsa (2023). "Anti-GD2 CAR-NKT cells in relapsed or refractory neuroblastoma: updated phase 1 trial interim results." Nature Medicine **29**(6): 1379-1388.

Herbst, R. S., J. C. Soria, M. Kowanetz, G. D. Fine, O. Hamid, M. S. Gordon, J. A. Sosman, D. F. McDermott, J. D. Powderly, S. N. Gettinger, H. E. Kohrt, L. Horn, D. P. Lawrence, S. Rost, M. Leabman, Y. Xiao, A. Mokatrin, H. Koeppen, P. S. Hegde, I. Mellman, D. S. Chen and F. S. Hodi (2014). "Predictive correlates of response to the anti-PD-L1 antibody MPDL3280A in cancer patients." Nature **515**(7528): 563-567.

Hodi, F. S., S. J. O'Day, D. F. McDermott, R. W. Weber, J. A. Sosman, J. B. Haanen, R. Gonzalez, C. Robert, D. Schadendorf, J. C. Hassel, W. Akerley, A. J. van den Eertwegh, J. Lutzky, P. Lorigan, J. M. Vaubel, G. P. Linette, D. Hogg, C. H. Ottensmeier, C. Lebbé, C. Peschel, I. Quirt, J. I. Clark, J. D. Wolchok, J. S. Weber, J. Tian, M. J. Yellin, G. M. Nichol, A. Hoos and W. J. Urba (2010). "Improved survival with ipilimumab in patients with metastatic melanoma." N Engl J Med **363**(8): 711-723.

Hoefman, S., I. Ottevaere, J. Baumeister and M. L. Sargentini-Maier (2015). "Pre-Clinical Intravenous Serum Pharmacokinetics of Albumin Binding and Non-Half-Life Extended Nanobodies®." Antibodies **4**(3): 141-156.

Holland, M. C., J. U. Wurthner, P. J. Morley, M. A. Birchler, J. Lambert, M. Albayaty, A. P. Serone, R. Wilson, Y. Chen, R. M. Forrest, J. C. Cordy, D. A. Lipson and A. I. Bayliffe (2013). "Autoantibodies to variable heavy (VH) chain Ig sequences in humans impact the safety and clinical pharmacology of a VH domain antibody antagonist of TNF-α receptor 1." J Clin Immunol **33**(7): 1192-1203.

Howard, F. D., J. A. Ledbetter, J. Wong, C. P. Bieber, E. B. Stinson and L. A. Herzenberg (1981). "A human T lymphocyte differentiation marker defined by monoclonal antibodies that block E-rosette formation." J Immunol **126**(6): 2117-2122.

Hu, S., L. Shively, A. Raubitschek, M. Sherman, L. E. Williams, J. Y. Wong, J. E. Shively and A. M. Wu (1996). "Minibody: A novel engineered anti-carcinoembryonic antigen antibody fragment (single-chain Fv-CH3) which exhibits rapid, high-level targeting of xenografts." Cancer Res **56**(13): 3055-3061.

Hu, Y. and J. Huang (2020). "The Chimeric Antigen Receptor Detection Toolkit." Front Immunol **11**: 1770.

Hu, Z. B., W. Ma, C. C. Uphoff, K. Metge, S. M. Gignac and H. G. Drexler (1993). "Myeloperoxidase: expression and modulation in a large panel of human leukemia-lymphoma cell lines." Blood **82**(5): 1599-1607.

Huang, A. C., M. A. Postow, R. J. Orlowski, R. Mick, B. Bengsch, S. Manne, W. Xu, S. Harmon, J. R. Giles, B. Wenz, M. Adamow, D. Kuk, K. S. Panageas, C. Carrera, P. Wong, F. Quagliarello, B. Wubbenhorst, K. D'Andrea, K. E. Pauken, R. S. Herati, R. P. Staupe, J. M. Schenkel, S. McGettigan, S. Kothari, S. M. George, R. H. Vonderheide, R. K. Amaravadi, G. C. Karakousis, L. M. Schuchter, X. Xu, K. L. Nathanson, J. D. Wolchok, T. C. Gangadhar and E. J. Wherry (2017). "T-cell invigoration to tumour burden ratio associated with anti-PD-1 response." Nature **545**(7652): 60-65.

Huh, W. K., E. A. Joura, A. R. Giuliano, O. E. Iversen, R. P. de Andrade, K. A. Ault, D. Bartholomew, R. M. Cestero, E. N. Fedrizzi, A. L. Hirschberg, M. H. Mayrand, A. M. Ruiz-Sternberg, J. T. Stapleton, D. J. Wiley, A. Ferenczy, R. Kurman, B. M. Ronnett, M. H. Stoler, J. Cuzick, S. M. Garland, S. K. Kjaer, O. M. Bautista, R. Haupt, E. Moeller, M. Ritter, C. C. Roberts, C. Shields and A. Luxembourg (2017). "Final efficacy, immunogenicity, and safety analyses of a nine-valent human papillomavirus vaccine in women aged 16-26 years: a randomised, double-blind trial." Lancet **390**(10108): 2143-2159.

Hünig, T., G. Tiefenthaler, K. H. Meyer zum Büschenfelde and S. C. Meuer (1987). "Alternative pathway activation of T cells by binding of CD2 to its cell-surface ligand." Nature **326**(6110): 298-301.

Hünig, T., G. Tiefenthaler, K. H. M. zum Büschenfelde and S. C. Meuer (1987). "Alternative pathway activation of T cells by binding of CD2 to its cell-surface ligand." Nature **326**(6110): 298-301.

Ingram, J. R., F. I. Schmidt and H. L. Ploegh (2018). "Exploiting Nanobodies' Singular Traits." Annual Review of Immunology **36**(1): 695-715.

Iordanova, B. and E. T. Ahrens (2012). "In vivo magnetic resonance imaging of ferritin-based reporter visualizes native neuroblast migration." Neuroimage **59**(2): 1004-1012.

Iwai, Y., M. Ishida, Y. Tanaka, T. Okazaki, T. Honjo and N. Minato (2002). "Involvement of PD-L1 on tumor cells in the escape from host immune system and tumor immunotherapy by PD-L1 blockade." Proc Natl Acad Sci U S A **99**(19): 12293-12297.

Jafari, M., A. Maali, M. A. Shokrgozar and Z. Sharifzadeh (2023). "Editorial: Nanobody-based cancer immunotherapy and immunoimaging." Front Immunol **14**: 1213386.

Jain, R. K. (1990). "Vascular and interstitial barriers to delivery of therapeutic agents in tumors." Cancer and Metastasis Reviews **9**(3): 253-266.

Jain, R. K. (1994). "Barriers to drug delivery in solid tumors." Sci Am **271**(1): 58-65.

Jin, B. K., S. Odongo, M. Radwanska and S. Magez (2023). "Nanobodies: A Review of Generation, Diagnostics and Therapeutics." Int J Mol Sci **24**(6).

Joura, E. A., A. R. Giuliano, O. E. Iversen, C. Bouchard, C. Mao, J. Mehlsen, E. D. Moreira, Jr., Y. Ngan, L. K. Petersen, E. Lazcano-Ponce, P. Pitisuttithum, J. A. Restrepo, G. Stuart, L. Woelber, Y. C. Yang, J. Cuzick, S. M. Garland, W. Huh, S. K. Kjaer, O. M. Bautista, I. S. Chan, J. Chen, R. Gesser, E. Moeller, M. Ritter, S. Vuocolo

and A. Luxembourg (2015). "A 9-valent HPV vaccine against infection and intraepithelial neoplasia in women." N Engl J Med **372**(8): 711-723.

Jovčevska, I. and S. Muyldermans (2020). "The Therapeutic Potential of Nanobodies." BioDrugs **34**(1): 11-26.

Jung, L. K., A. K. Roy and H. R. Chakkalath (1992). "CD7 augments T cell proliferation via the interleukin-2 autocrine pathway." Cell Immunol **141**(1): 189-199.

Kang, L., C. Li, Z. T. Rosenkrans, J. W. Engle, R. Wang, D. Jiang, X. Xu and W. Cai (2021). "Noninvasive Evaluation of CD20 Expression Using (64)Cu-Labeled F(ab')(2) Fragments of Obinutuzumab in Lymphoma." J Nucl Med **62**(3): 372-378.

Kantoff, P. W., C. S. Higano, N. D. Shore, E. R. Berger, E. J. Small, D. F. Penson, C. H. Redfern, A. C. Ferrari, R. Dreicer, R. B. Sims, Y. Xu, M. W. Frohlich and P. F. Schellhammer (2010). "Sipuleucel-T immunotherapy for castration-resistant prostate cancer." N Engl J Med **363**(5): 411-422.

Kasten, B. B., H. A. Houson, J. M. Coleman, J. W. Leavenworth, J. M. Markert, A. M. Wu, F. Salazar, R. Tavaré, A. V. F. Massicano, G. Y. Gillespie, S. E. Lapi, J. M. Warram and A. G. Sorace (2021). "Positron emission tomography imaging with 89Zr-labeled anti-CD8 cys-diabody reveals CD8+ cell infiltration during oncolytic virus therapy in a glioma murine model." Scientific Reports **11**(1): 15384.

Katz, S. I., M. Hammer, S. J. Bagley, C. Aggarwal, J. M. Bauml, J. C. Thompson, A. C. Nachiappan, C. B. Simone, 2nd and C. J. Langer (2018). "Radiologic Pseudoprogression during Anti-PD-1 Therapy for Advanced Non-Small Cell Lung Cancer." J Thorac Oncol **13**(7): 978-986.

Kenanova, V. and A. M. Wu (2006). "Tailoring antibodies for radionuclide delivery." Expert Opin Drug Deliv **3**(1): 53-70.

Keu, K. V., T. H. Witney, S. Yaghoubi, J. Rosenberg, A. Kurien, R. Magnusson, J. Williams, F. Habte, J. R. Wagner, S. Forman, C. Brown, M. Allen-Auerbach, J. Czernin, W. Tang, M. C. Jensen, B. Badie and S. S. Gambhir (2017). "Reporter gene imaging of targeted T cell immunotherapy in recurrent glioma." Sci Transl Med **9**(373).

Keyaerts, M., C. Xavier, J. Heemskerk, N. Devoogdt, H. Everaert, C. Ackaert, M. Vanhoeij, F. P. Duhoux, T. Gevaert, P. Simon, D. Schallier, C. Fontaine, I. Vaneycken, C. Vanhove, J. De Greve, J. Lamote, V. Caveliers and T. Lahoutte (2016). "Phase I Study of 68Ga-HER2-Nanobody for PET/CT Assessment of HER2 Expression in Breast Carcinoma." J Nucl Med **57**(1): 27-33.

Khong, H. T. and N. P. Restifo (2002). "Natural selection of tumor variants in the generation of “tumor escape” phenotypes." Nature Immunology **3**(11): 999-1005.

Killock, D. (2017). "Leveraging ADCC to enhance anti-HER2 therapy." Nature Reviews Clinical Oncology **14**(4): 200-200.

Kircher, M. F., J. R. Allport, E. E. Graves, V. Love, L. Josephson, A. H. Lichtman and R. Weissleder (2003). "In vivo high resolution three-dimensional imaging of antigen-specific cytotoxic T-lymphocyte trafficking to tumors." Cancer Res **63**(20): 6838-6846.

Kist de Ruijter, L., P. P. van de Donk, J. S. Hooiveld-Noeken, D. Giesen, S. G. Elias, M. N. Lub-de Hooge, S. F. Oosting, M. Jalving, W. Timens, A. H. Brouwers, T. C. Kwee, J. A. Gietema, R. S. N. Fehrmann, B. M. Fine, S. M. Sanabria Bohórquez, M. Yadav, H. Koeppen, J. Jing, S. Guelman, M. T. Lin, M. J. Mamounas, J. R. Eastham, P. K. Kimes, S. P. Williams, A. Ungewickell, D. J. A. de Groot and E. G. E. de Vries (2022). "Whole-body CD8(+) T cell visualization before and during cancer immunotherapy: a phase 1/2 trial." Nat Med **28**(12): 2601-2610.

Klar, R., S. Schober, M. Rami, S. Mall, J. Merl, S. M. Hauck, M. Ueffing, A. Admon, J. Slotta-Huspenina, M. Schwaiger, S. Stevanović, R. A. Oostendorp, D. H. Busch, C. Peschel and A. M. Krackhardt (2014). "Therapeutic targeting of naturally presented myeloperoxidase-derived HLA peptide ligands on myeloid leukemia cells by TCR-transgenic T cells." Leukemia **28**(12): 2355-2366.

Klarenbeek, A., K. El Mazouari, A. Desmyter, C. Blanchetot, A. Hultberg, N. de Jonge, R. C. Roovers, C. Cambillau, S. Spinelli, J. Del-Favero, T. Verrips, H. J. de Haard and I. Achour (2015). "Camelid Ig V genes reveal significant human homology not seen in therapeutic target genes, providing for a powerful therapeutic antibody platform." MAbs **7**(4): 693-706.

Knowles, S. M. and A. M. Wu (2012). "Advances in immuno-positron emission tomography: antibodies for molecular imaging in oncology." J Clin Oncol **30**(31): 3884-3892.

Knowles, S. M., K. A. Zettlitz, R. Tavaré, M. M. Rochefort, F. B. Salazar, D. B. Stout, P. J. Yazaki, R. E. Reiter and A. M. Wu (2014). "Quantitative immunoPET of prostate cancer xenografts with 89Zr- and 124I-labeled anti-PSCA A11 minibody." J Nucl Med **55**(3): 452-459.

Kolkman, J. A. and D. A. Law (2010). "Nanobodies – from llamas to therapeutic proteins." Drug Discovery Today: Technologies **7**(2): e139-e146.

Koyama, S., E. A. Akbay, Y. Y. Li, G. S. Herter-Sprie, K. A. Buczkowski, W. G. Richards, L. Gandhi, A. J. Redig, S. J. Rodig, H. Asahina, R. E. Jones, M. M. Kulkarni, M. Kuraguchi, S. Palakurthi, P. E. Fecci, B. E. Johnson, P. A. Janne, J. A. Engelman, S. P. Gangadharan, D. B. Costa, G. J. Freeman, R. Bueno, F. S. Hodi, G. Dranoff, K. K. Wong and P. S. Hammerman (2016). "Adaptive resistance to therapeutic PD-1 blockade is associated with upregulation of alternative immune checkpoints." Nat Commun **7**: 10501.

Kramer, C. S. and A. Dimitrakopoulou-Strauss (2022). "Immuno-Imaging (PET/SPECT)-Quo Vadis?" Molecules **27**(10).

Krasniqi, A., M. D'Huyvetter, C. Xavier, K. Van der Jeught, S. Muyldermans, J. Van Der Heyden, T. Lahoutte, J. Tavernier and N. Devoogdt (2017). "Theranostic Radiolabeled Anti-CD20 sdAb for Targeted Radionuclide Therapy of Non-Hodgkin Lymphoma." Molecular Cancer Therapeutics **16**(12): 2828-2839.

Krebs, S., A. Ahad, L. M. Carter, J. Eyquem, C. Brand, M. Bell, V. Ponomarev, T. Reiner, C. F. Meares, S. Gottschalk, M. Sadelain, S. M. Larson and W. A. Weber (2018). "Antibody with Infinite Affinity for In Vivo Tracking of Genetically Engineered Lymphocytes." J Nucl Med **59**(12): 1894-1900.

Krekorian, M., G. O. Fruhwirth, M. Srinivas, C. G. Figdor, S. Heskamp, T. H. Witney and E. Aarntzen (2019). "Imaging of T-cells and their responses during anti-cancer immunotherapy." Theranostics **9**(25): 7924-7947.

Kristensen, L. K., C. Fröhlich, C. Christensen, M. C. Melander, T. T. Poulsen, G. R. Galler, J. Lantto, I. D. Horak, M. Kragh, C. H. Nielsen and A. Kjaer (2019). "CD4(+) and CD8a(+) PET imaging predicts response to novel PD-1 checkpoint inhibitor: studies of Sym021 in syngeneic mouse cancer models." Theranostics **9**(26): 8221-8238.

Kubli, S. P., T. Berger, D. V. Araujo, L. L. Siu and T. W. Mak (2021). "Beyond immune checkpoint blockade: emerging immunological strategies." Nature Reviews Drug Discovery.

Kunz, P., K. Zinner, N. Mücke, T. Bartoschik, S. Muyldermans and J. D. Hoheisel (2018). "The structural basis of nanobody unfolding reversibility and thermoresistance." Sci Rep **8**(1): 7934.

Kurtys, E., L. Lim, F. Man, A. Volpe and G. Fruhwirth (2018). "In vivo tracking of CAR-T by [18f] BF4-PET/CT in human breast cancer xenografts reveals differences in CAR-T tumour retention." Cytotherapy **20**(5): S20.

Labun, K., T. G. Montague, M. Krause, Y. N. Torres Cleuren, H. Tjeldnes and E. Valen (2019). "CHOPCHOP v3: expanding the CRISPR web toolbox beyond genome editing." Nucleic Acids Res **47**(W1): W171-w174.

Larimer, B. M., E. Wehrenberg-Klee, A. Caraballo and U. Mahmood (2016). "Quantitative CD3 PET Imaging Predicts Tumor Growth Response to Anti-CTLA-4 Therapy." J Nucl Med **57**(10): 1607-1611.

Lassi, K. and N. A. Dawson (2010). "Update on castrate-resistant prostate cancer: 2010." Curr Opin Oncol **22**(3): 263-267.

Lazarovits, A. I., N. Osman, C. E. Le Feuvre, S. C. Ley and M. J. Crumpton (1994). "CD7 is associated with CD3 and CD45 on human T cells." J Immunol **153**(9): 3956-3966.

Le, D. T., E. Lutz, J. N. Uram, E. A. Sugar, B. Onners, S. Solt, L. Zheng, L. A. Diaz, Jr., R. C. Donehower, E. M. Jaffee and D. A. Laheru (2013). "Evaluation of ipilimumab in combination with allogeneic pancreatic tumor cells transfected with a GM-CSF gene in previously treated pancreatic cancer." J Immunother **36**(7): 382-389.

Lecocq, Q., Y. De Vlaeminck, H. Hanssens, M. D'Huyvetter, G. Raes, C. Goyvaerts, M. Keyaerts, N. Devoogdt and K. Breckpot (2019). "Theranostics in immuno-oncology using nanobody derivatives." Theranostics **9**(25): 7772-7791.

Lee, D. W., R. Gardner, D. L. Porter, C. U. Louis, N. Ahmed, M. Jensen, S. A. Grupp and C. L. Mackall (2014). "Current concepts in the diagnosis and management of cytokine release syndrome." Blood **124**(2): 188-195.

Lee, J. H., E. Shklovskaya, S. Y. Lim, M. S. Carlino, A. M. Menzies, A. Stewart, B. Pedersen, M. Irvine, S. Alavi, J. Y. H. Yang, D. Strbenac, R. P. M. Saw, J. F. Thompson, J. S. Wilmott, R. A. Scolyer, G. V. Long, R. F. Kefford and H. Rizos (2020). "Transcriptional downregulation of MHC class I and melanoma de- differentiation in resistance to PD-1 inhibition." Nature Communications **11**(1): 1897.

Lee, J. S. and E. Ruppin (2019). "Multiomics Prediction of Response Rates to Therapies to Inhibit Programmed Cell Death 1 and Programmed Cell Death 1 Ligand 1." JAMA Oncology **5**(11): 1614-1618.

Lee, S. H., H. Soh, J. H. Chung, E. H. Cho, S. J. Lee, J. M. Ju, J. H. Sheen, H. Kim, S. J. Oh, S. J. Lee, J. Chung, K. Choi, S. Y. Kim and J. S. Ryu (2020). "Feasibility of real-time in vivo 89Zr-DFO-labeled CAR T-cell trafficking using PET imaging." PLoS One **15**(1): e0223814.

Leland, P., D. Kumar, S. Nimmagadda, S. R. Bauer, R. K. Puri and B. H. Joshi (2023). "Characterization of chimeric antigen receptor modified T cells expressing scFv-IL-13Rα2 after radiolabeling with (89)Zirconium oxine for PET imaging." J Transl Med **21**(1): 367.

Lepareur, N. (2022). "Cold Kit Labeling: The Future of 68Ga Radiopharmaceuticals?" Frontiers in Medicine **9**.

Lewis, R. E., J. M. Cruse, C. M. Sanders, R. N. Webb, B. F. Tillman, K. L. Beason, J. Lam and J. Koehler (2006). "The immunophenotype of pre-TALL/LBL revisited." Exp Mol Pathol **81**(2): 162-165.

Li, A., Y. Wu, F. Tang, W. Li, X. Feng and Z. Yao (2016). "In Vivo Magnetic Resonance Imaging of CD8+ T Lymphocytes Recruiting to Glioblastoma in Mice." Cancer Biotherapy and Radiopharmaceuticals **31**(9): 317-323.

Li, J., W. Li, K. Huang, Y. Zhang, G. Kupfer and Q. Zhao (2018). "Chimeric antigen receptor T cell (CAR-T) immunotherapy for solid tumors: lessons learned and strategies for moving forward." J Hematol Oncol **11**(1): 22.

Liu, L., Q. Ye, Y. Wu, W.-Y. Hsieh, C.-L. Chen, H.-H. Shen, S.-J. Wang, H. Zhang, T. K. Hitchens and C. Ho (2012). "Tracking T-cells in vivo with a new nano-sized MRI contrast agent." Nanomedicine: Nanotechnology, Biology and Medicine **8**(8): 1345-1354.

Liu, Y., K. Ao, F. Bao, Y. Cheng, Y. Hao, H. Zhang, S. Fu, J. Xu and Q. Wu (2022). "Development of a Bispecific Nanobody Targeting CD20 on B-Cell Lymphoma Cells and CD3 on T Cells." Vaccines (Basel) **10**(8).

Liu, Y., J. Zugazagoitia, F. S. Ahmed, B. S. Henick, S. N. Gettinger, R. S. Herbst, K. A. Schalper and D. L. Rimm (2020). "Immune Cell PD-L1 Colocalizes with Macrophages and Is Associated with Outcome in PD-1 Pathway Blockade Therapy." Clin Cancer Res **26**(4): 970-977.

Liu, Z. and Z. Li (2014). "Molecular imaging in tracking tumor-specific cytotoxic T lymphocytes (CTLs)." Theranostics **4**(10): 990-1001.

Lobach, D. F., L. L. Hensley, W. Ho and B. F. Haynes (1985). "Human T cell antigen expression during the early stages of fetal thymic maturation." J Immunol **135**(3): 1752-1759.

Long, G. V., J. S. Weber, J. Larkin, V. Atkinson, J. J. Grob, D. Schadendorf, R. Dummer, C. Robert, I. Márquez-Rodas, C. McNeil, H. Schmidt, K. Briscoe, J. F. Baurain, F. S. Hodi and J. D. Wolchok (2017). "Nivolumab for Patients With Advanced

Melanoma Treated Beyond Progression: Analysis of 2 Phase 3 Clinical Trials." JAMA Oncol **3**(11): 1511-1519.

Loubaki, L., T. Tremblay and R. Bazin (2013). "In vivo depletion of leukocytes and platelets following injection of T cell-specific antibodies into mice." J Immunol Methods **393**(1-2): 38-44.

Louis, C. U., K. Straathof, C. M. Bollard, S. Ennamuri, C. Gerken, T. T. Lopez, M. H. Huls, A. Sheehan, M. F. Wu, H. Liu, A. Gee, M. K. Brenner, C. M. Rooney, H. E. Heslop and S. Gottschalk (2010). "Adoptive transfer of EBV-specific T cells results in sustained clinical responses in patients with locoregional nasopharyngeal carcinoma." J Immunother **33**(9): 983-990.

Lu, P., Y. Liu, J. Yang, X. Zhang, X. Yang, H. Wang, L. Wang, Q. Wang, D. Jin, J. Li and X. Huang (2022). "Naturally selected CD7 CAR-T therapy without genetic manipulations for T-ALL/LBL: first-in-human phase 1 clinical trial." Blood **140**(4): 321-334.

Lugat, A., C. Bailly, M. Chérel, C. Rousseau, F. Kraeber-Bodéré, C. Bodet-Milin and M. Bourgeois (2022). "Immuno-PET: Design options and clinical proof-of-concept." Front Med (Lausanne) **9**: 1026083.

Lv, G., X. Sun, L. Qiu, Y. Sun, K. Li, Q. Liu, Q. Zhao, S. Qin and J. Lin (2020). "PET Imaging of Tumor PD-L1 Expression with a Highly Specific Nonblocking Single-Domain Antibody." J Nucl Med **61**(1): 117-122.

Mall, S., N. Yusufi, R. Wagner, R. Klar, H. Bianchi, K. Steiger, M. Straub, S. Audehm, I. Laitinen, M. Aichler, C. Peschel, S. Ziegler, M. Mustafa, M. Schwaiger, C. D'Alessandria and A. M. Krackhardt (2016). "Immuno-PET Imaging of Engineered Human T Cells in Tumors." Cancer Res **76**(14): 4113-4123.

Maloney, D. G., B. Smith and A. Rose (2002). "Rituximab: mechanism of action and resistance." Semin Oncol **29**(1 Suppl 2): 2-9.

Manafi-Farid, R., B. Ataeinia, S. Ranjbar, Z. Jamshidi Araghi, M. M. Moradi, C. Pirich and M. Beheshti (2022). "ImmunoPET: Antibody-Based PET Imaging in Solid Tumors." Front Med (Lausanne) **9**: 916693.

Martin, T., S. Z. Usmani, J. G. Berdeja, A. Jakubowiak, M. Agha, A. D. Cohen, P. Hari, D. Avigan, A. Deol, M. Htut, A. Lesokhin, N. C. Munshi, E. O'Donnell, A. K. Stewart, J. M. Schecter, J. D. Goldberg, C. C. Jackson, T.-M. Yeh, A. Banerjee, A. Allred, E. Zudaire, W. Deraedt, D. Madduri, Y. Olyslager, C. Zhou, L. Pacaud, Y. Lin and S. Jagannath (2021). "Updated Results from CARTITUDE-1: Phase 1b/2Study of Ciltacabtagene Autoleucel, a B-Cell Maturation Antigen-Directed Chimeric Antigen Receptor T Cell Therapy, in Patients With Relapsed/Refractory Multiple Myeloma." Blood **138**(Supplement 1): 549-549.

Masopust, D. and J. M. Schenkel (2013). "The integration of T cell migration, differentiation and function." Nat Rev Immunol **13**(5): 309-320.

Maude, S. L., N. Frey, P. A. Shaw, R. Aplenc, D. M. Barrett, N. J. Bunin, A. Chew, V. E. Gonzalez, Z. Zheng, S. F. Lacey, Y. D. Mahnke, J. J. Melenhorst, S. R. Rheingold, A. Shen, D. T. Teachey, B. L. Levine, C. H. June, D. L. Porter and S. A.

Grupp (2014). "Chimeric antigen receptor T cells for sustained remissions in leukemia." N Engl J Med **371**(16): 1507-1517.

Maude, S. L., M. A. Pulsipher, M. W. Boyer, S. A. Grupp, S. M. Davies, C. L. Phillips, M. R. Verneris, K. J. August, K. Schlis, T. A. Driscoll, R. Mody, C. M. Capitini, C. H. June, B. L. Levine, P. A. Wood, L. Yi and J. E. Levine (2016). "Efficacy and Safety of CTL019 in the First US Phase II Multicenter Trial in Pediatric Relapsed/Refractory Acute Lymphoblastic Leukemia: Results of an Interim Analysis." Blood **128**(22): 2801-2801.

Mayer, K. E., S. Mall, N. Yusufi, D. Gosmann, K. Steiger, L. Russelli, H. O. Bianchi, S. Audehm, R. Wagner, E. Bräunlein, A. Stelzl, F. Bassermann, W. Weichert, W. Weber, M. Schwaiger, C. D'Alessandria and A. M. Krackhardt (2018). "T-cell functionality testing is highly relevant to developing novel immuno-tracers monitoring T cells in the context of immunotherapies and revealed CD7 as an attractive target." Theranostics **8**(21): 6070-6087.

McCracken, M. N., D. N. Vatakis, D. Dixit, J. McLaughlin, J. A. Zack and O. N. Witte (2015). "Noninvasive detection of tumor-infiltrating T cells by PET reporter imaging." J Clin Invest **125**(5): 1815-1826.

Meuer, S. C., R. E. Hussey, M. Fabbi, D. Fox, O. Acuto, K. A. Fitzgerald, J. C. Hodgdon, J. P. Protentis, S. F. Schlossman and E. L. Reinherz (1984). "An alternative pathway of T-cell activation: a functional role for the 50 kd T11 sheep erythrocyte receptor protein." Cell **36**(4): 897-906.

Meyer, S., J. H. Leusen and P. Boross (2014). "Regulation of complement and modulation of its activity in monoclonal antibody therapy of cancer." MAbs **6**(5): 1133-1144.

Moek, K. L., D. Giesen, I. C. Kok, D. J. A. de Groot, M. Jalving, R. S. N. Fehrmann, M. N. Lub-de Hooge, A. H. Brouwers and E. G. E. de Vries (2017). "Theranostics Using Antibodies and Antibody-Related Therapeutics." J Nucl Med **58**(Suppl 2): 83s-90s.

Moingeon, P., H.-C. Chang, P. H. Sayre, L. K. Clayton, A. Alcover, P. Gardner and E. L. Reinherz (1989). "The Structural Biology of CD2." Immunological Reviews **111**(1): 111-144.

Motzer, R. J., N. M. Tannir, D. F. McDermott, O. Arén Frontera, B. Melichar, T. K. Choueiri, E. R. Plimack, P. Barthélémy, C. Porta, S. George, T. Powles, F. Donskov, V. Neiman, C. K. Kollmannsberger, P. Salman, H. Gurney, R. Hawkins, A. Ravaud, M. O. Grimm, S. Bracarda, C. H. Barrios, Y. Tomita, D. Castellano, B. I. Rini, A. C. Chen, S. Mekan, M. B. McHenry, M. Wind-Rotolo, J. Doan, P. Sharma, H. J. Hammers and B. Escudier (2018). "Nivolumab plus Ipilimumab versus Sunitinib in Advanced Renal-Cell Carcinoma." N Engl J Med **378**(14): 1277-1290.

Munshi, N. C., L. D. Anderson, Jr., N. Shah, D. Madduri, J. Berdeja, S. Lonial, N. Raje, Y. Lin, D. Siegel, A. Oriol, P. Moreau, I. Yakoub-Agha, M. Delforge, M. Cavo, H. Einsele, H. Goldschmidt, K. Weisel, A. Rambaldi, D. Reece, F. Petrocca, M. Massaro, J. N. Connarn, S. Kaiser, P. Patel, L. Huang, T. B. Campbell, K. Hege and J. San-Miguel (2021). "Idecabtagene Vicleucel in Relapsed and Refractory Multiple Myeloma." N Engl J Med **384**(8): 705-716.

Murty, S., L. Labanieh, T. Murty, G. Gowrishankar, T. Haywood, I. S. Alam, C. Beinat, E. Robinson, A. Aalipour, D. D. Klysz, J. R. Cochran, R. G. Majzner, C. L. Mackall and S. S. Gambhir (2020). "PET Reporter Gene Imaging and Ganciclovir-Mediated Ablation of Chimeric Antigen Receptor T Cells in Solid Tumors." Cancer Res **80**(21): 4731-4740.

Nagy, K., M. Tóth, P. Major, G. Patay, G. Egri, J. Häggkvist, A. Varrone, L. Farde, C. Halldin and B. Gulyás (2013). "Performance evaluation of the small-animal nanoScan PET/MRI system." J Nucl Med **54**(10): 1825-1832.

Natarajan, A., A. T. Mayer, R. E. Reeves, C. M. Nagamine and S. S. Gambhir (2017). "Development of Novel ImmunoPET Tracers to Image Human PD-1 Checkpoint Expression on Tumor-Infiltrating Lymphocytes in a Humanized Mouse Model." Mol Imaging Biol **19**(6): 903-914.

Natarajan, A., C. B. Patel, F. Habte and S. S. Gambhir (2018). "Dosimetry Prediction for Clinical Translation of (64)Cu-Pembrolizumab ImmunoPET Targeting Human PD-1 Expression." Sci Rep **8**(1): 633.

Neelapu, S. S., F. L. Locke, N. L. Bartlett, L. J. Lekakis, D. B. Miklos, C. A. Jacobson, I. Braunschweig, O. O. Oluwole, T. Siddiqi, Y. Lin, J. M. Timmerman, P. J. Stiff, J. W. Friedberg, I. W. Flinn, A. Goy, B. T. Hill, M. R. Smith, A. Deol, U. Farooq, P. McSweeney, J. Munoz, I. Avivi, J. E. Castro, J. R. Westin, J. C. Chavez, A. Ghobadi, K. V. Komanduri, R. Levy, E. D. Jacobsen, T. E. Witzig, P. Reagan, A. Bot, J. Rossi, L. Navale, Y. Jiang, J. Aycock, M. Elias, D. Chang, J. Wiezorek and W. Y. Go (2017). "Axicabtagene Ciloleucel CAR T-Cell Therapy in Refractory Large B-Cell Lymphoma." New England Journal of Medicine **377**(26): 2531-2544.

Ngwa, W., O. C. Irabor, J. D. Schoenfeld, J. Hesser, S. Demaria and S. C. Formenti (2018). "Using immunotherapy to boost the abscopal effect." Nat Rev Cancer **18**(5): 313-322.

Niemeijer, A. N., D. Leung, M. C. Huisman, I. Bahce, O. S. Hoekstra, G. van Dongen, R. Boellaard, S. Du, W. Hayes, R. Smith, A. D. Windhorst, N. H. Hendrikse, A. Poot, D. J. Vugts, E. Thunnissen, P. Morin, D. Lipovsek, D. J. Donnelly, S. J. Bonacorsi, L. M. Velasquez, T. D. de Gruijl, E. F. Smit and A. J. de Langen (2018). "Whole body PD-1 and PD-L1 positron emission tomography in patients with non-small-cell lung cancer." Nat Commun **9**(1): 4664.

Nord, K., E. Gunneriusson, J. Ringdahl, S. Ståhl, M. Uhlén and P. A. Nygren (1997). "Binding proteins selected from combinatorial libraries of an alpha-helical bacterial receptor domain." Nat Biotechnol **15**(8): 772-777.

O'Day, S. J., O. Hamid and W. J. Urba (2007). "Targeting cytotoxic T-lymphocyte antigen-4 (CTLA-4): a novel strategy for the treatment of melanoma and other malignancies." Cancer **110**(12): 2614-2627.

Olafsen, T., S. J. Sirk, S. Olma, C. K. Shen and A. M. Wu (2012). "ImmunoPET using engineered antibody fragments: fluorine-18 labeled diabodies for same-day imaging." Tumour Biol **33**(3): 669-677.

Olafsen, T. and A. M. Wu (2010). "Antibody vectors for imaging." Semin Nucl Med **40**(3): 167-181.

Oliveira, G. and C. J. Wu (2023). "Dynamics and specificities of T cells in cancer immunotherapy." Nat Rev Cancer **23**(5): 295-316.

Oliveira, S., G. A. M. S. van Dongen, M. S.-v. Walsum, R. C. Roovers, J. C. Stam, W. Mali, P. J. van Diest and P. M. P. van Bergen en Henegouwen (2012). "Rapid Visualization of Human Tumor Xenografts through Optical Imaging with a Near-Infrared Fluorescent Anti–Epidermal Growth Factor Receptor Nanobody." Molecular Imaging **11**(1): 7290.2011.00025.

Orcutt, K. D., G. P. Adams, A. M. Wu, M. D. Silva, C. Harwell, J. Hoppin, M. Matsumura, M. Kotsuma, J. Greenberg, A. M. Scott and R. A. Beckman (2017). "Molecular Simulation of Receptor Occupancy and Tumor Penetration of an Antibody and Smaller Scaffolds: Application to Molecular Imaging." Mol Imaging Biol **19**(5): 656-664.

Oroujeni, M., S. S. Rinne, A. Vorobyeva, A. Loftenius, J. Feldwisch, P. Jonasson, V. Chernov, A. Orlova, F. Y. Frejd and V. Tolmachev (2021). "Preclinical Evaluation of (99m)Tc-ZHER2:41071, a Second-Generation Affibody-Based HER2-Visualizing Imaging Probe with a Low Renal Uptake." Int J Mol Sci **22**(5).

Pandit-Taskar, N., M. A. Postow, M. D. Hellmann, J. J. Harding, C. A. Barker, J. A. O'Donoghue, M. Ziolkowska, S. Ruan, S. K. Lyashchenko, F. Tsai, M. Farwell, T. C. Mitchell, R. Korn, W. Le, J. S. Lewis, W. A. Weber, D. Behera, I. Wilson, M. Gordon, A. M. Wu and J. D. Wolchok (2020). "First-in-Humans Imaging with (89)Zr-Df-IAB22M2C Anti-CD8 Minibody in Patients with Solid Malignancies: Preliminary Pharmacokinetics, Biodistribution, and Lesion Targeting." J Nucl Med **61**(4): 512-519.

Papadopoulos, K. P., R. Isaacs, S. Bilic, K. Kentsch, H. A. Huet, M. Hofmann, D. Rasco, N. Kundamal, Z. Tang, J. Cooksey and A. Mahipal (2015). "Unexpected hepatotoxicity in a phase I study of TAS266, a novel tetravalent agonistic Nanobody® targeting the DR5 receptor." Cancer Chemother Pharmacol **75**(5): 887-895.

Papp, K. A., M. A. Weinberg, A. Morris and K. Reich (2021). "IL17A/F nanobody sonelokimab in patients with plaque psoriasis: a multicentre, randomised, placebo-controlled, phase 2b study." Lancet **397**(10284): 1564-1575.

Parente-Pereira, A. C., J. Burnet, D. Ellison, J. Foster, D. M. Davies, S. van der Stegen, S. Burbridge, L. Chiapero-Stanke, S. Wilkie, S. Mather and J. Maher (2011). "Trafficking of CAR-engineered human T cells following regional or systemic adoptive transfer in SCID beige mice." J Clin Immunol **31**(4): 710-718.

Park, H. J., G. H. Kim, K. W. Kim, C. W. Lee, S. Yoon, Y. K. Chae, S. H. Tirumani and N. H. Ramaiya (2021). "Comparison of RECIST 1.1 and iRECIST in Patients Treated with Immune Checkpoint Inhibitors: A Systematic Review and Meta-Analysis." Cancers (Basel) **13**(1).

Parseghian, C. M., M. Patnana, P. Bhosale, K. R. Hess, Y. T. Shih, B. Kim, S. Kopetz, M. J. Overman, G. R. Varadhachary, M. Javle, A. Naing, S. Piha-Paul, D. Hong, H. Le, V. Subbiah and S. Pant (2018). "Evaluating for Pseudoprogression in Colorectal and Pancreatic Tumors Treated With Immunotherapy." J Immunother **41**(6): 284-291.

Patel, S. A. and A. J. Minn (2018). "Combination Cancer Therapy with Immune Checkpoint Blockade: Mechanisms and Strategies." Immunity **48**(3): 417-433.

Pérez, J. M., J. G. Renisio, J. J. Prompers, C. J. van Platerink, C. Cambillau, H. Darbon and L. G. Frenken (2001). "Thermal unfolding of a llama antibody fragment: a two-state reversible process." Biochemistry **40**(1): 74-83.

Perico, M. E., M. Chinol, A. Nacca, E. Luison, G. Paganelli and S. Canevari (2001). "The humoral immune response to macrocyclic chelating agent DOTA depends on the carrier molecule." J Nucl Med **42**(11): 1697-1703.

Perk, L. R., M. J. Vosjan, G. W. Visser, M. Budde, P. Jurek, G. E. Kiefer and G. A. van Dongen (2010). "p-Isothiocyanatobenzyl-desferrioxamine: a new bifunctional chelate for facile radiolabeling of monoclonal antibodies with zirconium-89 for immuno-PET imaging." Eur J Nucl Med Mol Imaging **37**(2): 250-259.

Peterson, A. and B. Seed (1987). "Monoclonal antibody and ligand binding sites of the T cell erythrocyte receptor (CD2)." Nature **329**(6142): 842-846.

Peyvandi, F., S. Cataland, M. Scully, P. Coppo, P. Knoebl, J. A. Kremer Hovinga, A. Metjian, J. de la Rubia, K. Pavenski, J. Minkue Mi Edou, H. De Winter and F. Callewaert (2021). "Caplacizumab prevents refractoriness and mortality in acquired thrombotic thrombocytopenic purpura: integrated analysis." Blood Adv **5**(8): 2137-2141.

Pimm, M. V. and S. J. Gribben (1994). "Prevention of renal tubule re-absorption of radiometal (indium-111) labelled Fab fragment of a monoclonal antibody in mice by systemic administration of lysine." Eur J Nucl Med **21**(7): 663-665.

Pittet, M. J., J. Grimm, C. R. Berger, T. Tamura, G. Wojtkiewicz, M. Nahrendorf, P. Romero, F. K. Swirski and R. Weissleder (2007). "In vivo imaging of T cell delivery to tumors after adoptive transfer therapy." Proc Natl Acad Sci U S A **104**(30): 12457-12461.

Png, Y. T., N. Vinanica, T. Kamiya, N. Shimasaki, E. Coustan-Smith and D. Campana (2017). "Blockade of CD7 expression in T cells for effective chimeric antigen receptor targeting of T-cell malignancies." Blood Adv **1**(25): 2348-2360.

Porter, D. L., W. T. Hwang, N. V. Frey, S. F. Lacey, P. A. Shaw, A. W. Loren, A. Bagg, K. T. Marcucci, A. Shen, V. Gonzalez, D. Ambrose, S. A. Grupp, A. Chew, Z. Zheng, M. C. Milone, B. L. Levine, J. J. Melenhorst and C. H. June (2015). "Chimeric antigen receptor T cells persist and induce sustained remissions in relapsed refractory chronic lymphocytic leukemia." Sci Transl Med **7**(303): 303ra139.

Postow, M. A., M. K. Callahan and J. D. Wolchok (2015). "Immune Checkpoint Blockade in Cancer Therapy." J Clin Oncol **33**(17): 1974-1982.

Powles, T., P. H. O'Donnell, C. Massard, H. T. Arkenau, T. W. Friedlander, C. J. Hoimes, J. L. Lee, M. Ong, S. S. Sridhar, N. J. Vogelzang, M. N. Fishman, J. Zhang, S. Srinivas, J. Parikh, J. Antal, X. Jin, A. K. Gupta, Y. Ben and N. M. Hahn (2017). "Efficacy and Safety of Durvalumab in Locally Advanced or Metastatic Urothelial Carcinoma: Updated Results From a Phase 1/2 Open-label Study." JAMA Oncol **3**(9): e172411.

Rapoport, A. P., E. A. Stadtmauer, G. K. Binder-Scholl, O. Goloubeva, D. T. Vogl, S. F. Lacey, A. Z. Badros, A. Garfall, B. Weiss, J. Finklestein, I. Kulikovskaya, S. K. Sinha, S. Kronsberg, M. Gupta, S. Bond, L. Melchiori, J. E. Brewer, A. D. Bennett, A. B. Gerry, N. J. Pumphrey, D. Williams, H. K. Tayton-Martin, L. Ribeiro, T. Holdich, S. Yanovich,

N. Hardy, J. Yared, N. Kerr, S. Philip, S. Westphal, D. L. Siegel, B. L. Levine, B. K. Jakobsen, M. Kalos and C. H. June (2015). "NY-ESO-1-specific TCR-engineered T cells mediate sustained antigen-specific antitumor effects in myeloma." Nat Med **21**(8): 914-921.

Rashidian, M., J. R. Ingram, M. Dougan, A. Dongre, K. A. Whang, C. LeGall, J. J. Cragnolini, B. Bierie, M. Gostissa, J. Gorman, G. M. Grotenbreg, A. Bhan, R. A. Weinberg and H. L. Ploegh (2017). "Predicting the response to CTLA-4 blockade by longitudinal noninvasive monitoring of CD8 T cells." J Exp Med **214**(8): 2243-2255.

Restifo, N. P., M. E. Dudley and S. A. Rosenberg (2012). "Adoptive immunotherapy for cancer: harnessing the T cell response." Nat Rev Immunol **12**(4): 269-281.

Robbins, P. F., R. A. Morgan, S. A. Feldman, J. C. Yang, R. M. Sherry, M. E. Dudley, J. R. Wunderlich, A. V. Nahvi, L. J. Helman, C. L. Mackall, U. S. Kammula, M. S. Hughes, N. P. Restifo, M. Raffeld, C. C. Lee, C. L. Levy, Y. F. Li, M. El-Gamil, S. L. Schwarz, C. Laurencot and S. A. Rosenberg (2011). "Tumor regression in patients with metastatic synovial cell sarcoma and melanoma using genetically engineered lymphocytes reactive with NY-ESO-1." J Clin Oncol **29**(7): 917-924.

Robert, C., J. Schachter, G. V. Long, A. Arance, J. J. Grob, L. Mortier, A. Daud, M. S. Carlino, C. McNeil, M. Lotem, J. Larkin, P. Lorigan, B. Neyns, C. U. Blank, O. Hamid, C. Mateus, R. Shapira-Frommer, M. Kosh, H. Zhou, N. Ibrahim, S. Ebbinghaus and A. Ribas (2015). "Pembrolizumab versus Ipilimumab in Advanced Melanoma." N Engl J Med **372**(26): 2521-2532.

Rooney, M. S., S. A. Shukla, C. J. Wu, G. Getz and N. Hacohen (2015). "Molecular and genetic properties of tumors associated with local immune cytolytic activity." Cell **160**(1-2): 48-61.

Rosenberg, J. E., J. Hoffman-Censits, T. Powles, M. S. van der Heijden, A. V. Balar, A. Necchi, N. Dawson, P. H. O'Donnell, A. Balmanoukian, Y. Loriot, S. Srinivas, M. M. Retz, P. Grivas, R. W. Joseph, M. D. Galsky, M. T. Fleming, D. P. Petrylak, J. L. Perez-Gracia, H. A. Burris, D. Castellano, C. Canil, J. Bellmunt, D. Bajorin, D. Nickles, R. Bourgon, G. M. Frampton, N. Cui, S. Mariathasan, O. Abidoye, G. D. Fine and R. Dreicer (2016). "Atezolizumab in patients with locally advanced and metastatic urothelial carcinoma who have progressed following treatment with platinum-based chemotherapy: a single-arm, multicentre, phase 2 trial." Lancet **387**(10031): 1909-1920.

Rosenberg, S. A., J. C. Yang, R. M. Sherry, U. S. Kammula, M. S. Hughes, G. Q. Phan, D. E. Citrin, N. P. Restifo, P. F. Robbins, J. R. Wunderlich, K. E. Morton, C. M. Laurencot, S. M. Steinberg, D. E. White and M. E. Dudley (2011). "Durable complete responses in heavily pretreated patients with metastatic melanoma using T-cell transfer immunotherapy." Clin Cancer Res **17**(13): 4550-4557.

Rosenberg, S. A., J. R. Yannelli, J. C. Yang, S. L. Topalian, D. J. Schwartzentruber, J. S. Weber, D. R. Parkinson, C. A. Seipp, J. H. Einhorn and D. E. White (1994). "Treatment of patients with metastatic melanoma with autologous tumor-infiltrating lymphocytes and interleukin 2." J Natl Cancer Inst **86**(15): 1159-1166.

Sahin, U. and Ö. Türeci (2018). "Personalized vaccines for cancer immunotherapy." Science **359**(6382): 1355-1360.

Saini, S., H. Korf, S. Liang, R. Verbeke, B. Manshian, K. Raemdonck, I. Lentacker, C. Gysemans, S. C. De Smedt and U. Himmelreich (2019). "Challenges for labeling and longitudinal tracking of adoptively transferred autoreactive T lymphocytes in an experimental type-1 diabetes model." Magma **32**(3): 295-305.

Salema, V. and L. Fernández (2013). "High yield purification of nanobodies from the periplasm of E. coli as fusions with the maltose binding protein." Protein Expr Purif **91**(1): 42-48.

Sato, N., H. Wu, K. O. Asiedu, L. P. Szajek, G. L. Griffiths and P. L. Choyke (2015). "(89)Zr-Oxine Complex PET Cell Imaging in Monitoring Cell-based Therapies." Radiology **275**(2): 490-500.

Schuster, S. J., M. R. Bishop, C. S. Tam, E. K. Waller, P. Borchmann, J. P. McGuirk, U. Jäger, S. Jaglowski, C. Andreadis, J. R. Westin, I. Fleury, V. Bachanova, S. R. Foley, P. J. Ho, S. Mielke, J. M. Magenau, H. Holte, S. Pantano, L. B. Pacaud, R. Awasthi, J. Chu, Ö. Anak, G. Salles and R. T. Maziarz (2019). "Tisagenlecleucel in Adult Relapsed or Refractory Diffuse Large B-Cell Lymphoma." N Engl J Med **380**(1): 45-56.

Schwartzentruber, D. J., D. H. Lawson, J. M. Richards, R. M. Conry, D. M. Miller, J. Treisman, F. Gailani, L. Riley, K. Conlon, B. Pockaj, K. L. Kendra, R. L. White, R. Gonzalez, T. M. Kuzel, B. Curti, P. D. Leming, E. D. Whitman, J. Balkissoon, D. S. Reintgen, H. Kaufman, F. M. Marincola, M. J. Merino, S. A. Rosenberg, P. Choyke, D. Vena and P. Hwu (2011). "gp100 peptide vaccine and interleukin-2 in patients with advanced melanoma." N Engl J Med **364**(22): 2119-2127.

Scott, A. M., J. D. Wolchok and L. J. Old (2012). "Antibody therapy of cancer." Nat Rev Cancer **12**(4): 278-287.

Scott, C. F., Jr., S. Bolender, G. D. McIntyre, J. Holldack, J. M. Lambert, Y. P. Venkatesh, C. Morimoto, J. Ritz and S. F. Schlossman (1989). "Activation of human cytolytic cells through CD2/T11. Comparison of the requirements for the induction and direction of lysis of tumor targets by T cells and NK cells." J Immunol **142**(11): 4105-4112.

Scully, M., S. R. Cataland, F. Peyvandi, P. Coppo, P. Knöbl, J. A. Kremer Hovinga, A. Metjian, J. de la Rubia, K. Pavenski, F. Callewaert, D. Biswas, H. De Winter and R. K. Zeldin (2019). "Caplacizumab Treatment for Acquired Thrombotic Thrombocytopenic Purpura." N Engl J Med **380**(4): 335-346.

Selvaraj, P., M. L. Plunkett, M. Dustin, M. E. Sanders, S. Shaw and T. A. Springer (1987). "The T lymphocyte glycoprotein CD2 binds the cell surface ligand LFA-3." Nature **326**(6111): 400-403.

Seo, J. W., R. Tavaré, L. M. Mahakian, M. T. Silvestrini, S. Tam, E. S. Ingham, F. B. Salazar, A. D. Borowsky, A. M. Wu and K. W. Ferrara (2018). "CD8(+) T-Cell Density Imaging with (64)Cu-Labeled Cys-Diabody Informs Immunotherapy Protocols." Clin Cancer Res **24**(20): 4976-4987.

Seymour, L., J. Bogaerts, A. Perrone, R. Ford, L. H. Schwartz, S. Mandrekar, N. U. Lin, S. Litière, J. Dancey, A. Chen, F. S. Hodi, P. Therasse, O. S. Hoekstra, L. K. Shankar, J. D. Wolchok, M. Ballinger, C. Caramella and E. G. E. de Vries (2017).

"iRECIST: guidelines for response criteria for use in trials testing immunotherapeutics." The Lancet Oncology **18**(3): e143-e152.

Sheng, B., K. Zhang, S. Tian, R. Ma, Z. Li, H. Wu, T. Wang, L. Jiang, F. You, G. An, H. Meng, L. Yang and X. Liu (2023). "CD7 protein plays a crucial role in T cell infiltration in tumors." Heliyon **9**(6): e16961.

Shimizu, Y., G. A. van Seventer, E. Ennis, W. Newman, K. J. Horgan and S. Shaw (1992). "Crosslinking of the T cell-specific accessory molecules CD7 and CD28 modulates T cell adhesion." J Exp Med **175**(2): 577-582.

Shukla, S. A., P. Bachireddy, B. Schilling, C. Galonska, Q. Zhan, C. Bango, R. Langer, P. C. Lee, D. Gusenleitner, D. B. Keskin, M. Babadi, A. Mohammad, A. Gnirke, K. Clement, Z. J. Cartun, E. M. Van Allen, D. Miao, Y. Huang, A. Snyder, T. Merghoub, J. D. Wolchok, L. A. Garraway, A. Meissner, J. S. Weber, N. Hacohen, D. Neuberg, P. R. Potts, G. F. Murphy, C. G. Lian, D. Schadendorf, F. S. Hodi and C. J. Wu (2018). "Cancer-Germline Antigen Expression Discriminates Clinical Outcome to CTLA-4 Blockade." Cell **173**(3): 624-633.e628.

Sommermeyer, D., M. Hudecek, P. L. Kosasih, T. Gogishvili, D. G. Maloney, C. J. Turtle and S. R. Riddell (2016). "Chimeric antigen receptor-modified T cells derived from defined CD8+ and CD4+ subsets confer superior antitumor reactivity in vivo." Leukemia **30**(2): 492-500.

Sosabowski, J. K. and S. J. Mather (2006). "Conjugation of DOTA-like chelating agents to peptides and radiolabeling with trivalent metallic isotopes." Nat Protoc **1**(2): 972-976.

Sperling, A. I., J. A. Auger, B. D. Ehst, I. C. Rulifson, C. B. Thompson and J. A. Bluestone (1996). "CD28/B7 interactions deliver a unique signal to naive T cells that regulates cell survival but not early proliferation." J Immunol **157**(9): 3909-3917.

Sta Maria, N. S., L. A. Khawli, V. Pachipulusu, S. W. Lin, L. Zheng, D. Cohrs, X. Liu, P. Hu, A. L. Epstein and R. E. Jacobs (2021). "Spatio-temporal biodistribution of (89)Zr-oxine labeled huLym-1-A-BB3z-CAR T-cells by PET imaging in a preclinical tumor model." Sci Rep **11**(1): 15077.

Stillwell, R. and B. E. Bierer (2001). "T cell signal transduction and the role of CD7 in costimulation." Immunol Res **24**(1): 31-52.

Sugiyama, H., T. S. McCormick, K. D. Cooper and N. J. Korman (2008). "Alefacept in the treatment of psoriasis." Clin Dermatol **26**(5): 503-508.

Sun, R., E. J. Limkin, M. Vakalopoulou, L. Dercle, S. Champiat, S. R. Han, L. Verlingue, D. Brandao, A. Lancia, S. Ammari, A. Hollebecque, J. Y. Scoazec, A. Marabelle, C. Massard, J. C. Soria, C. Robert, N. Paragios, E. Deutsch and C. Ferté (2018). "A radiomics approach to assess tumour-infiltrating CD8 cells and response to anti-PD-1 or anti-PD-L1 immunotherapy: an imaging biomarker, retrospective multicohort study." Lancet Oncol **19**(9): 1180-1191.

Suzuki, T., A. Ishii-Watabe, M. Tada, T. Kobayashi, T. Kanayasu-Toyoda, T. Kawanishi and T. Yamaguchi (2010). "Importance of neonatal FcR in regulating the serum half-life of therapeutic proteins containing the Fc domain of human IgG1: a

comparative study of the affinity of monoclonal antibodies and Fc-fusion proteins to human neonatal FcR." J Immunol **184**(4): 1968-1976.

Tannous, B. A., J. Grimm, K. F. Perry, J. W. Chen, R. Weissleder and X. O. Breakefield (2006). "Metabolic biotinylation of cell surface receptors for in vivo imaging." Nat Methods **3**(5): 391-396.

Tavaré, R., H. Escuin-Ordinas, S. Mok, M. N. McCracken, K. A. Zettlitz, F. B. Salazar, O. N. Witte, A. Ribas and A. M. Wu (2016). "An Effective Immuno-PET Imaging Method to Monitor CD8-Dependent Responses to Immunotherapy." Cancer Res **76**(1): 73-82.

Tavaré, R., M. N. McCracken, K. A. Zettlitz, S. M. Knowles, F. B. Salazar, T. Olafsen, O. N. Witte and A. M. Wu (2014). "Engineered antibody fragments for immuno-PET imaging of endogenous CD8+ T cells in vivo." Proc Natl Acad Sci U S A **111**(3): 1108-1113.

Tawbi, H. A., D. Schadendorf, E. J. Lipson, P. A. Ascierto, L. Matamala, E. Castillo Gutiérrez, P. Rutkowski, H. J. Gogas, C. D. Lao, J. J. De Menezes, S. Dalle, A. Arance, J. J. Grob, S. Srivastava, M. Abaskharoun, M. Hamilton, S. Keidel, K. L. Simonsen, A. M. Sobiesk, B. Li, F. S. Hodi and G. V. Long (2022). "Relatlimab and Nivolumab versus Nivolumab in Untreated Advanced Melanoma." N Engl J Med **386**(1): 24-34.

Tazdait, M., L. Mezquita, J. Lahmar, R. Ferrara, F. Bidault, S. Ammari, C. Balleyguier, D. Planchard, A. Gazzah, J. C. Soria, A. Marabelle, B. Besse and C. Caramella (2018). "Patterns of responses in metastatic NSCLC during PD-1 or PDL-1 inhibitor therapy: Comparison of RECIST 1.1, irRECIST and iRECIST criteria." Eur J Cancer **88**: 38-47.

Thurber, G. M., M. M. Schmidt and K. D. Wittrup (2008). "Factors determining antibody distribution in tumors." Trends in Pharmacological Sciences **29**(2): 57-61.

Topalian, S. L., J. M. Taube, R. A. Anders and D. M. Pardoll (2016). "Mechanism-driven biomarkers to guide immune checkpoint blockade in cancer therapy." Nat Rev Cancer **16**(5): 275-287.

Tsai, W. K., K. A. Zettlitz, R. Tavaré, N. Kobayashi, R. E. Reiter and A. M. Wu (2018). "Dual-Modality ImmunoPET/Fluorescence Imaging of Prostate Cancer with an Anti-PSCA Cys-Minibody." Theranostics **8**(21): 5903-5914.

Tumeh, P. C., C. L. Harview, J. H. Yearley, I. P. Shintaku, E. J. Taylor, L. Robert, B. Chmielowski, M. Spasic, G. Henry, V. Ciobanu, A. N. West, M. Carmona, C. Kivork, E. Seja, G. Cherry, A. J. Gutierrez, T. R. Grogan, C. Mateus, G. Tomasic, J. A. Glaspy, R. O. Emerson, H. Robins, R. H. Pierce, D. A. Elashoff, C. Robert and A. Ribas (2014). "PD-1 blockade induces responses by inhibiting adaptive immune resistance." Nature **515**(7528): 568-571.

Twyman-Saint Victor, C., A. J. Rech, A. Maity, R. Rengan, K. E. Pauken, E. Stelekati, J. L. Benci, B. Xu, H. Dada, P. M. Odorizzi, R. S. Herati, K. D. Mansfield, D. Patsch, R. K. Amaravadi, L. M. Schuchter, H. Ishwaran, R. Mick, D. A. Pryma, X. Xu, M. D. Feldman, T. C. Gangadhar, S. M. Hahn, E. J. Wherry, R. H. Vonderheide and A. J. Minn (2015). "Radiation and dual checkpoint blockade activate non-redundant immune mechanisms in cancer." Nature **520**(7547): 373-377.

van de Donk, P. P., T. T. Wind, J. S. Hooiveld-Noeken, E. L. van der Veen, A. Glaudemans, A. Diepstra, M. Jalving, E. G. E. de Vries, E. F. J. de Vries and G. A. P. Hospers (2021). "Interleukin-2 PET imaging in patients with metastatic melanoma before and during immune checkpoint inhibitor therapy." Eur J Nucl Med Mol Imaging **48**(13): 4369-4376.

van den Eertwegh, A. J., J. Versluis, H. P. van den Berg, S. J. Santegoets, R. J. van Moorselaar, T. M. van der Sluis, H. E. Gall, T. C. Harding, K. Jooss, I. Lowy, H. M. Pinedo, R. J. Scheper, A. G. Stam, B. M. von Blomberg, T. D. de Gruijl, K. Hege, N. Sacks and W. R. Gerritsen (2012). "Combined immunotherapy with granulocyte-macrophage colony-stimulating factor-transduced allogeneic prostate cancer cells and ipilimumab in patients with metastatic castration-resistant prostate cancer: a phase 1 dose-escalation trial." Lancet Oncol **13**(5): 509-517.

van der Linden, R. H., L. G. Frenken, B. de Geus, M. M. Harmsen, R. C. Ruuls, W. Stok, L. de Ron, S. Wilson, P. Davis and C. T. Verrips (1999). "Comparison of physical chemical properties of llama VHH antibody fragments and mouse monoclonal antibodies." Biochim Biophys Acta **1431**(1): 37-46.

van Kemenade, F. J., E. Tellegen, M. M. Maurice, A. C. Lankester, T. W. Kuijpers, M. Brouwer, R. de Jong, F. Miedema and R. A. van Lier (1994). "Simultaneous regulation of CD2 adhesion and signaling functions by a novel CD2 monoclonal antibody." J Immunol **152**(9): 4425-4432.

Verdegaal, E. M., N. F. de Miranda, M. Visser, T. Harryvan, M. M. van Buuren, R. S. Andersen, S. R. Hadrup, C. E. van der Minne, R. Schotte, H. Spits, J. B. Haanen, E. H. Kapiteijn, T. N. Schumacher and S. H. van der Burg (2016). "Neoantigen landscape dynamics during human melanoma-T cell interactions." Nature **536**(7614): 91-95.

Verhaar, E. R., A. W. Woodham and H. L. Ploegh (2021). "Nanobodies in cancer." Semin Immunol **52**: 101425.

Vincke, C., R. Loris, D. Saerens, S. Martinez-Rodriguez, S. Muyldermans and K. Conrath (2009). "General strategy to humanize a camelid single-domain antibody and identification of a universal humanized nanobody scaffold." J Biol Chem **284**(5): 3273-3284.

Vosjan, M. J., L. R. Perk, R. C. Roovers, G. W. Visser, M. Stigter-van Walsum, P. M. van Bergen En Henegouwen and G. A. van Dongen (2011). "Facile labelling of an anti-epidermal growth factor receptor Nanobody with 68Ga via a novel bifunctional desferal chelate for immuno-PET." Eur J Nucl Med Mol Imaging **38**(4): 753-763.

Vosjan, M. J., L. R. Perk, G. W. Visser, M. Budde, P. Jurek, G. E. Kiefer and G. A. van Dongen (2010). "Conjugation and radiolabeling of monoclonal antibodies with zirconium-89 for PET imaging using the bifunctional chelate p-isothiocyanatobenzyl-desferrioxamine." Nat Protoc **5**(4): 739-743.

Vosjan, M. J., J. Vercammen, J. A. Kolkman, M. Stigter-van Walsum, H. Revets and G. A. van Dongen (2012). "Nanobodies targeting the hepatocyte growth factor: potential new drugs for molecular cancer therapy." Mol Cancer Ther **11**(4): 1017-1025.

Waldman, A. D., J. M. Fritz and M. J. Lenardo (2020). "A guide to cancer immunotherapy: from T cell basic science to clinical practice." Nat Rev Immunol **20**(11): 651-668.

Wang, G., X. Ji, H. Wang, X. Tang, X. Xing and J. Ji (2023). "PTPRD/PTPRT mutation correlates to treatment outcomes of immunotherapy and immune landscape in pan-cancers." Chin J Cancer Res **35**(3): 316-330.

Wang, M., J. Munoz, A. Goy, F. L. Locke, C. A. Jacobson, B. T. Hill, J. M. Timmerman, H. Holmes, S. Jaglowski, I. W. Flinn, P. A. McSweeney, D. B. Miklos, J. M. Pagel, M. J. Kersten, N. Milpied, H. Fung, M. S. Topp, R. Houot, A. Beitinjaneh, W. Peng, L. Zheng, J. M. Rossi, R. K. Jain, A. V. Rao and P. M. Reagan (2020). "KTE-X19 CAR T-Cell Therapy in Relapsed or Refractory Mantle-Cell Lymphoma." N Engl J Med **382**(14): 1331-1342.

Wang, X., M. Mathieu and R. J. Brezski (2018). "IgG Fc engineering to modulate antibody effector functions." Protein Cell **9**(1): 63-73.

Wang, Z. and W. Han (2018). "Biomarkers of cytokine release syndrome and neurotoxicity related to CAR-T cell therapy." Biomark Res **6**: 4.

Ward, E. S., J. Zhou, V. Ghetie and R. J. Ober (2003). "Evidence to support the cellular mechanism involved in serum IgG homeostasis in humans." Int Immunol **15**(2): 187-195.

Weber, J. S., S. P. D'Angelo, D. Minor, F. S. Hodi, R. Gutzmer, B. Neyns, C. Hoeller, N. I. Khushalani, W. H. Miller, Jr., C. D. Lao, G. P. Linette, L. Thomas, P. Lorigan, K. F. Grossmann, J. C. Hassel, M. Maio, M. Sznol, P. A. Ascierto, P. Mohr, B. Chmielowski, A. Bryce, I. M. Svane, J. J. Grob, A. M. Krackhardt, C. Horak, A. Lambert, A. S. Yang and J. Larkin (2015). "Nivolumab versus chemotherapy in patients with advanced melanoma who progressed after anti-CTLA-4 treatment (CheckMate 037): a randomised, controlled, open-label, phase 3 trial." Lancet Oncol **16**(4): 375-384.

Wei, W., Z. T. Rosenkrans, J. Liu, G. Huang, Q. Y. Luo and W. Cai (2020). "ImmunoPET: Concept, Design, and Applications." Chem Rev **120**(8): 3787-3851.

Weinstein, J. N. and W. van Osdol (1992). "Early intervention in cancer using monoclonal antibodies and other biological ligands: micropharmacology and the "binding site barrier"." Cancer Res **52**(9 Suppl): 2747s-2751s.

Weisser, N. E. and J. C. Hall (2009). "Applications of single-chain variable fragment antibodies in therapeutics and diagnostics." Biotechnology Advances **27**(4): 502-520.

Weist, M. R., R. Starr, B. Aguilar, J. Chea, J. K. Miles, E. Poku, E. Gerdts, X. Yang, S. J. Priceman, S. J. Forman, D. Colcher, C. E. Brown and J. E. Shively (2018). "PET of Adoptively Transferred Chimeric Antigen Receptor T Cells with (89)Zr-Oxine." J Nucl Med **59**(10): 1531-1537.

Wild, M. K., W. Strittmatter, S. Matzku, B. Schraven and S. C. Meuer (1999). "Tumor therapy with bispecific antibody: the targeting and triggering steps can be separated employing a CD2-based strategy." J Immunol **163**(4): 2064-2072.

Williams, M. B. and E. C. Butcher (1997). "Homing of naive and memory T lymphocyte subsets to Peyer's patches, lymph nodes, and spleen." J Immunol **159**(4): 1746-1752.

Wolchok, J. D., V. Chiarion-Sileni, R. Gonzalez, P. Rutkowski, J. J. Grob, C. L. Cowey, C. D. Lao, J. Wagstaff, D. Schadendorf, P. F. Ferrucci, M. Smylie, R. Dummer,

A. Hill, D. Hogg, J. Haanen, M. S. Carlino, O. Bechter, M. Maio, I. Marquez-Rodas, M. Guidoboni, G. McArthur, C. Lebbé, P. A. Ascierto, G. V. Long, J. Cebon, J. Sosman, M. A. Postow, M. K. Callahan, D. Walker, L. Rollin, R. Bhore, F. S. Hodi and J. Larkin (2017). "Overall Survival with Combined Nivolumab and Ipilimumab in Advanced Melanoma." N Engl J Med **377**(14): 1345-1356.

Wolchok, J. D., O. Hamid, A. Ribas, C. Robert, R. Kefford, W.-J. Hwu, J. S. Weber, A. M. Joshua, T. C. Gangadhar, R. S. Dronca, A. Daud, A. Patnaik, R. W. Joseph, H. M. Zarour, X. N. Li, D. Xue, S. Ebbinghaus, S. P. Kang, A. M. Perrone and F. S. Hodi (2015). "Atypical patterns of response in patients (pts) with metastatic melanoma treated with pembrolizumab (MK-3475) in KEYNOTE-001." Journal of Clinical Oncology **33**(15_suppl): 3000-3000.

Wolchok, J. D., H. Kluger, M. K. Callahan, M. A. Postow, N. A. Rizvi, A. M. Lesokhin, N. H. Segal, C. E. Ariyan, R. A. Gordon, K. Reed, M. M. Burke, A. Caldwell, S. A. Kronenberg, B. U. Agunwamba, X. Zhang, I. Lowy, H. D. Inzunza, W. Feely, C. E. Horak, Q. Hong, A. J. Korman, J. M. Wigginton, A. Gupta and M. Sznol (2013). "Nivolumab plus ipilimumab in advanced melanoma." N Engl J Med **369**(2): 122-133.

Xavier, C., A. Blykers, I. Vaneycken, M. D'Huyvetter, J. Heemskerk, T. Lahoutte, N. Devoogdt and V. Caveliers (2016). "(18)F-nanobody for PET imaging of HER2 overexpressing tumors." Nucl Med Biol **43**(4): 247-252.

Xavier, C., I. Vaneycken, M. D'Huyvetter, J. Heemskerk, M. Keyaerts, C. Vincke, N. Devoogdt, S. Muyldermans, T. Lahoutte and V. Caveliers (2013). "Synthesis, preclinical validation, dosimetry, and toxicity of 68Ga-NOTA-anti-HER2 Nanobodies for iPET imaging of HER2 receptor expression in cancer." J Nucl Med **54**(5): 776-784.

Xing, Y., G. Chand, C. Liu, G. J. R. Cook, J. O'Doherty, L. Zhao, N. C. L. Wong, L. K. Meszaros, H. H. Ting and J. Zhao (2019). "Early Phase I Study of a (99m)Tc-Labeled Anti-Programmed Death Ligand-1 (PD-L1) Single-Domain Antibody in SPECT/CT Assessment of PD-L1 Expression in Non-Small Cell Lung Cancer." J Nucl Med **60**(9): 1213-1220.

Yan, J., P. Wang, M. Zhu, G. Li, E. Romão, S. Xiong and Y. Wan (2015). "Characterization and applications of Nanobodies against human procalcitonin selected from a novel naïve Nanobody phage display library." J Nanobiotechnology **13**: 33.

Yang, Z. Z., D. M. Grote, S. C. Ziesmer, T. Niki, M. Hirashima, A. J. Novak, T. E. Witzig and S. M. Ansell (2012). "IL-12 upregulates TIM-3 expression and induces T cell exhaustion in patients with follicular B cell non-Hodgkin lymphoma." J Clin Invest **122**(4): 1271-1282.

Yoon, J. K., B. N. Park, E. K. Ryu, Y. S. An and S. J. Lee (2020). "Current Perspectives on (89)Zr-PET Imaging." Int J Mol Sci **21**(12).

Yusufi, N., S. Mall, H. O. Bianchi, K. Steiger, S. Reder, R. Klar, S. Audehm, M. Mustafa, S. Nekolla, C. Peschel, M. Schwaiger, A. M. Krackhardt and C. D'Alessandria (2017). "In-depth Characterization of a TCR-specific Tracer for Sensitive Detection of Tumor-directed Transgenic T Cells by Immuno-PET." Theranostics **7**(9): 2402-2416.

Zacharakis, N., H. Chinnasamy, M. Black, H. Xu, Y. C. Lu, Z. Zheng, A. Pasetto, M. Langhan, T. Shelton, T. Prickett, J. Gartner, L. Jia, K. Trebska-McGowan, R. P. Somerville, P. F. Robbins, S. A. Rosenberg, S. L. Goff and S. A. Feldman (2018).

"Immune recognition of somatic mutations leading to complete durable regression in metastatic breast cancer." Nat Med **24**(6): 724-730.

Zhang, L., J. R. Conejo-Garcia, D. Katsaros, P. A. Gimotty, M. Massobrio, G. Regnani, A. Makrigiannakis, H. Gray, K. Schlienger, M. N. Liebman, S. C. Rubin and G. Coukos (2003). "Intratumoral T cells, recurrence, and survival in epithelial ovarian cancer." N Engl J Med **348**(3): 203-213.

Zhang, M., X. Fu, H. Meng, M. Wang, Y. Wang, L. Zhang, L. Li, X. Li, X. Wang, Z. Sun, H. Yu, Z. Li, F. Nan, Y. Chang, Z. Zhou, J. Yan, J. Li, X. Wu, G. Pan, Y. Zhao, Y.-S. Chen, F. You and L. Yang (2021). "A Single-Arm, Open-Label, Pilot Trial of Autologous CD7-CAR-T Cells for CD7 Positive Relapsed and Refractory T-Lymphoblastic Leukemia/Lymphoma." Blood **138**(Supplement 1): 3829-3829.

Zhang, Y. and Z. Zhang (2020). "The history and advances in cancer immunotherapy: understanding the characteristics of tumor-infiltrating immune cells and their therapeutic implications." Cell Mol Immunol **17**(8): 807-821.

Zhao, H., C. Wang, Y. Yang, Y. Sun, W. Wei, C. Wang, L. Wan, C. Zhu, L. Li, G. Huang and J. Liu (2021). "ImmunoPET imaging of human CD8+ T cells with novel 68Ga-labeled nanobody companion diagnostic agents." Journal of Nanobiotechnology **19**(1): 42.

8. Acknowledgements

I extend a sincere thank you to Prof. Angela Krackhardt, whose guidance, expertise, and unwavering commitment to scholarly excellence have left an indelible mark on my academic journey. Professor Krackhardt's mentorship has been transformative, providing not only invaluable insights into the intricacies of my research but also fostering an environment where curiosity and innovation thrive.

A special mention goes to Dr. D'Alessandria, whose mentorship has been an enlightening addition to my academic experience. Dr. D'Alessandria's unique perspective and insightful critiques have significantly enhanced the quality and depth of my work.

As I reflect on the collaborative efforts within the laboratory, my appreciation deepens for every member who contributed to the vibrant and intellectually stimulating research atmosphere. Each one of you played an indispensable role in shaping the ideas and outcomes of this dissertation. The collective energy and commitment to excellence within our research community have been instrumental in pushing the boundaries of knowledge.

I am profoundly grateful for the unwavering support and encouragement provided by my family throughout this arduous academic journey. Their sacrifices and steadfast belief in my capabilities have been the bedrock of my perseverance. To my friends, your camaraderie and shared experiences have not only lightened the academic load but have added immeasurable joy to this transformative process. I owe a debt of gratitude to my partner, whose unwavering support and love have been my anchor during the most challenging phases of this dissertation.

My deepest appreciation goes out to everyone who has been part of this transformative experience. This dissertation is not just a culmination of individual efforts but a testament to the collective support, wisdom, and inspiration provided by my family, friends, partner, lab members, Prof. Angela Krackhardt, and Dr. D'Alessandria.